Fuel Analysis and Licensing Code: FALCON MOD01

Volume 3: Verification and Validation

WARNING:
Please read the Export Control and License Agreement on the back cover before removing the Wrapping Material.

Technical Report

Fuel Analysis and Licensing Code: FALCON MOD01

Volume 3: Verification and Validation

1011309

Final Report, December 2004

EPRI Project Manager
S. Yagnik

EPRI • 3412 Hillview Avenue, Palo Alto, California 94304 • PO Box 10412, Palo Alto, California 94303 • USA
800.313.3774 • 650.855.2121 • askepri@epri.com • www.epri.com

ORGANIZATION(S) THAT PREPARED THIS DOCUMENT

ANATECH Corp

ORDERING INFORMATION

Requests for copies of this report should be directed to EPRI Orders and Conferences, 1355 Willow Way, Suite 278, Concord, CA 94520, (800) 313-3774, press 2 or internally x5379, (925) 609-9169, (925) 609-1310 (fax).

CITATIONS

This report was prepared by

ANATECH Corp.
5435 Oberlin Drive
San Diego, California 92121

Principal Investigator
W. F. Lyon
M. N. Jahingir
R. O. Montgomery

This report describes research sponsored by EPRI.

The report is a corporate document that should be cited in the literature in the following manner:

Fuel Analysis and Licensing Code: FALCON MOD01: Volume 3: Verification and Validation, EPRI, Palo Alto, CA: 2004. 1011309.

REPORT SUMMARY

FALCON Mod01 software and accompanying three-volume documentation are being released as the state-of-the-art light water reactor (LWR) fuel performance analysis and modeling code validated to high burn-up. Based on a robust finite element numerical structure, FALCON is capable of analyzing both steady state and transient fuel behavior with a seamless transition between the two modes. FALCON is the culmination of focused developmental activities since 1996 (with its origins in EPRI's two historic fuel performance codes developed in the 1980s: ESCORE and FREY).

Background

Historically, EPRI has been supporting two codes to provide fuel analysis capabilities to utilities: ESCORE for steady state reload analysis and FREY for fuel reliability and off-normal transient analysis. In 1996, EPRI initiated development of FALCON (Fuel Analysis and Licensing Code—New) to address the need for more detailed fuel behavioral analysis, which had become necessary for the fuel designs and operational changes of recent years. The traditional separation of fuel analysis methodologies between steady state and transient had constrained the ability to address important fuel behavioral problems that fall into both regimes. Further, many users of ESCORE and FREY had requested program enhancements (for example, validation to higher burn-ups, ability to deal with newer cladding materials, MOX fuel, and burnable absorbers).

Objectives

To provide a robust and independent code that is validated up to high burn-ups to support fuel performance analyses, reload design, and licensing activities.

Approach

Using the existing experience base from ESCORE and FREY, FALCON's developers focused their efforts on three major tasks: (1) assimilate a robust numerical scheme with fully coupled thermal and mechanical iterations to perform steady state and transient analyses seamlessly in a single code; (2) incorporate pellet and cladding material and behavior models required for steady state and transient fuel performance analysis, with an emphasis to upgrade these models for high burn-up applications where appropriate; and (3) extensively benchmark, verify, and validate the code using a wide variety of test reactor experiments and commercial reactor fuel rod data. The developers also completed a detailed three-part documentation on the code: (a) Theoretical and Numerical Bases (EPRI report 1011307), (b) User's Manual (1011308), and (c) Verification and Validation (1011309). These reports are an integral part of the FALCON Mod01 release.

Results

Various interim versions of FALCON have already been used in support of a variety of recent industry demands, including fuel rod design evaluations, analysis of reactivity-initiated accident

(RIA) tests, development of revised RIA acceptance criteria, analytical support for the Argonne National Laboratory - Nuclear Regulatory Commission Loss of Coolant Accident (ANL-NRC LOCA) program, and dry storage of high burn-up spent fuel. As a result, this formal release of FALCON has not only undergone substantial improvements compared to ESCORE and FREY, but has been duly validated up to high burn-up for modern high-duty fuel operations.

EPRI Perspective

Although licensing analyses have traditionally been performed by fuel vendors, and many utilities continue to rely on vendor-supplied services, an increasing number of utilities prefer to acquire the tools necessary to perform licensing analyses or to conduct independent verification of vendor calculations. FALCON is an essential tool for such work.

Fuel behavior during both normal and off-normal operations is a complex interaction of thermal mechanical and chemical processes. Under some abnormal operational conditions, these processes can threaten fuel integrity and increase demands for more detailed fuel licensing analyses. The large economic benefits of increased fuel use have led to many fuel design changes in recent years. However, no comparable improvements in fuel analysis capabilities have been introduced in the last decade. For optimum plant operation, the detailed behavior of fuel rods under anticipated high-burn-up operations needs to be understood and licensed. As new results emerge from various poolside fuel inspections and hot cell post-irradiation examination (PIE) programs, an analytical capability is indispensable to understand and interpret the results. EPRI anticipates that FALCON will be the tool to meet these challenges.

A FALCON Users Group has been formed, and depending on subsequent utility guidance, the code also may be submitted for design review to obtain Appendix B Quality Assurance (QA) status and NRC approval in the future.

Keywords

Fuel performance and modeling
Finite element methods
High burn-up fuel behavior
Steady state fuel operation
Fuel response to transients
Fission gas release
Core reload and licensing
Operational transients
Postulated accidents

EXECUTIVE SUMMARY

This document presents a summary of the verification and validation of the capabilities of the nuclear fuel behavior program FALCON version MOD01. It is a companion document to Volume 1: Theoretical and Numerical Bases, and Volume 2: User's Manual. Evolving from its origins as a purely transient nuclear fuel behavior code, the focus of recent FALCON development activities has been the addition of the material property and behavioral models required for steady state analysis capability. Along with an emphasis on increasing the validated burnup range, the steady state modifications constitute the primary differences in FALCON MOD01 as compared to the previous versions of the code. The transient capabilities of FALCON were extensively evaluated and documented previously in a special purpose version of the code, FALCON Beta RIA. However, a limited number of submodel, separate effects, and integral fuel rod verification and validation cases have also been included in this report to demonstrate the transient capabilities and applications of FALCON MOD01.

The primary goal of the verification and validation program is to demonstrate the predictive capability of FALCON MOD01 for both PWR and BWR LWR fuels under steady state and transient operating conditions. A fuel rod database was developed that contains 159 cases primarily consisting of instrumented, test program, and commercial fuel rods, but also including analytical and separate effects simulations designed to verify specific behavioral submodels within the code. The criteria used for the selection of the fuel rods cases were based on a combination of factors including emphasis on high burnup (rod average burnups up to or exceeding ~ 70 GWd/TU), relevancy of fuel rod design, and availability of applicable/required experimentally measured data. The verification activity was conducted as an iterative benchmark testing and revision process. This process focused on the primary material property and behavioral models recently added or modified as part of the steady state analysis development program. It was accomplished by using several selected subsets from the fuel rod database tailored to provide the relevant measured data for the following technical areas of evaluation: fuel temperature, fission gas release, cladding diametral creep strain, and cladding irradiation (axial) growth. Once the verification process was completed, validation testing was conducted as a single run of the remaining inventory of fuel rod cases. The final step in the validation process was the comparison of the calculated values to experimentally measured data for fuel temperature, fission gas release, cladding diametral creep strain, cladding irradiation (axial) growth, cladding corrosion, fuel rod internal void volume, and fuel rod internal pressure.

The verification and validation activity summarized herein, has established the steady state applicability of FALCON MOD01 for fuel performance evaluations. This activity has also provided guidance for the continued development of FALCON to further improve its capabilities to address extended fuel utilization and higher fuel duty issues in both steady state and transient operational regimes.

CONTENTS

LIST OF FIGURES

LIST OF TABLES

1
INTRODUCTION

This document provides an overview and a summary of the results from the FALCON MOD01 verification (benchmark testing) and validation (V&V) process. The current effort focused primarily on the code's steady state analysis capability. However, a limited number of submodel, separate effects, and integral fuel rod V&V cases have also been included in this report to demonstrate the transient capabilities and applications of FALCON MOD01. The transient capabilities of FALCON have been extensively evaluated and documented previously in conjunction with the release of a special purpose version of the code modified specifically to analyze reactivity initiated accidents (RIA), FALCON Beta RIA. The theoretical and numerical bases document for FALCON Beta RIA was submitted for review at the request of the U. S. Nuclear Regulatory Commission (NRC) [1]. A revised theoretical and numerical bases document and users manual for FALCON MOD01 have been published as companions to this report [2, 3].

A review of the overall V&V approach, including the development of the fuel rod case database and case selection criteria and prioritization, is presented in Section 2. Section 3 contains an evaluation of the calculational results from the V&V cases based on comparisons with experimental data. The relevant areas of comparison include:

- fuel temperature,
- fission gas release,
- cladding creep,
- cladding irradiation growth,
- cladding corrosion,
- fuel rod internal void volume,
- fuel rod internal pressure,
- coolant channel boundary conditions, and
- transient fuel rod behavior.

Section 4 summarizes the evaluation of the steady state and transient performance of FALCON and discusses recommendations for future development activities. References are listed at the end of each section.

1.1 References

1. Montgomery, R.O., Rashid, Y.R., "FALCON BETA-RIA: Fuel Analysis for Reactivity Initiated Accident, Vol. 1: Theoretical and Numerical Bases," ANATECH Report ANA-02-0356, October 2002.
2. *Fuel Analysis and Licensing Code: Falcon MOD01: Volume 1: Theoretical and Numerical Bases,* EPRI, Palo Alto, CA: 2004. 1011307.
3. *Fuel Analysis and Licensing Code: Falcon MOD01: Volume 2: User's Manual,* EPRI, Palo Alto, CA: 2004. 1011308.

2
DATABASE

This section provides an overview of the development of the FALCON V&V fuel rod case database. The general approach to the development of the database was presented in detail in the alpha release document [1]. That document defined the overall strategy and the case selection criteria and prioritization.

2.1 Approach

The initial task of the V&V plan was to develop an extensive database of analysis cases built upon the existing ESCORE and FREY V&V databases. The combination of these two databases has been supplemented with data from experiments and irradiation programs that have become available since the completion of ESCORE and FREY. The priority for selection of these cases is an emphasis on data to support steady state analysis of extended duty and high burnup fuel. Recommendations from the review of the ESCORE V&V by S. M. Stoller were also utilized [2, 3, 4]. In this review, criteria were established to provide guidance for future fuel performance code benchmarking. These criteria have been used to aid in the selection of cases for the steady state portion of the FALCON V&V database. The general characteristics of the supplementary cases selected to populate the database are summarized below.

- Emphasize high burnup, inventory to extend to 70 GWd/TU average rod burnup or beyond
- Representative of current fuel designs
- Representative of specific phenomena observed in high burnup fuel behavior, i.e. rim formation

Additional recommendations for fuel rod test cases were made during the peer review process. These focused primarily on instrumented research rods to be used for the development of specific fuel performance models within FALCON. For example, recommendations were made for cases to benchmark and/or verify fuel densification, relocation, fission gas release, thermal conductivity (including Gd-bearing fuel), and cladding creep. These recommendations were incorporated into the V&V database development plan.

The database development plan also included the selection of relevant submodel, separate effects, and integral fuel rod transient V&V cases. These cases were selected from the database developed for the testing and verification of FREY-01 and FALCON Beta RIA [5, 6].

2.2 Database Population

The population of fuel rod cases is generally divided into three groups: (1) instrumented research rods, (2) non-instrumented research rods, and (3) commercial fuel rods. The FALCON V&V plan designates rods from groups 1 and 2 to be used in verification activities (model development, testing, and calibration) and those from group 3 for validation to demonstrate the code's predictive capability for commercial fuel rods. Several separate effects cases were also used to demonstrate and verify specific code submodels. Additionally, a small number of commercial rods from group 3 were used for verification to increase the representation of high burnup fuel behavioral phenomena and commercial designs in this category.

A large number of cases representing a wide range of fuel design variants, irradiation environments, and burnups were identified for potential inclusion into the FALCON V&V database. The sources for these cases include the ESCORE and FREY V&V databases, Halden test reactor programs (both from reports and from the Halden Test Fuel Database [TFDB]), and EPRI, U.S. Department of Energy, NRC, and commercial utility fuel test programs. An analysis data request form was developed to facilitate gathering data for inclusion into the FALCON V&V database. This form lists detailed data requirements including fuel and cladding dimensions, thermal hydraulic parameters, rod design data, and power history/axial shape data needed for FALCON fuel performance analyses. Units and default values (if applicable) for the various parameters are also listed and prioritized. In addition, recommendations are included to specify the format of electronic data for power histories, axial shapes, and other distribution data such as that required for PWR corrosion analyses.

Approximately 270 FALCON input decks were developed and entered into the FALCON V&V database. Of these, 159 were chosen for V&V analyses based primarily on 1) the relevance of the fuel rod design, 2) burnup level, and 3) the quality and quantity of measured data available. This group is comprised of approximately a 50/50 mixture of commercial fuel rods and instrumented/non-instrumented research rods. Table 2-1 contains a list of the V&V case rods along with a grid indicating measured data availability. High burnup cases were emphasized in the selection process resulting in more than half of the selected cases within the database having an average fuel rod burnup above 40 GWd/TU. A breakdown of the burnup distribution of the benchmark and V&V cases is displayed in Figure 2-1. A complete listing of the FALCON V&V fuel rod database, including sources for the rod information and measured data, is shown in Appendix A.

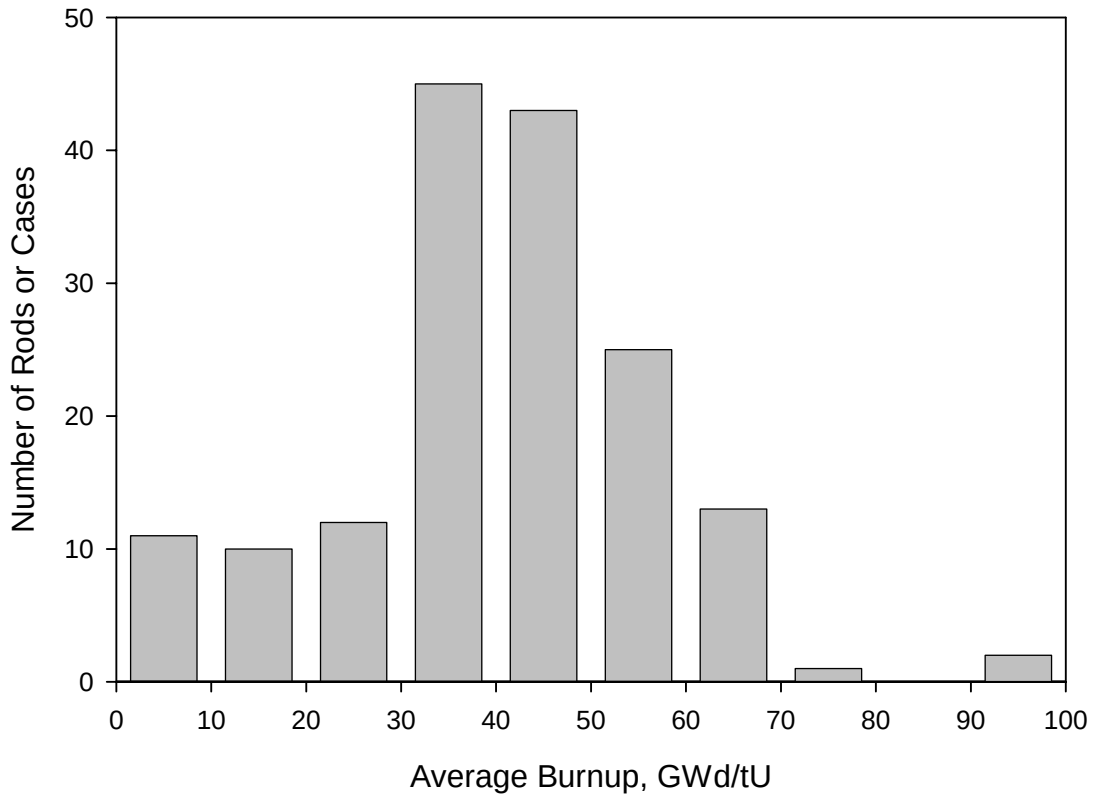

Figure 2-1
Verification and Validation Database Fuel Rod Burnup Distribution

Table 2-1
Verification and Validation Database Inventory

Group	Type	No of Rods	Avg BU GWd/TU	Temp	FGR	Clad Creep	Corrosion	Axial Growth	Void Vol.	Int. Pressure
Annular Flow	channel geom	1	-	X[1]						
CABRI REP Na-5	PWR	1	64.00			X		X		
Calvert Cliffs	14x14 PWR	2	42.80		X	X			X	
Calvert Cliffs Extended BU	14x14 PWR	12	57.97		X	X	X	X	X	X
DOE/BR-3	PWR	1	59.60		X					
Dresden 2	9x9 BWR	10	32.93		X	X	X	X		
Enthalpy Rise	channel geom	1	-	X[2]						
FRF-1	BWR	1	0	X		X				
Ft. Calhoun	14x14 PWR	2	47.40		X		X		X	
Grand Gulf LTA-901	9x9 BWR	19	39.90		X	X	X	X	X	
Grohnde	16x16 PWR	6	46			X	X	X		
HB Robinson	15x15 PWR	11	64.27		X	X	X	X	X	X
HBC	PWR	1	48.20		X					
HBEP	PWR/BWR	4	45.50		X					
HBEP ABB	8X8 BWR	6	45.75		X	X	X	X	X	X
HBEP BNFL	PWR	5	37.85		X				X	
IFA 418	HBWR	1	13.60		X					
IFA 432.3	HBWR	1	28.90		X					
IFA 504	HBWR	3	26.40	X						
IFA 505.5	HBWR	3	40.00	X						
IFA 509.1	HBWR	3	14.00	X						
IFA 515.10	HBWR	2	76.00	X						

Table 2-1 (continued)
Verification and Validation Database Inventory

Group	Type	No of Rods	Avg BU GWd/TU	Temp	FGR	Clad Creep	Corrosion	Axial Growth	Void Vol.	Int. Pressure
IFA 519.9	HBWR	1	91.20		X					
IFA 533.2	HBWR	1	51.50		X					
IFA 562.1	HBWR	6	14.00	X						
IFA 597 (base irrad)	HBWR	1	63.30		X					
IFA 636.1	HBWR	2	21.00	X						
KKL	8x8 GE10 BWR	3	27.3		X	X	X	X	X	X
Limerick	9x9 GE11 BWR	7	55.33		X	X	X	X	X	
Oconee	15x15 PWR	1	45.80		X	X	X		X	X
OPPD/DOE	PWR	3	40.30		X				X	
Over Ramp	PWR	3	23.80		X			X		
PBF GC2-2	BWR	2	0	X						
PBF PCM-2	PWR	1	0	X						
Peach Bottom 3	8x8 BWR	2	33.63		X				X	X
PETTEN/DOE	PWR	9	39.15		X					
Quad Cities 1	8x8 BWR	1	42.00		X					
RISO III	PWR/BWR	4	44.00		X					
Super Ramp	PWR	1	45.20		X					
Transient Conduction	fuel only	1	-	X						
Tribulation	PWR	4	56.50		X					
Verticle Pipe Flow	channel geom	1	-	X[1]						
Zorita	PWR	9	44.45		X				X	

1 - cladding wall temperature, 2 - coolant enthalpy

2.3 References

1. "FALCON – Fuel Analysis and Licensing Code, Vol. 1: Summary Report on Development Activities," ANATECH Report ANA-97-0230, December 1997.
2. Sunderland, D., Harbottle, J., "An Assessment of the Validation of the ESCORE I Code," Stoller Report to S. Levy for EPRI Project 2061-26, August 1991.
3. Sunderland, D., Harbottle, J., "Selection of Rods to Re-Evaluate ESCORE I by Use of Discriminating Criteria," Stoller Report to S. Levy for EPRI Project 2061-26, August 1991.
4. Sunderland, D., Harbottle, J., "Review of New Fuel Performance Data," Stoller Report to S. Levy for EPRI Project 2061-26, August 1991.
5. Montgomery, R.O., Zangari, A.J., Rashid, Y.R., "FREY-01 – Fuel Rod Evaluation System, Vol. 4 Verification and Validation Manual," ANATECH Research Corporation, NP-3277-CCM, Rev. 2, January 1993.
6. Montgomery, R.O., Rashid, Y.R., "FALCON BETA-RIA: Fuel Analysis for Reactivity Initiated Accident, Vol. 1: Theoretical and Numerical Bases," ANATECH Report ANA-02-0356, October 2002.

3
VERIFICATION AND VALIDATION RESULTS

This section presents the results from the analyses completed during the FALCON V&V exercise. These include evaluation and testing of models for fuel rod temperature, fission gas release, cladding creep, cladding irradiation growth, and for integral effects including rod internal void volume and internal pressure. In addition, several cases were used to evaluate the coolant channel model and demonstrate the code's capability to model transients such as power/coolant mismatch (PCM), loss-of-coolant accident (LOCA), and RIA. Selected results for individual rods are presented to illustrate performance for particular effects, behaviors, or material properties along with cumulative data plots of predicted versus measured data from the entire fuel rod inventory. Statistical assessments of the performance of FALCON are also presented where applicable.

3.1 Fuel Temperature

Thermal testing is fundamental to determining the performance of a fuel rod behavior code in that the temperatures within the fuel rod drive most other physical phenomena and are of primary importance when determining integral fuel rod performance. In the current revision, FALCON MOD01 has undergone numerous upgrades that directly and indirectly impact thermal performance. These include a new radial power and burnup distribution model, fuel thermal conductivity model augmentations (revised burnup and gadolinia [Gd_2O_3] content), inclusion of relocation and densification models, new cladding creep models (which affect gap thickness), and a revised thermal/mechanical solution iteration procedure. These modifications along with others have dramatically improved the thermal performance of FALCON MOD01 under steady state operating conditions as compared to earlier versions of the code. These modifications and their impacts have been discussed in detail in the FALCON theory manual and other previously published reports [1, 2].

Thermal testing of FALCON as part of the steady state development phase and the steady state and transient verification phase was conducted by comparing calculated fuel temperatures to measured temperatures from instrumented test fuel rods and transient thermal simulations. The measured fuel temperatures are based on thermocouple readings taken during irradiation under reactor operational conditions. The transient thermal simulation is based on the analytical solution for transient heat conduction through an idealized bare fuel pellet. The verification case set consisted of 22 different cases as listed in Table 3-1. These cases provided a wide variety of both steady state and transient thermal conditions based on differing fill gas compositions, initial fuel/cladding gap thicknesses, fuel surface roughnesses, U-235 enrichments, gadolinia content, and burnup. Table 3-2 lists the results of the statistical assessment of the thermal verification cases. Figures 3-1 through 3-9 provide examples of the thermal performance of FALCON MOD01 as compared to measured data for individual rods. A cumulative sampling of data from

all the thermal verification cases plotted as functions of burnup, diametral gap thickness, and linear power, respectively, are shown in Figures 3-10 through 3-12. The distribution of temperature differentials (calculated – measured) based on this data is presented in Figure 3-13.

Table 3-1
Thermal Verification Cases

Case	Average Burnup (GWd/TU)	Number of Rods	Description
IFA 504	~ 26.4	3	He, Ar, Xe fill gases evaluated during startup 10% enrichment, 200 μm gap
IFA 505.5	~ 40	3	Various enrichments, fill gases, and gaps Rod 1: 10% enrichment, He-filled, 100 μm gap Rod 2: 6% enrichment, Xe-filled, 100 μm gap Rod 3: 10% enrichment, Xe-filled, 50 μm gap
IFA 509.1	~ 14	3	10% enrichment, He-filled Rod 1: 150 μm gap Rod 2: 225 μm gap Rod 3: 60 μm gap
IFA 515.10	~ 76	2	He-filled, 50 μm gap Rod A1: UO_2, 11.5% enrichment Rod A2: 8% Gd_2O_3, 13% enrichment
IFA 562.1	~ 14	6	3.95% enrichment, 60 – 72 μm gap Rod 5: He-filled, 0.78 μm fuel roughness Rod 6: He-filled, 1.38 μm fuel roughness Rod 7: Xe-filled, 0.55 μm fuel roughness Rod 10: Xe-filled, 1.5 μm fuel roughness Rod 11: He-filled, 0.45 μm fuel roughness Rod 12: He-filled, 1.3 μm fuel roughness
IFA 636.1	~21/17	2	75 μm gap Rod 2: 8% Gd_2O_3, 4.25% enrichment Rod 7: 3.94% enrichment
PBF GC 2-2	~0	2	Power oscillation test methodology Centerline and off center thermal couple locations Rod 522-2: Ar-filled, 63.5 μm gap Rod 522-4: He-filled, 190 μm gap
Transient Conduction	~0	1	1-D transient solution of Fourier law of heat conduction Idealized cylindrical geometry (bare fuel pellet) Low enrichment (0.1% to suppress radial power effects) Constant fuel thermal conductivity

Table 3-2
Thermal Verification Results Summary

Test Case	Fuel Centerline Temperature Standard Deviation	
	+/- °C	**+/- %**
IFA 504		
He Rod	22.04	3.46 %
Xe Rod	45.4	5.88 %
Ar Rod	51.4	7.9 %
IFA 505.5		
Rod 1	141.3	16.1 %
Rod 2	157.7	15.0 %
Rod 3	41.2	4.6 %
IFA 509.1		
Rod 1	47.74	4.0 %
Rod 2	130.5	10.0 %
Rod 3	116.1	8.8 %
IFA 515.10		
Rod A1	48.8	8.1 %
Rod A2 (Gd)	48.0	7.4 %
IFA 562.1		
Rod 5	107.6	14.3 %
Rod 6	147.6	19.3 %
Rod 7	164.1	18.2 %
Rod 10	115.2	12.1 %
Rod 11	51.9	6.6 %
Rod 12	118.1	14.9 %
IFA 636.1		
Rod 2 (Gd)	89.9	13.7 %
Rod 7	111.3	21.0 %
PBF GC 2-2		
Rod 522-2	42.8	0.6 %
Rod 522-4	60.1	0.9 %
Transient Conduction		
$\tau = 0.1$	6.0	0.3 %
$\tau = 0.2$	7.8	0.6 %
$\tau = 0.4$	1.9	0.1 %
Overall Average	78.1 °C	8.9 %

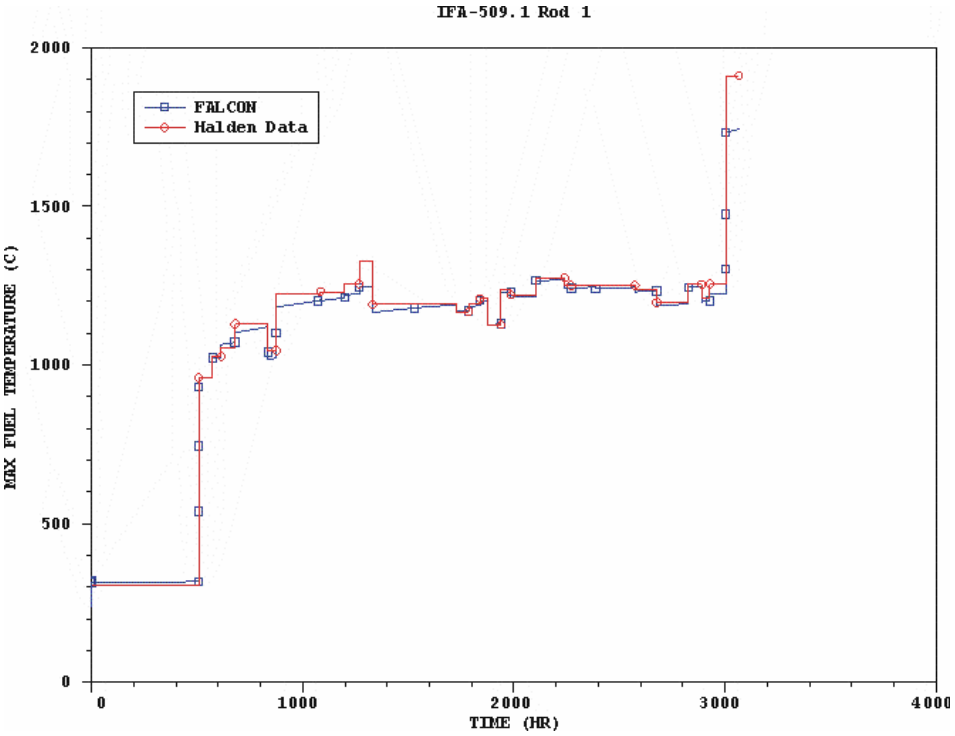

Figure 3-1
Calculated Fuel Temperatures Versus Measured Data for IFA-509.1 Rod 1

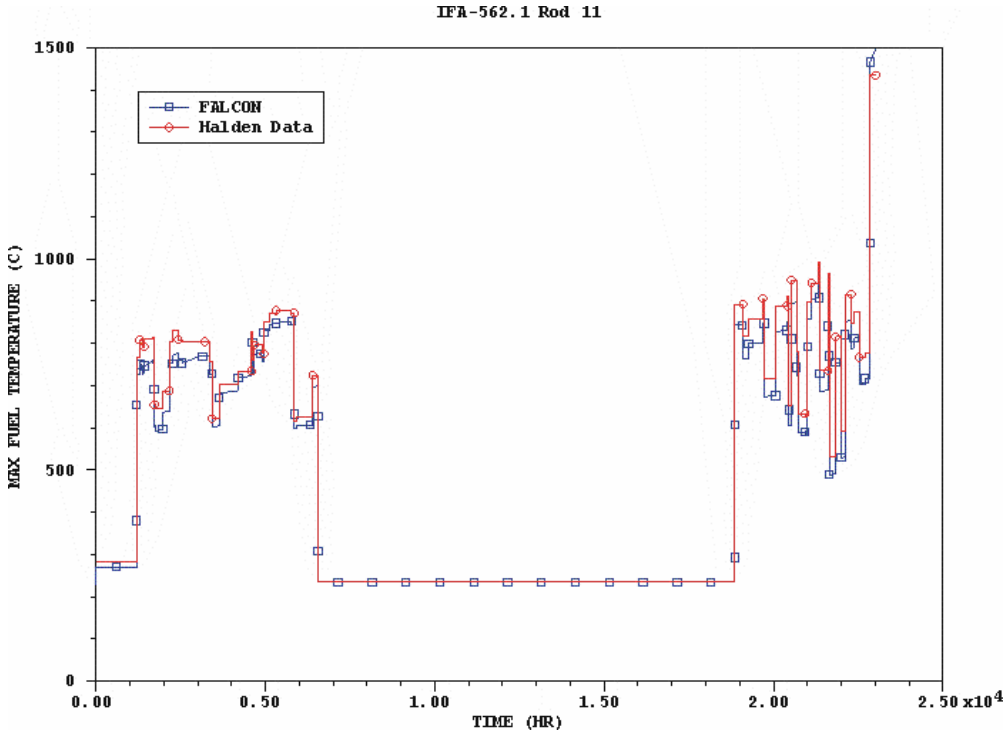

Figure 3-2
Calculated Fuel Temperatures Versus Measured Data for IFA-562.1 Rod 11

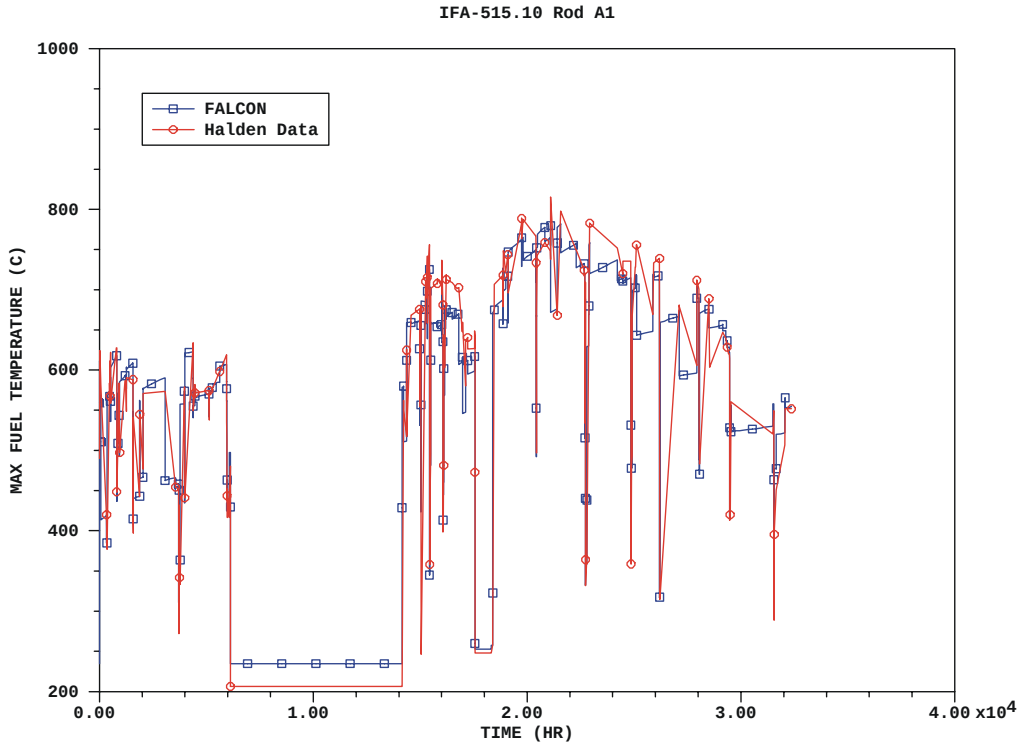

Figure 3-3
Calculated Fuel Temperatures Versus Measured Data for IFA-515.10 Rod A1

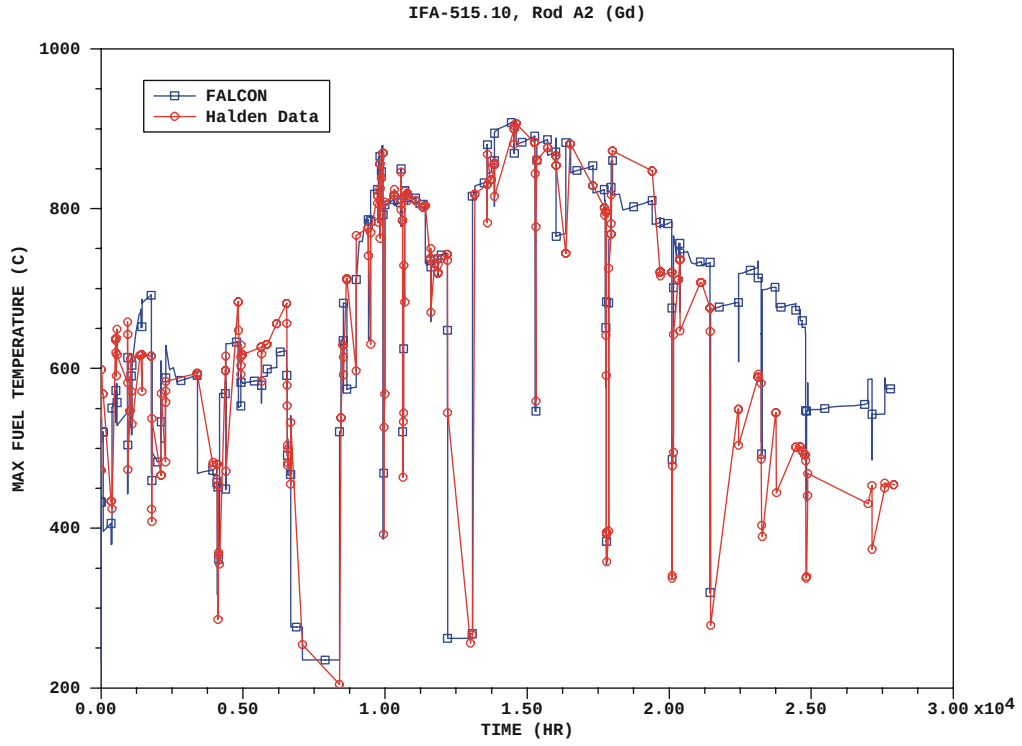

Figure 3-4
Calculated Fuel Temperatures Versus Measured Data for IFA-515.10 Rod A2

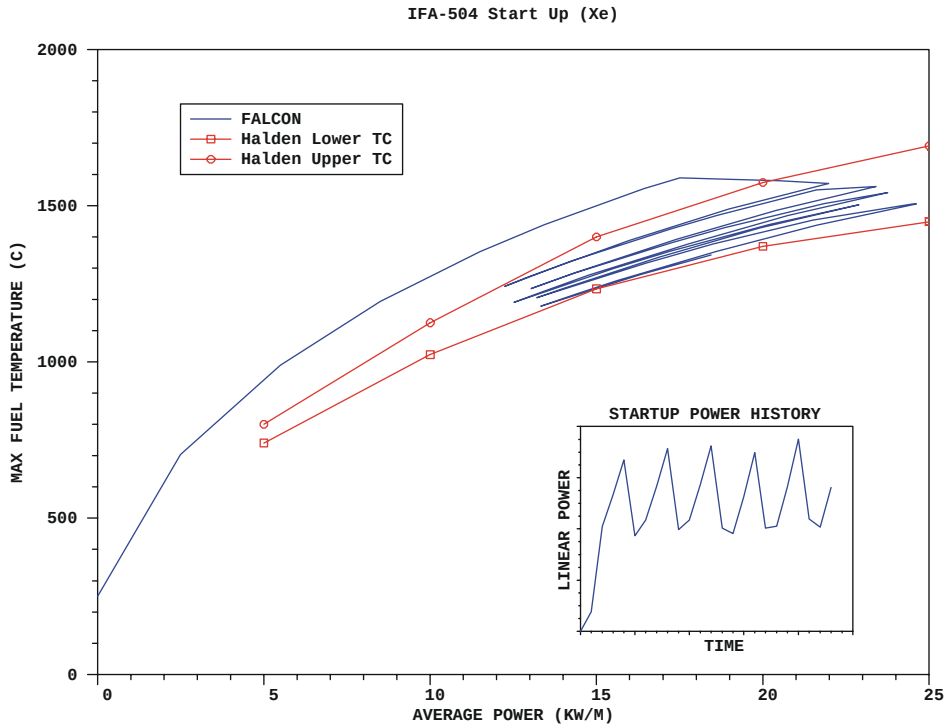

Figure 3-5
Calculated Fuel Temperatures Versus Measured Data for IFA-504 (Xe-Filled)

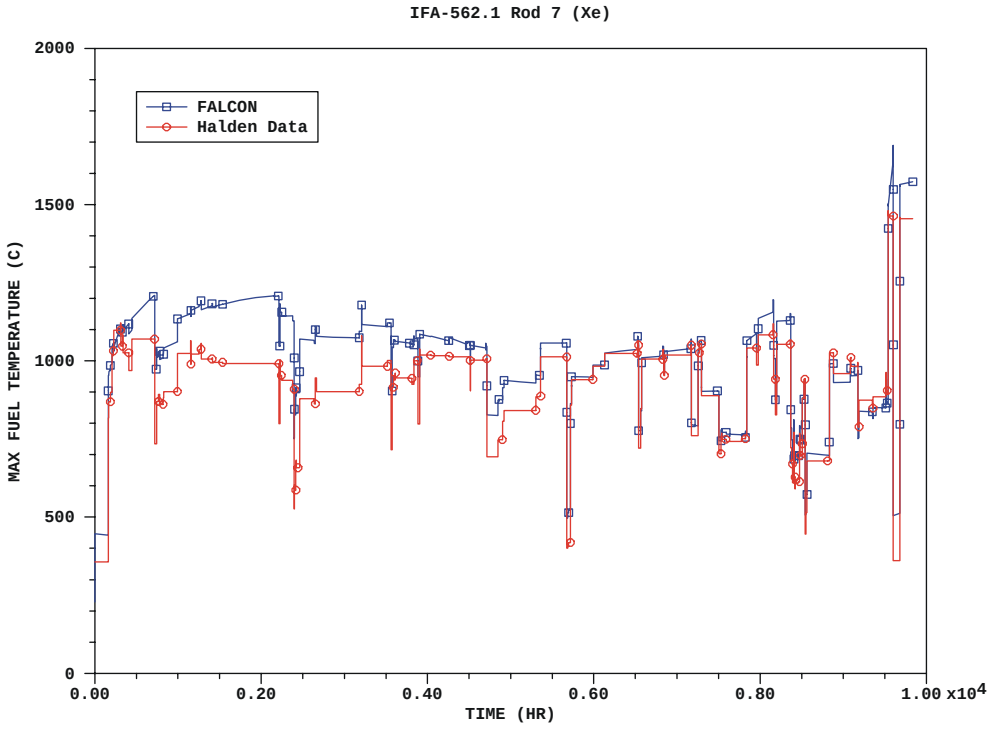

Figure 3-6
Calculated Fuel Temperatures Versus Measured Data for IFA-562.1 Rod 7 (Xe-filled)

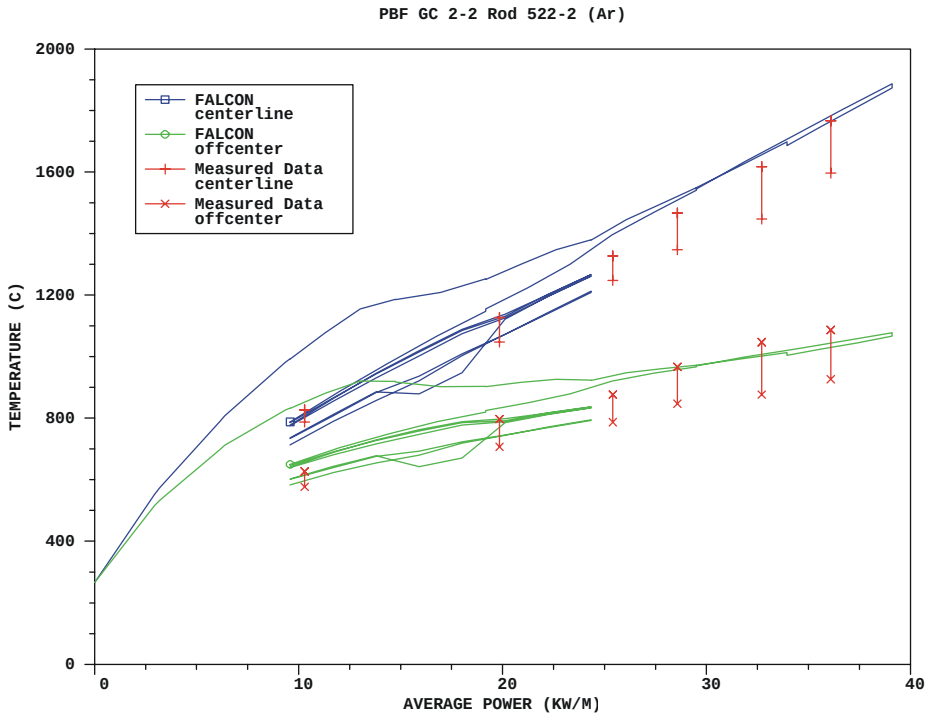

Figure 3-7
Calculated Fuel Temperatures Versus Measured Data for Centerline and Off-Center Thermocouple Locations in GC 2-2 Rod 522-2 (Ar-filled)

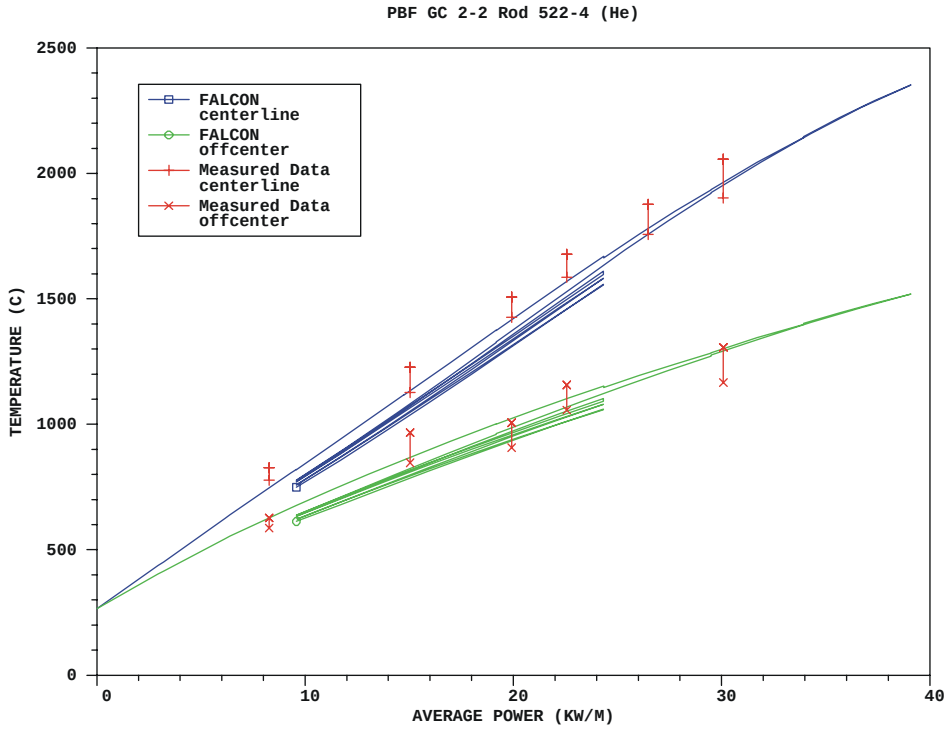

Figure 3-8
Calculated Fuel Temperatures Versus Measured Data for Centerline and Off-Center Thermocouple Locations in GC 2-2 Rod 522-4 (He-filled)

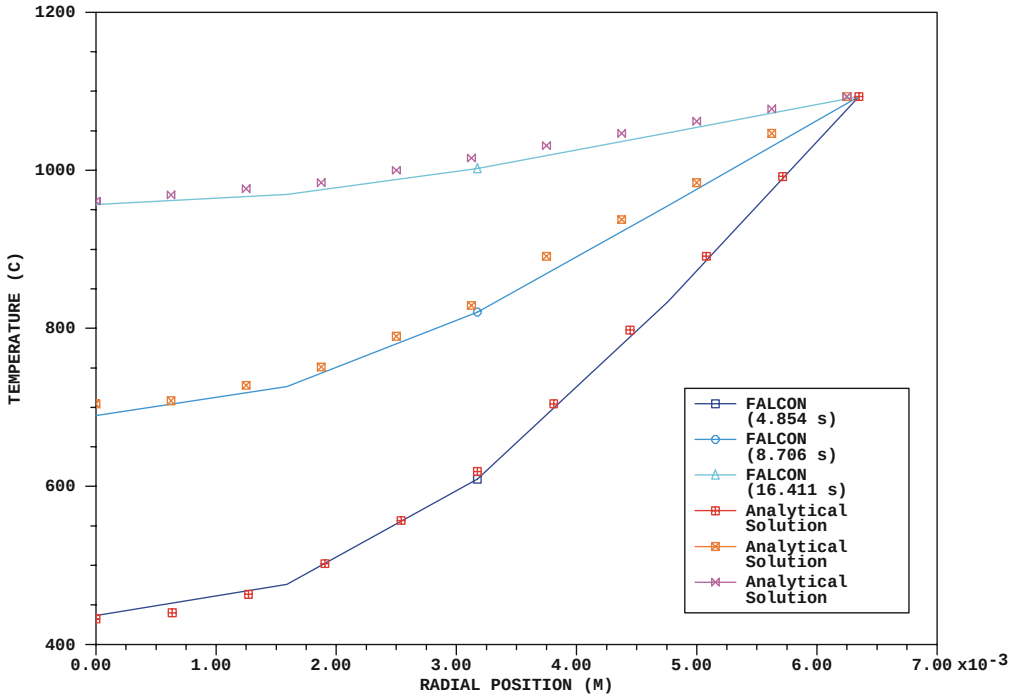

Figure 3-9
Calculated Fuel Temperatures Versus the 1-D Cylindrical Transient Thermal Solution for a Bare Fuel Pellet

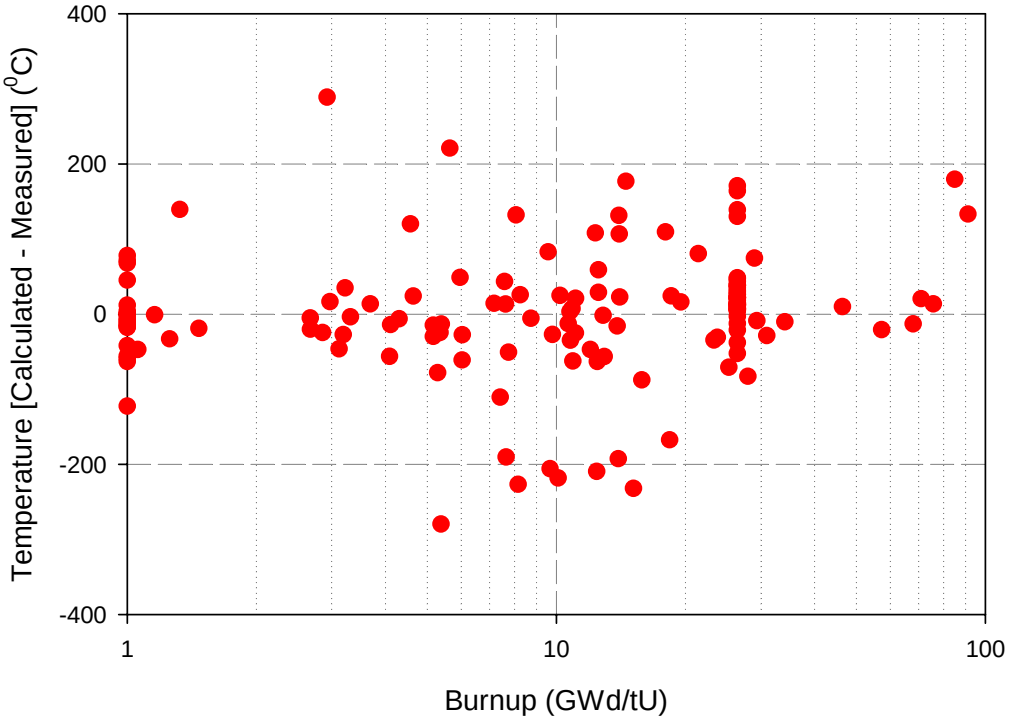

Figure 3-10
Cumulative Thermal Performance as a Function of Burnup

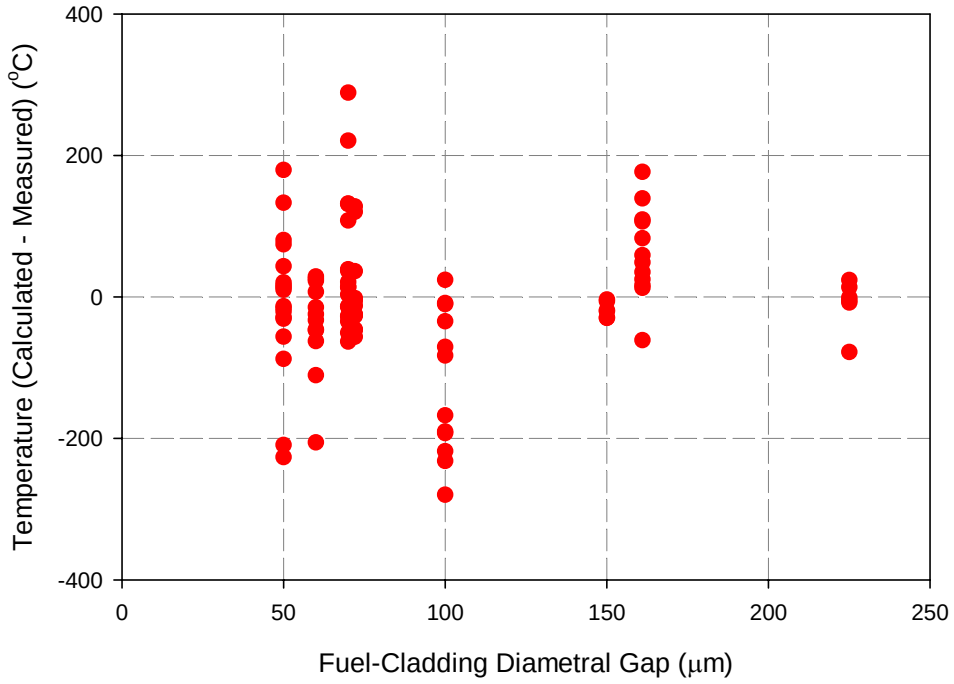

Figure 3-11
Cumulative Thermal Performance as a Function of Diametral Gap Thickness

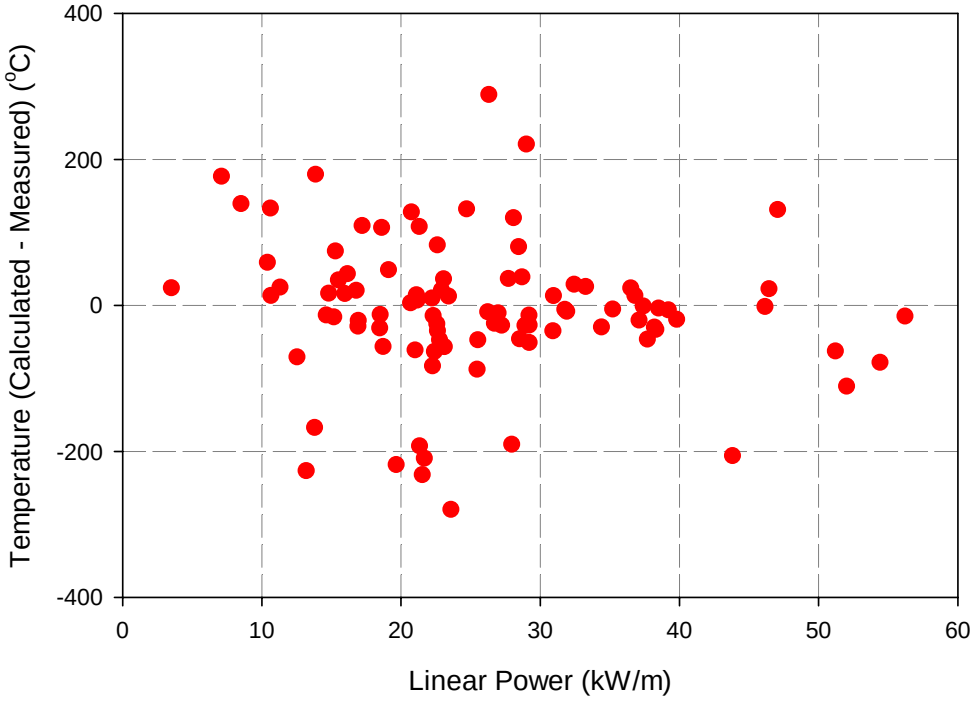

Figure 3-12
Cumulative Thermal Performance as a Function of Linear Power

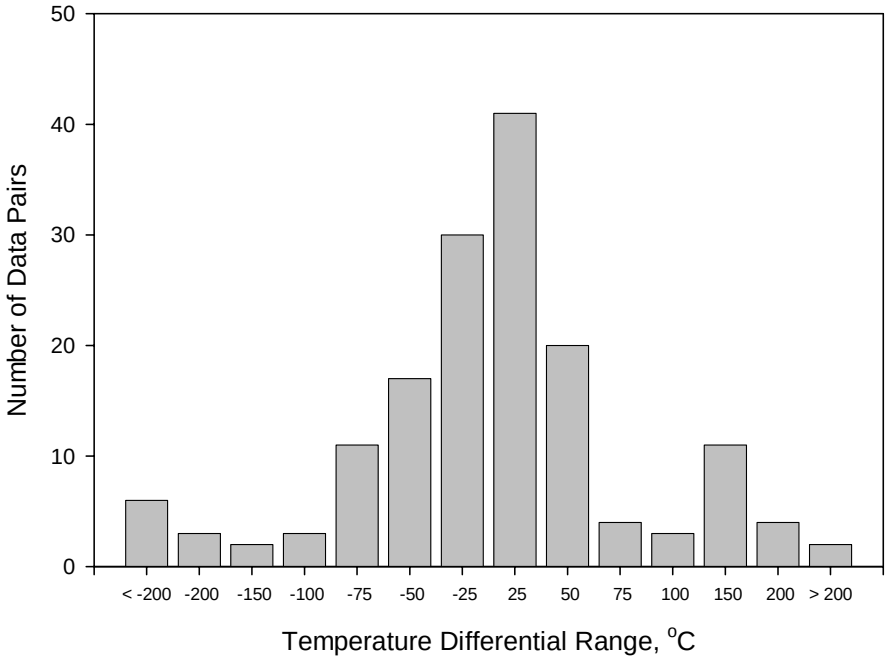

Figure 3-13
Temperature Differential Range Distribution

Comparing results from earlier versions of FALCON has shown dramatic improvement in the steady state thermal predictive capability especially in the areas of low initial gap conductivity (due to large initial gap width or low conductivity gas composition) and high burnup rods. As noted earlier, these changes are due primarily to modifications and improvements in the overall thermal/mechanical iteration procedure, fuel swelling, and fuel thermal conductivity models.

Figures 3-1 through 3-4 illustrate measured temperature history comparisons for several He-filled test rods. In Figures 3-1 and 3-2, IFA-509.1 Rod 1 and IFA 562.1 Rod 11, respectively, indicate very good agreement for relatively low burnup rods (~ 14 GWd/TU), whereas Figure 3-3, IFA-515.10 Rod A1, shows good agreement at much higher burnups (~ 76 GWd/TU). In Figure 3-4, the companion rod from IFA-515.10 that contains 8% Gd_2O_3, also indicates good agreement until a small divergence noted near the end of the irradiation. Limited data on irradiated Gd-doped fuel is available and this result may indicate more data is required at the higher burnup ranges.

The results from two test Xe-filled rods are shown in Figures 3-5 and 3-6. The first, IFA 504, is a sweep gas experiment and indicates good agreement between FALCON and the measured data. It should be noted that the data presented in the plot is of two forms: 1) the FALCON data represents a time history for the linear powers experienced during the simulation, whereas, 2) the measured data presented are thermocouple readings from the lower and upper portions of the rod presumably condensed and averaged over the entire history of the startup test for each linear power. The initial differences (seen at the lower linear powers) are the result of the effects of thermal cycling at startup. These effects include relocation, densification, and cracking. Once these effects subside, the FALCON predicted temperatures stay within the range of the measured data. In Figure 3-6, data for a Xe-filled rod from IFA-562.1 is presented. Early on in the

irradiation the FALCON predicted temperatures are somewhat higher than those measured, but indicate good agreement as the test proceeds to higher burnups.

Figures 3-7 and 3-8 show the results from the analysis of GC 2-2 rods 522-2 and 522-4. These rods were part of the NRC-sponsored Thermal Fuels Behavior Program conducted in the Power Burst Facility (PBF) [3]. Designed to measure gap conductance and its dependence on a variety of parameters including fill gas composition, fuel density, and initial gap width in BWR type test rods, this test program used a power oscillation methodology to infer gap conductance (which is not directly measurable). These rods featured thermocouples placed in pellet center and off-center locations. The data shown for comparison with FALCON fuel temperature calculations were obtained from these thermocouples during the power calibration phase of the irradiation. For the Ar-filled rod in Figure 3-7, the FALCON calculated temperatures show the effects of power cycling in the lower linear power range as discussed above regarding the Xe-filled rod in Figure 3-5. Once this effect subsides, the calculated off-center temperatures fall within the measured temperature ranges. The calculated centerline temperatures show a similar trend below 25 kW/m and a slight over prediction above this linear power. Given the power cycling history, it appears that the data from linear powers above 25 kW/m are still somewhat influenced by the effects of relocation, densification, and cracking. In Figure 3-8, the FALCON calculated temperatures show a smaller thermal cycling effect and fall primarily within the measured thermocouple data throughout the entire range of linear powers. Another trend noted within the testing regime is that the lower gap conductivity from Ar and Xe-filled rods tends to increase the thermal effects of relocation, densification, and cracking during power cycling.

Figure 3-9 depicts a comparison of calculated FALCON temperatures as a function of time and radial position to the analytical solution for a simplified transient heat conduction problem. A model was developed for a bare cylinder of UO_2 fuel (without heat generation and with constant fuel thermal conductivity) instantaneously heated from an initial temperature of 315.6 ºC (600 ºF) to 1093.3 ºC (2000 ºF). The results were then compared to analytical solutions available in the literature for corresponding times and radial positions [4]. The times shown in Figure 3-9 correspond to dimensionless time points (τ = 0.1, 0.2, and 0.4) designated in the analytical solution as shown in the reference. The dimensionless time parameter, τ, is defined by equation (1) below.

$$\tau = \frac{\alpha t}{R^2} \tag{1}$$

Where α = thermal diffusivity, t = time, and R = cylinder radius. Evaluation of the plots show that the FALCON calculated temperatures match the analytical solution extremely well indicating that the transient heat conduction methodology implemented in FALCON is accurate.

As shown in Figure 3-10, FALCON represents the majority of the temperature measurement data quite well with the vast majority of predicted temperatures falling with a band of +/- 100 ºC over the entire burnup range. Also, as indicated in Figures 3-11 and 3-12, there are no indicated biases or trends with initial diametral gap size nor linear power. Table 3-2 lists the standard deviation in both degrees C and as a percentage of the mean temperature measured during irradiation averaged over the time of irradiation for each case. The average standard deviation of +/- 78.1 ºC and +/- 8.9% represents the thermal predictive capability of FALCON MOD01 over

a wide variety of thermal conditions and rod types and geometries as represented by the selected verification cases. To provide some basis for comparison, the uncertainty associated with the power histories provided by Halden is reported to be approximately +/- 5%. This level of uncertainty in power can cause a fuel rod's centerline temperature to vary +/- 30 to 40 ºC or more depending upon geometry, composition, and power level. Additional uncertainty inherent in the material property and behavioral models employed as well as the temperature measurements themselves also contribute to the differences in calculated and measured values. Overall, the steady state and transient thermal performance of FALCON is judged to be quite good over a wide range of fuel rod conditions, powers, geometries, and fill gas and fuel compositions and provides a good foundation for the simulation of more integral rods effects such as fission gas release, internal pressure, and cladding response.

3.2 Fission Gas Release

A total of 29 fuel rod cases were chosen from the FALCON V&V database for fission gas release (FGR) model verification. These rods are shown in Table 3-3 and include test program and commercial rods. The primary function of the verification tests was to calibrate and evaluate the Forsberg - Massih and ESCORE FGR models as implemented in FALCON.

Once the verification activity was completed, an additional 86 cases, primarily test program and commercial fuel rods, were run to validate the FGR models in FALCON. Thus, a total of 115 fuel rod cases were used in the overall FGR testing program. These cases represented a wide variety of fuel rod designs and included two fundamental irradiation regimes: 1) long term steady state irradiation, and 2) power ramp or "bump" tests.

The Forsberg - Massih FGR model was run in the "default mode", using the recently implemented NFIR fuel thermal conductivity and the Limbäck and Andersson creep models. For the "bump" tests, the Forsberg - Massih model was coupled with the FALCON transient FGR model (EPRI/CE), that is based on thermal anneal studies. The latter being used only during the ramp and hold phases of the power history for the cases bump tested. This approach was not used for the ESCORE FGR model. However, during testing it was found that more consistent results were obtained from the ESCORE FGR model when it was run in conjunction with the MATPRO cladding creep and fuel thermal conductivity models. This result was not unexpected given that the MATPRO models more closely mimic the thermal and mechanical response of the ESCORE code and therefore, the calibration basis of the ESCORE FGR model. This combination of models is recommended when running FALCON in what is termed "ESCORE-emulation mode". The calculated FGR data from both models were compared to the measured data. A summary of the results is provided in Table 3-4. Figures 3-14 through 3-20 provide examples of the performance of both the Forsberg – Massih and ESCORE FGR models as compared to measured data for individual fuel rods. A cumulative plot of the performance of both models is shown in Figure 3-21. Figures 3-22 and 3-23 illustrate the distribution of the differences between the calculated and measured FGR values for each model.

Figure 3-14 illustrates the performance of both the Forsberg – Massih and ESCORE FGR models for a Calvert Cliffs Extended Burnup PWR fuel rod UFE067. This rod is an example of a commercial PWR fuel rod irradiated under steady state conditions. Both models calculate a FGR value near the measured value of 2.6%. Readily noticeable in this plot is the difference between

the two model's approach to release or kinetic behavior. The ESCORE model shows an almost immediate onset of release at a rate that stays fairly constant throughout the power history. In contrast, Forsberg – Massih shows two incubation periods each followed by fairly rapid release, indicative of the two-stage saturation and release methodology employed in this model.

The RISO III, AN2 fuel rod is an example of a PWR rod initially irradiated under steady state conditions and then refabricated and retested using a transient or bump test mode of operation. The bump test consisted of a series of power ramps followed by high power hold periods. The entire test lasted approximately 72 hours. Figures 3-15 and 3-16 show the response of both FGR models during base irradiation and bump testing, respectively. During the steady state base irradiation, the measured gas release is low in these rods at ~ 0.2%. The Forsberg Massih model predicts a steady state gas release of 0.012%, while the ESCORE model predicts 2.7%. As can be seen in Figure 3-16, both models respond to the increase in power that occurs during the initial portion of the bump test and subsequently release large fractions of gas during the high power hold period. As noted earlier, the Forsberg – Massih model is coupled to the EPRI/CE transient FGR model for application to power ramp tests. The result from the combined Forsberg – Massih and EPRI/CE approach produces a calculated value of 27.3% versus a - measured value of 29.7%. The ESCORE model predicts 18% FGR for this rod.

Table 3-3
Fission Gas Release Verification Cases

Case	Average Burnup (GWd/TU)	Number of Rods	Description Rod Type, Irradiation History
DOE/Br-3	59.6	1	PWR, steady state
Grand Gulf	39.9	2	BWR, commercial, steady state
HB Robinson	64.3	2	PWR, commercial, steady state
HBC	48.2	1	PWR, steady state
HBEP	45.5	4	PWR & BWR, steady state
IFA 418	13.6	1	HBWR, steady state
IFA 432.3	28.9	1	HBWR, steady state
IFA 519.9	91.2	1	HBWR, steady state
IFA 533.2	51.5	1	HBWR, steady state
IFA 597	61.1	1	BWR, steady state, base irradiation only
KKL	45.1	2	BWR, commercial, steady state
Limerick	55.3	2	BWR, commercial, steady state
Over Ramp	23.8	1	PWR, steady state & ramp
RISO III	44.0	4	PWR/BWR, steady state & ramp
Super Ramp	45.2	1	PWR, steady state & ramp
Tribulation	56.5	4	PWR, steady state

Table 3-4
Fission Gas Release Verification and Validation Results

Verification Cases						
Program	**Rod**	**Measured FGR %**	**ESCORE Model**	**ESCORE Δ**	**Forsberg – Massih Model**	**Forsberg – Massih Δ**
DOE/Br-3	36I82	33.8	72.01	38.21	46.43	12.63
Grand Gulf	A02	5.2	2.57	-2.63	0.17	-5.03
	A06	3.5	5.42	1.92	0.99	-2.51
HB Robinson	A10	2.5	2.55	0.05	8.93	6.43
	R01	1.6	2.59	0.99	3.83	2.23
HBC	BN-1066	5.3	42.88	37.58	11.44	6.14
HBEP	GE 8D10-1	5.2	2.96	-2.24	0.48	-4.72
	GE 8D10-2	0.1	0.9	0.8	0.01	-0.09
	GE 8D14-2	< 0.2	0.75	0.6	0.0	-0.2
	W 01-7-A	0.5	1.3	0.8	0.08	-0.42
IFA 418	2	0.2	1.16	0.96	0.75	0.55
IFA 432.3	3	10 +/- 10	11.39	1.39	2.53	-7.47
IFA 519.9	DH	57.4	42.28	-15.12	34.94	-22.46
IFA 533.2	808	~ 6 – 8	28.49	21.49	17.5	10.5
IFA 597 (base)	8	~10	97.73	87.73	30.6	20.6
KKL	F5	11.64	1.92	-9.72	4.47	-7.17
	F6	8.1	1.24	-6.86	0.3	-7.8
Limerick	J4	13.12	1.7	-11.42	0.3	-12.82
	J6	16.72	1.68	-15.04	0.29	-16.43
Over Ramp	A10/3	30.3	21.51	-8.79	22.73	-7.57
RISO III	AN2	29.7	17.96	-11.74	27.29	-2.41
	AN3	35.5	15.84	-19.66	26.28	-9.22
	GE4	27	16.45	-10.55	19.37	-7.63
	GE7	14.4	9.35	-5.05	20.63	6.23
Super Ramp	PK2/1	28.3	12.05	-16.25	18.32	-9.98
Tribulation	W-109	0.75	2.48	1.73	1.15	0.4
	W-217	0.2	1.12	0.92	0.01	-0.19
	W-220	1.3	2.43	1.13	0.07	-1.23
	W-324	6.7	2.61	-4.09	3.08	-3.62

Table 3-4 (continued)
Fission Gas Release Verification and Validation Results

Validation Cases						
Program	**Rod**	**Measured FGR %**	**ESCORE Model**	**ESCORE Δ**	**Forsberg – Massih Model**	**Forsberg – Massih Δ**
Calvert Cliffs-1	AHS008	0.3	77.6	77.3	0.013	-0.287
	NBD 144	1.5	93.55	92.05	0.029	-1.471
Calvert Cliffs Ext Burnup	BEN 013	2.3	2.58	0.28	0.739	-1.561
	BFJ 027	2	2.52	0.52	0.716	-1.284
	BFL 009	1.6	2.7	1.1	0.505	-1.095
	UFE 067	2.6	2.16	-0.44	2.882	0.282
	UFE 019	0.9	1.59	0.69	0.157	-0.743
	BFM 034	3.8	2.92	-0.88	1.038	-2.762
	BFM 070	3.1	2.72	-0.38	0.828	-2.272
	BFM 071	2.3	2.46	0.16	0.658	-1.642
	BFM 073	2.9	2.66	-0.24	0.807	-2.093
	BFM 156	1.4	2.31	0.91	0.442	-0.958
Dresden-2	220 A1	0.12	0.6	0.48	0.004	-0.116
	228 A1	0.88	0.56	-0.32	0.004	-0.876
	B2	0.06	0.52	0.46	0.584	0.524
	B9	0.65	0.58	-0.07	0.004	-0.646
	F9	0.24	0.6	0.36	0.004	-0.236
	H8	0.13	0.63	0.5	0.004	-0.126
Fort Calhoun	KJD 125	0.45	3.38	2.93	0.021	-0.429
	KJE 076	0.62	3.63	3.01	0.023	-0.597

Table 3-4 (continued)
Fission Gas Release Verification and Validation Results

Validation Cases (continued)						
Program	**Rod**	**Measured FGR %**	**ESCORE Model**	**ESCORE Δ**	**Forsberg – Massih Model**	**Forsberg – Massih Δ**
Grand Gulf	901 A05	4.4	3.52	-0.88	0.77	-3.63
	901 B01	9	0.96	-8.04	0.177	-8.823
	901 D02	1.2	1.13	-0.07	0.057	-1.143
	901 E09	0.8	3.09	2.29	1.13	0.33
	901 F08	0.3	0.99	0.69	0.088	-0.212
	901 K05	2.3	3	0.7	1.077	-1.223
	901 B04	2	1.39	-0.61	0.083	-1.917
	901 D01	1.8	2.38	0.58	0.688	-1.112
	901 D09	1.3	3.05	1.75	1.161	-0.139
	901 E01	2.9	3.53	0.63	0.756	-2.144
	901 F01	3.1	3.18	0.08	0.845	-2.255
	901 F09	3.8	3.56	-0.24	1.167	-2.633
	901 H06	2.1	1.25	-0.85	0.124	-1.976
	901 H09	2.9	0.82	-2.08	0.331	-2.569
	901 K04	3.7	5.51	1.81	1.315	-2.385
	901 K06	2.1	2.32	0.22	1.023	-1.077
	901 K08	1.2	0.73	-0.47	0.191	-1.009
HBEP	ABB A184	0.3	1.38	1.08	0.019	-0.281
	ABB A186	3.4	1.35	-2.05	0.009	-3.391
	ABB A364	1	1.8	0.8	0.179	-0.821
	ABB H8364	17.3	2.5	-14.8	1.202	-16.098
	ABB H8366	11.2	2.93	-8.27	0.879	-10.321
	BNFL AK	4.1	10.92	6.82	3.636	-0.464
	BNFL BH	7.6	29.01	21.41	4.633	-2.967
	BNFL BP	7.3	27.58	20.28	1.146	-6.154
	BNFL CQ	6.6	32.29	25.69	1.6	-5.0
	BNFL DF	4.0	12.4	8.4	4.772	0.772
HB Robinson	A02	2.4	2.15	-0.25	0.717	-1.683
	B01	2	2.59	0.59	0.878	-1.122
	B05	2.3	2.15	-0.15	0.873	-1.426
	E02	2.1	2.42	0.32	0.823	-1.276
	F07	1.4	1.9	0.5	0.228	-1.172
	G10	1.9	1.91	0.01	0.228	-1.672
	H05	1.4	1.27	-0.13	0.009	-1.391
	R05	2.2	2.71	0.51	0.896	-1.304
	S02	2.4	2.73	0.33	0.913	-1.487

Table 3-4 (continued)
Fission Gas Release Verification and Validation Results

Validation Cases (continued)						
Program	**Rod**	**Measured FGR %**	**ESCORE Model**	**ESCORE Δ**	**Forsberg – Massih Model**	**Forsberg – Massih Δ**
KKL	D02	8.2	1.62	-6.58	2.098	-6.102
Limerick	E9	19.31	1.69	-17.62	0.301	-19.009
	F9	19.4	1.68	-17.72	0.31	-19.09
	G1	15.59	1.58	-14.01	0.198	-15.392
	J3	10.88	1.64	-9.24	0.191	-10.689
	J7	6.33	1.66	-4.67	0.229	-6.101
Oconee	A1	2.2	4.8	2.6	1.965	-0.235
OPPD	KJE 076	0.6	1.48	0.88	0.009	-0.591
	JKN 052	0.3	1.07	0.77	0.007	-0.293
	KKM 095	0.4	1.34	0.94	0.009	-0.391
Peach Bottom 3	DJD 224	4.8	0.6	-4.2	0.018	-4.782
Petten	123	40.8	27.56	-13.24	31.54	-9.26
	124	33.6	19.3	-14.3	23.87	-9.73
	V 305	25.6	12.82	-12.78	15.55	-10.05
	V 404	12.6	8.47	-4.13	12.81	0.21
	V 302	35	19.56	-15.44	21.94	-13.06
	V 401	26.6	9.69	-16.91	20.21	-6.39
	V 402	42.2	20.85	-21.35	28.7	-13.5
	V 403	29.5	13.34	-16.16	22.92	-6.58
	V 405	11.4	27.58	16.18	31.55	20.15
Quad Cities	G7	0.3	1.26	0.96	0.008	-0.292
Zorita	328	11.7	30.85	19.15	13.52	1.82
	331	11.7	13.85	2.15	38.3	26.6
	332	20.9	22.46	1.56	23.88	2.98
	334	23	88.38	65.38	72.64	49.64
	335	12.4	13.79	1.39	14.94	2.54
	344	16.9	13.81	-3.09	19.13	2.23
	384	23.9	92.25	68.35	77.54	53.64
	386	22.6	37.63	15.03	25.56	2.96
	385	13.2	15.87	2.67	22.02	8.82

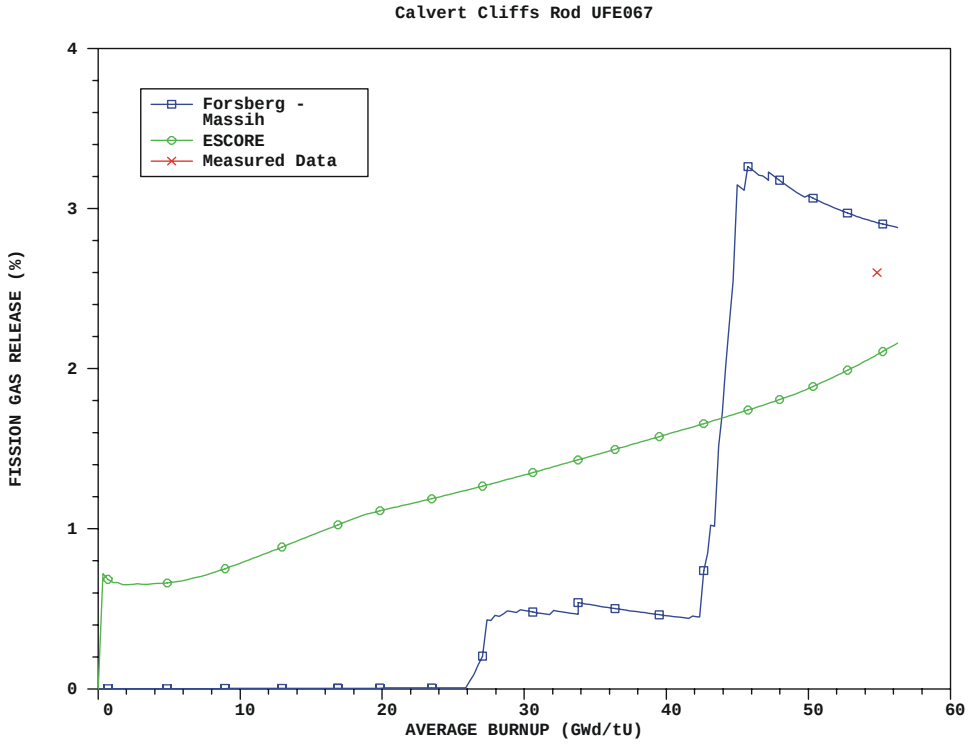

Figure 3-14
Fission Gas Release Model Comparison - Calvert Cliffs Extended Burnup Rod UFE067

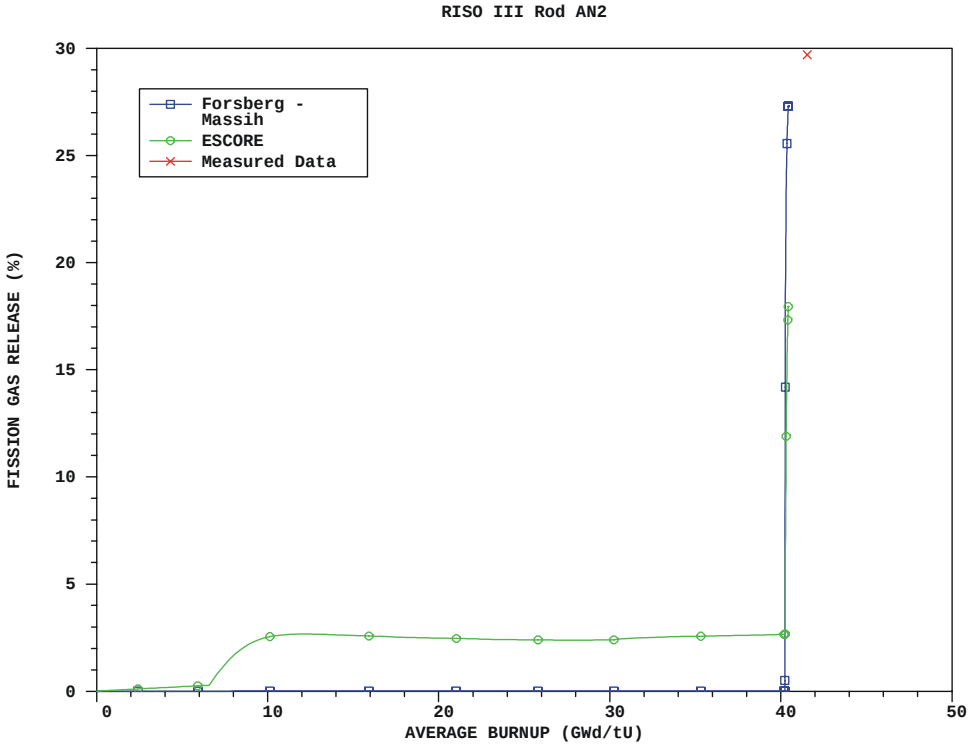

Figure 3-15
Fission Gas Release Model Comparison – RISO III Rod AN2

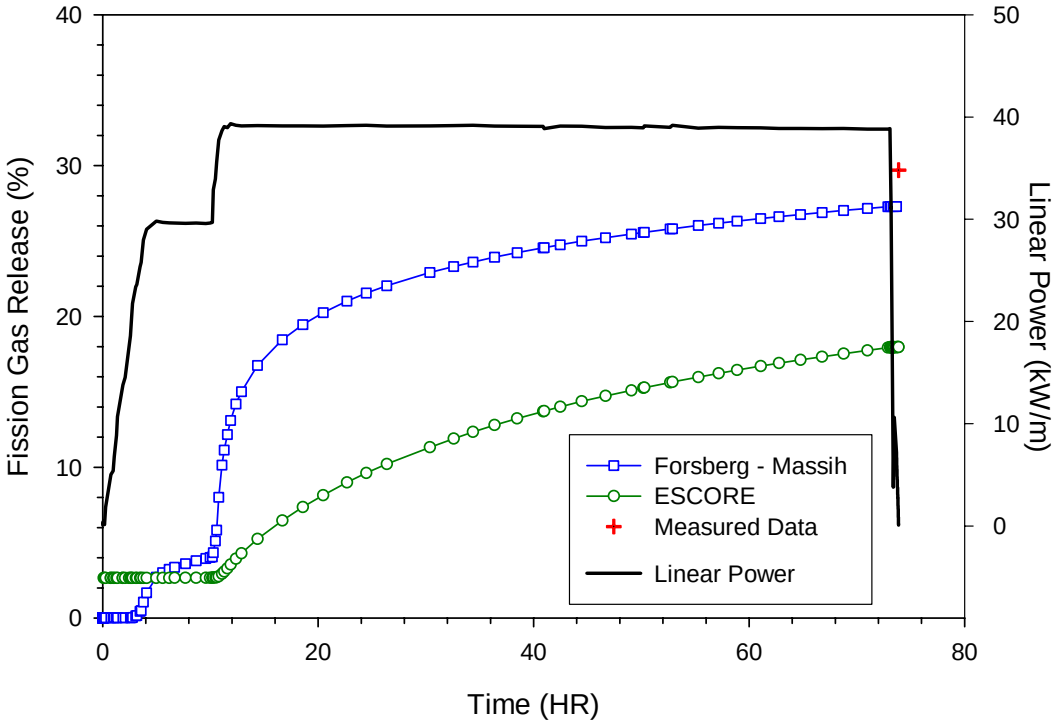

Figure 3-16
RISO III AN2 Bump Test Fission Gas Release and Power History

In contrast to AN2, RISO III rod AN3 was equipped with instrumentation that provided fuel rod temperature, internal pressure, and FGR as a function of time during a bump test. This data allows the evaluation of the kinetics of each FGR model to be evaluated during the power ramps and hold times. Figure 3-17 illustrates the overall FGR response (from base irradiation through the end of the bump test) for the Forsberg – Massih model coupled to the EPRI/CE transient model and the ESCORE FGR model. Figure 3-18 compares the FGR response of the two models to the measured FGR data during the bump test. Both models tend to follow the slope of the measured release during the first power ramp up to the hold at 40 kW/m linear power. However, neither model responds to the second and third power ramps well resulting in fairly large under predictions of the final measured FGR of 35.5%. The predicted release values were 26.3% and 15.8% for the Forsberg – Massih model coupled to the EPRI/CE transient model and the ESCORE FGR model, respectively.

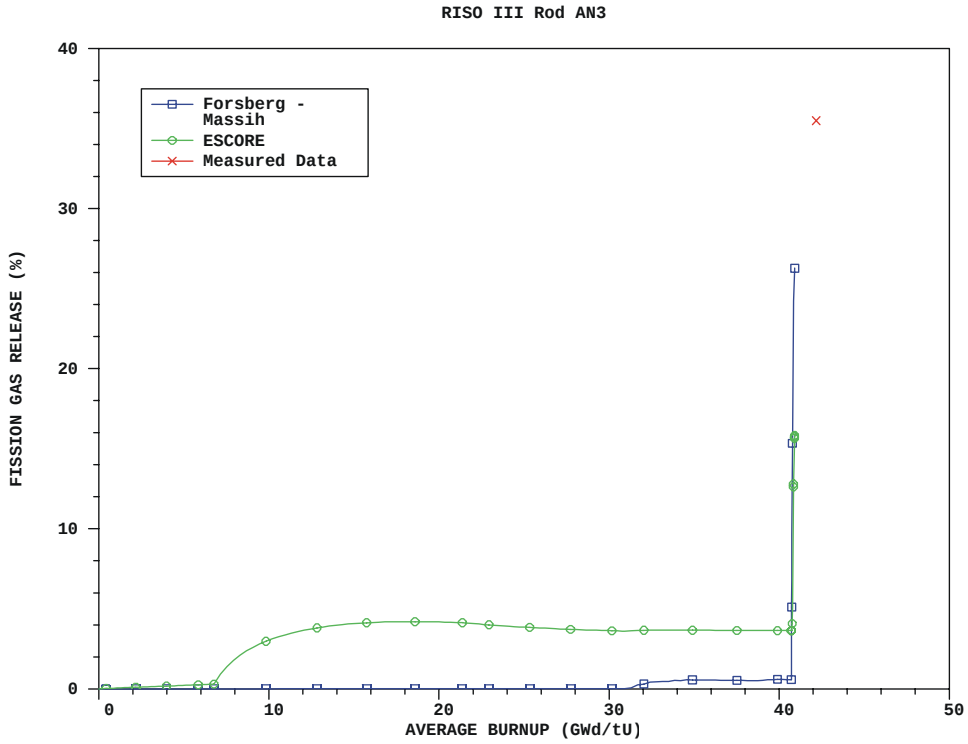

Figure 3-17
Fission Gas Release Model Comparison – RISO III Rod AN3

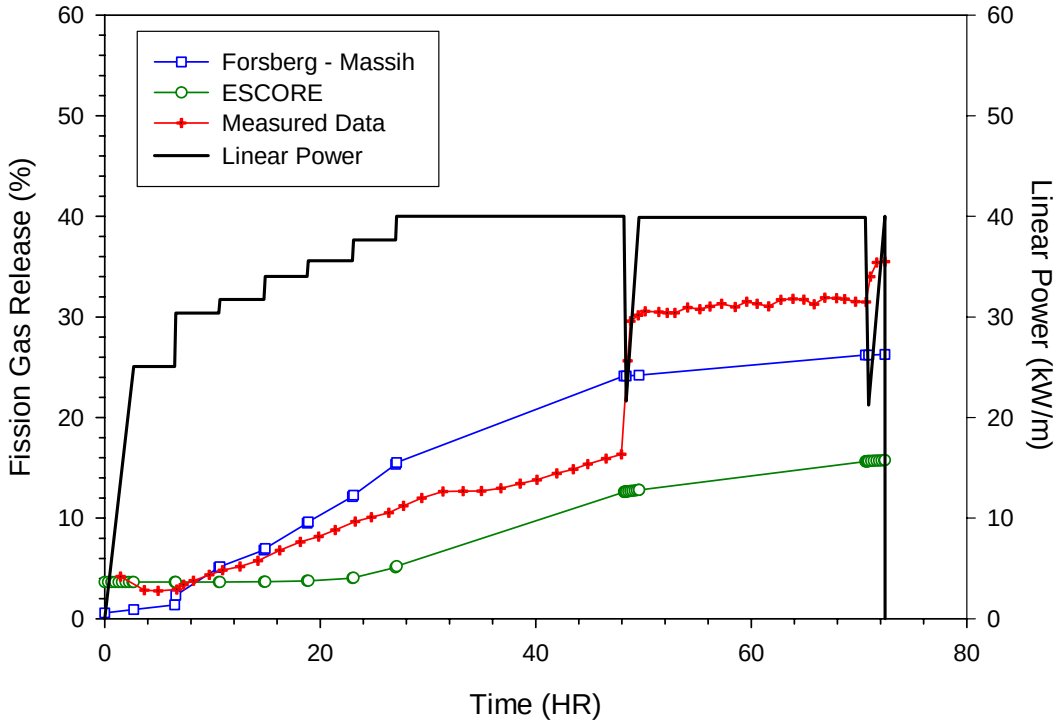

Figure 3-18
RISO III AN3 Bump Test Fission Gas Release and Power History

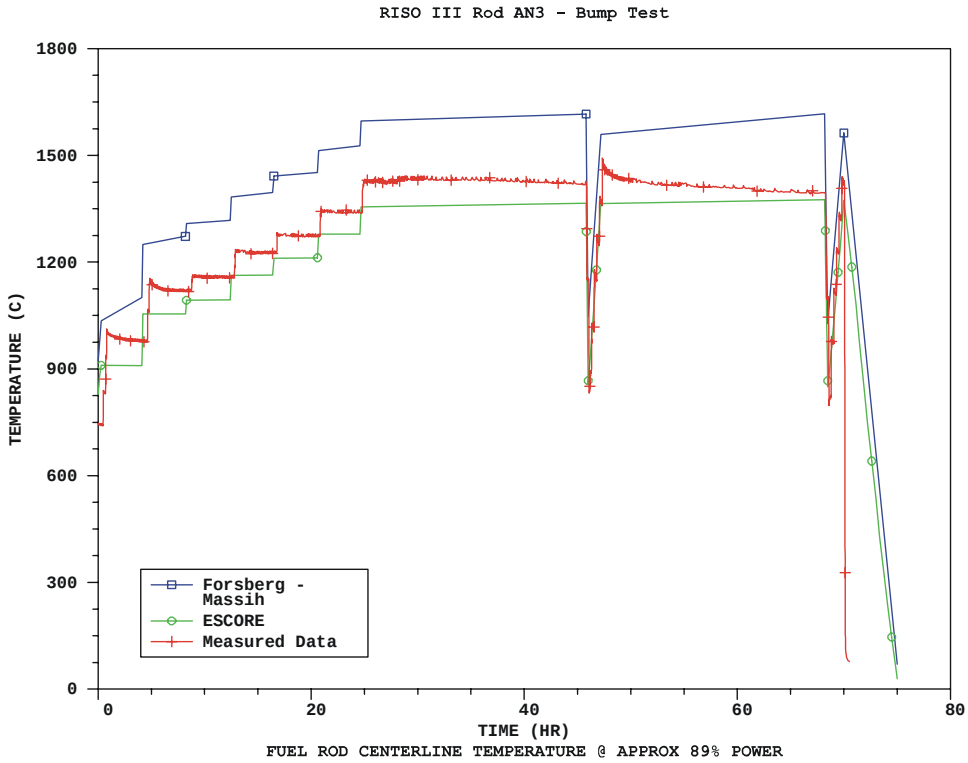

Figure 3-19
RISO III Rod AN3 – Bump Test Fuel Temperature

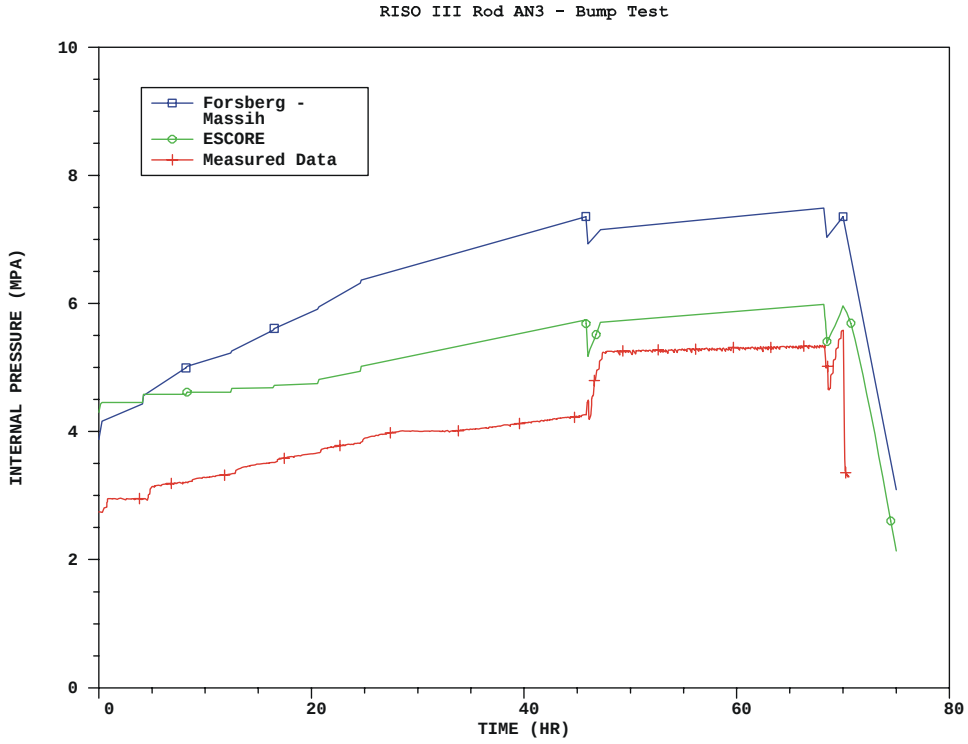

Figure 3-20
RISO III Rod AN3 – Bump Test Rod Internal Pressure

The next two figures (Figure 3-19 and 3-20) present the measured and calculated rod centerline temperature and rod internal pressure data. The fuel temperature track closely to the measured data. The higher temperatures predicted using the Forsberg – Massih FGR model coupled to the EPRI/CE transient FGR model are expected considering the higher release predicted over the first 50 hours of the bump test (see Figure 3-18). The ESCORE model predicts lower gas release throughout the majority of the test and the lower predicted temperatures reflect that. It should also be noted that the temperatures calculated by FALCON are at a somewhat higher power position within the rod than that designated for the thermocouple measurement due to limitations in the model used. The thermocouple measurements were taken inside a hollow pellet, while the temperatures reported for FALCON were taken from a solid pellet axial location with a similar, but slightly higher power (~ 0.92 versus 0.89 average power factor). Therefore, it is expected that the FALCON temperatures would be biased somewhat higher than those reported from the experiment. Differences between the responses of the two FGR models can be attributed to the two different fuel thermal conductivity models used; the NFIR model with the EPRI/CE FGR model, and MATPRO model with ESCORE FGR model. The internal pressure data shown in Figure 3-20 indicate that the calculated pressures over predict the measured fuel rod internal pressure. However, they tend to track the general shape and response of the pressure throughout the power history. Overall, although both models tend to under predict the release from bump tested rods, the approach using the Forsberg - Massih model coupled to the EPRI/CE transient FGR model appears to provide the better results. Further work is planned on revision of both the Forsberg - Massih and transient FGR models as implemented in FALCON to address these types of experiments.

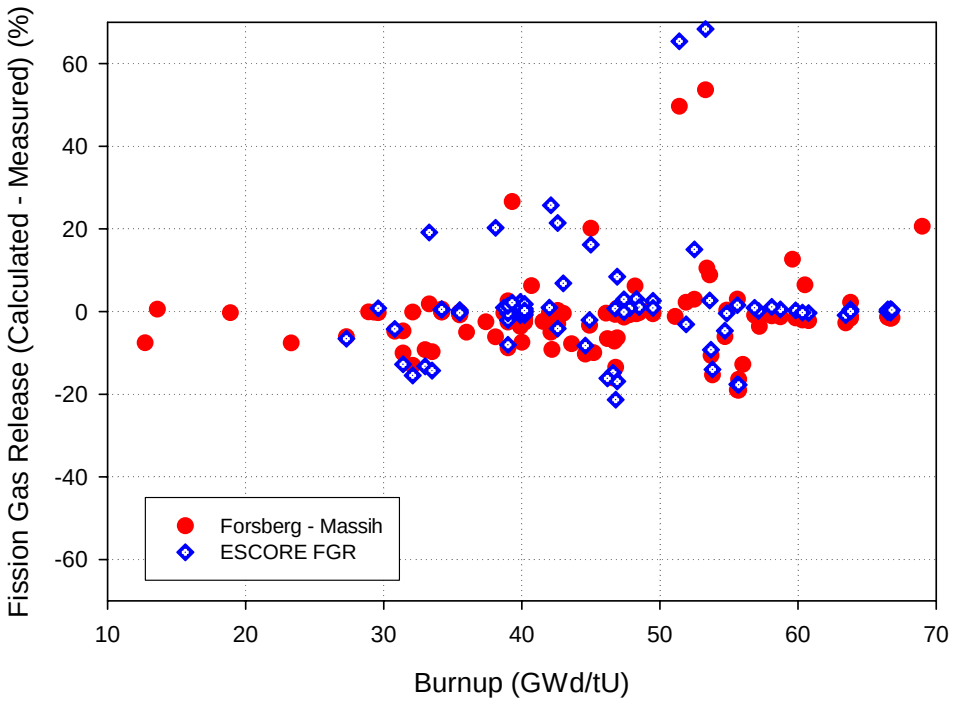

Figure 3-21
Fission Gas Release as a Function of Burnup

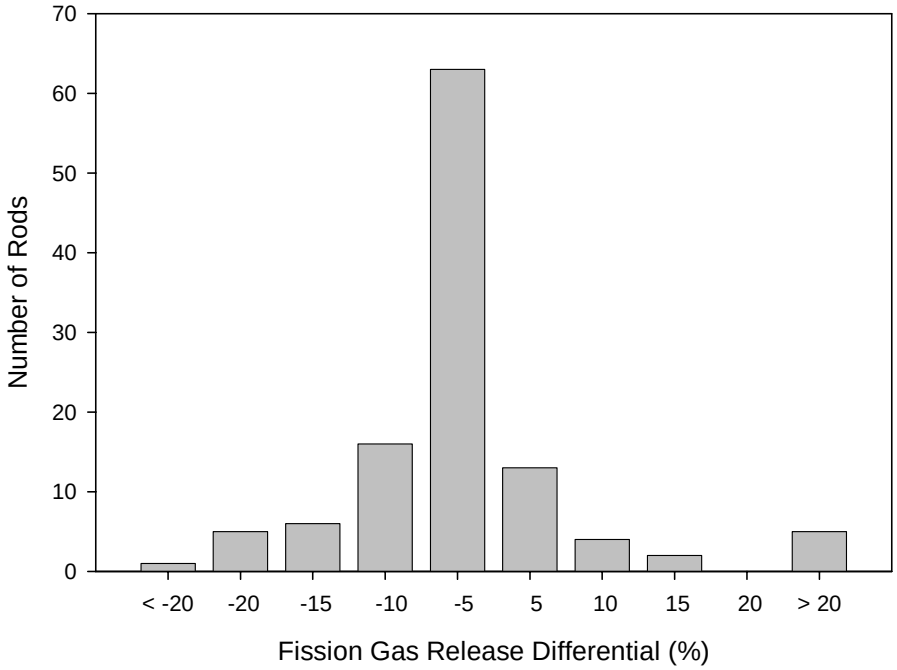

Figure 3-22
Differential Range Distribution for the Forsberg – Massih FGR Model

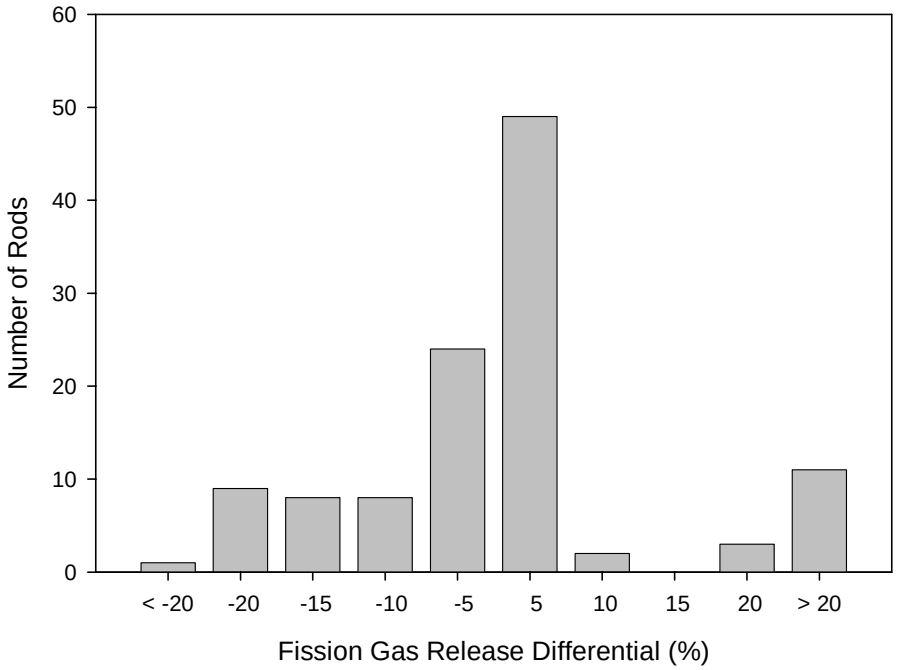

Figure 3-23
Differential Range Distribution for the ESCORE Fission Gas Release Model

Another trend noted in the results is that both models tended to fairly severely under predict the Limerick and KKL BWR rod data sets. These two data sets have relatively large measured FGR fractions, ~ 14.5% and ~ 9.3 on average, respectively. By comparison, the Grand Gulf and Dresden-2 BWR data sets average measured FGR fractions are ~ 2.8% and ~ 0.35%, respectively. Using either FGR model in FALCON results in reasonable predictions for the Grand Gulf and Dresden-2 BWR rods. Some discussion has taken place in the literature regarding these unusual FGR values, particularly for the Limerick rods. There has been speculation that perhaps the power histories do not accurately reflect the in-reactor conditions. No adequate explanation has yet been determined.

The above items notwithstanding, both the Forsberg – Massih and ESCORE FGR models in FALCON perform fairly well throughout the entire range of burnup, especially in the steady state regime that they were designed to address. And although reasonable results were obtained for several of the bump test cases (AN2, AN3, GE4, and GE7) using the combination of the Forsberg – Massih steady state and EPRI/CE transient FGR models, further testing and developed is planned in the area of transient FGR.

Overall, the distribution of the computed values from the Forsberg - Massih model, as shown in Figures 3-21 and 3-22, is good with a slight tendency toward under prediction. Almost 70% of the calculated values are within a band of +/- 5% of the measured FGR values. A gradual dispersal to a larger range can be seen at burnups beyond ~ 50 GWd/TU. However, the trend with burnup is fairly consistent and indications are that this model will perform reasonably well at high burnups. The overall average delta (calculated – measured) for the Forsberg – Massih FGR model is –1.3%. The ESCORE model tends to be more evenly distributed about the measured data with a slight tendency to over predict in the ~ 30-55 GWd/TU burnup range which reaches beyond the development basis burnup for this model. Approximately, 63% of the calculated values are within a band of +/- 5% of the measured FGR values as shown in Figure 3-23. The overall average delta for the ESCORE FGR model is 3.6%.

3.3 Cladding Creep

Table 3-5 lists the fuel rod cases chosen from the FALCON V&V database for cladding creep model V&V indicating average burnup as well as fuel design type. The primary focus of the verification tests was to evaluate the implementation of the Limbäck and Andersson model in FALCON. The additional 49 cases, primarily test program and commercial fuel rods, were run during the V&V exercise, bringing to 61 the total number fuel rod cases used in the overall creep testing program. Figures 3-24 through 3-27 provide examples of the performance of the model as compared to measured data for individual rods. A cumulative plot of the performance of the Limbäck and Andersson creep model is shown in Figure 3-28 and the axially averaged cladding strain differential distribution is shown in Figure 3-29.

Figures 3-24 through 3-27 indicate fairly good agreement between the creep strain calculated with the Limbäck and Andersson model as compared to measured data for the individual rods shown. Evaluation of the cumulative plot in Figure 3-28, however, indicates a trend beginning at ~ 35 GWd/TU burnup, to over predict cladding strain. This trend is also noted in the cladding strain differential plot in Figure 3-29. During code development and testing, it was noted that the interaction between the fuel and cladding after gap closure was contributing to the over

prediction of cladding strain. Modifications made to the fuel swelling model improved this performance. Additional planned modifications include a fuel relocation recovery model that will further increase the accuracy of FALCON cladding strain calculations. It should be noted that although this trend to over predict strain is present in some cases, the overall performance of the cladding strain calculations in FALCON are good with an axially averaged mean differential of only 0.0019 m/m for the inventory of V&V cases run.

Table 3-5
Cladding Creep Verification and Validation Cases

Verification Cases			
Case	**Average Burnup (GWd/TU)**	**Number of Rods**	**Description Rod Type**
Calvert Cliffs Extended Burnup	59.2	2	PWR
Grand Gulf	36.7	2	BWR
Grohnde	44.9	2	PWR
HB Robinson	62.2	2	PWR
KKL	45.2	2	BWR
Limerick	55.9	2	BWR
Validation Cases			
Calvert Cliffs Extended Burnup	57.7	10	PWR
Calvert Cliffs-1	30.5	2	PWR
Dresden-2	30.1	4	BWR
Grand Gulf	39.9	17	BWR
Grohnde	45	4	PWR
HB Robinson	63.9	9	PWR
KKL	27.3	1	BWR
Limerick	55.7	2	BWR

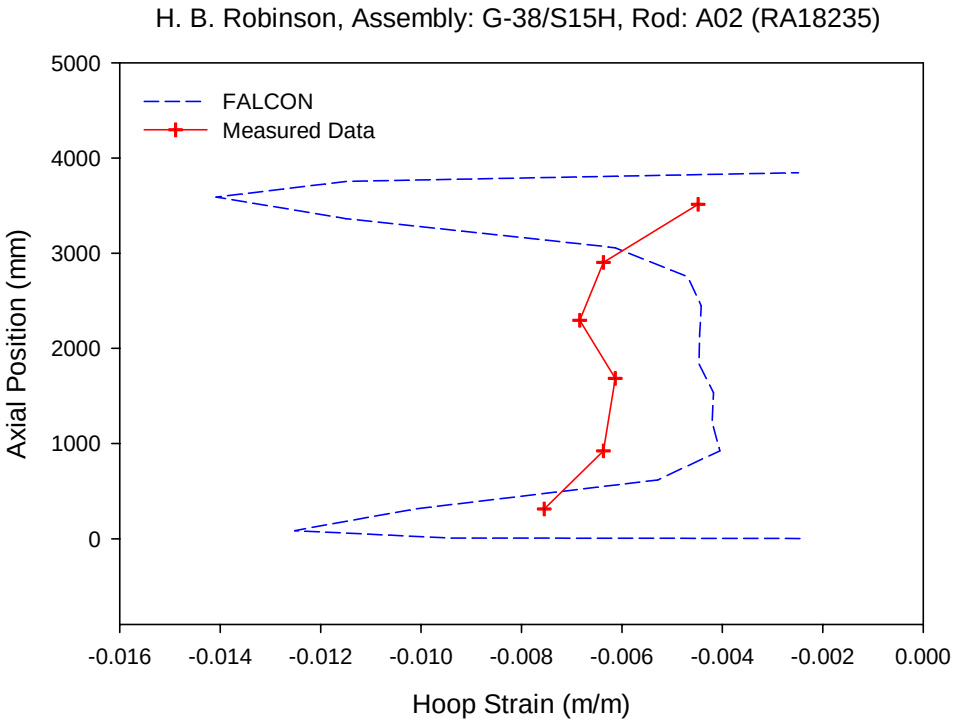

Figure 3-24
Calculated Cladding Creep Versus Measured Data for HB Robinson Rod A02

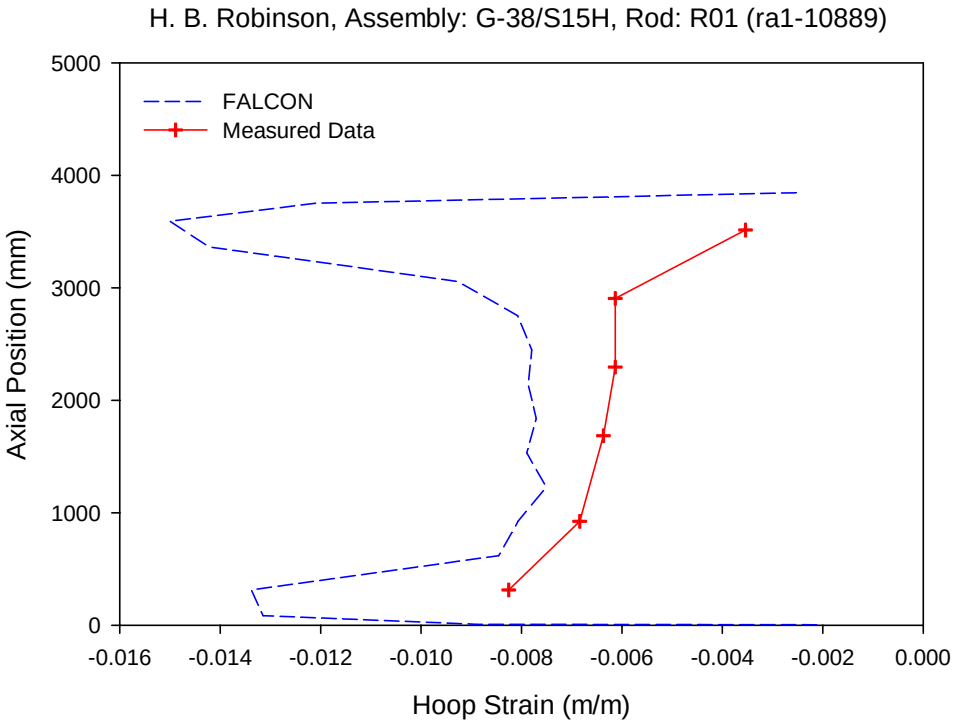

Figure 3-25
Calculated Cladding Creep Versus Measured Data for HB Robinson Rod R01

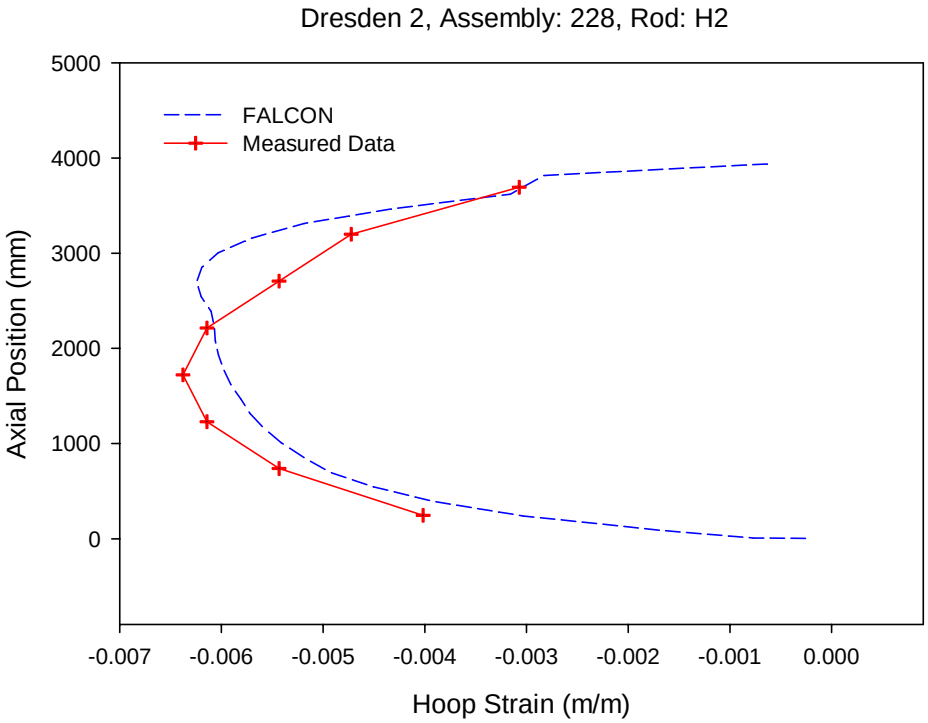

Figure 3-26
Calculated Cladding Creep Versus Measured Data for Dresden-2 Rod H2

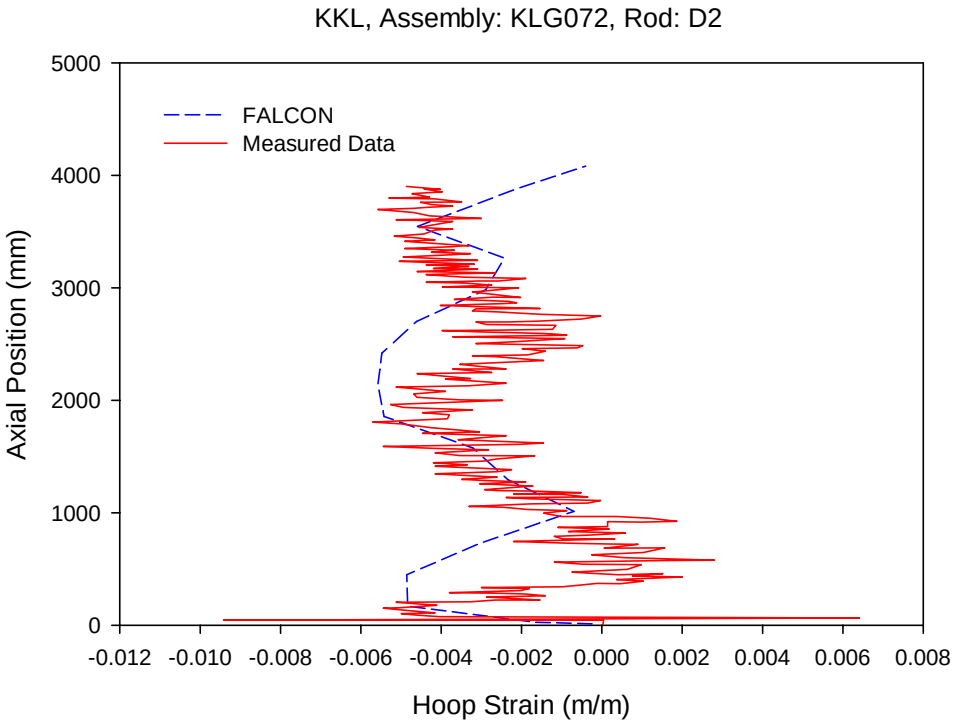

Figure 3-27
Calculated Cladding Creep Versus Measured Data for KKL Rod D2

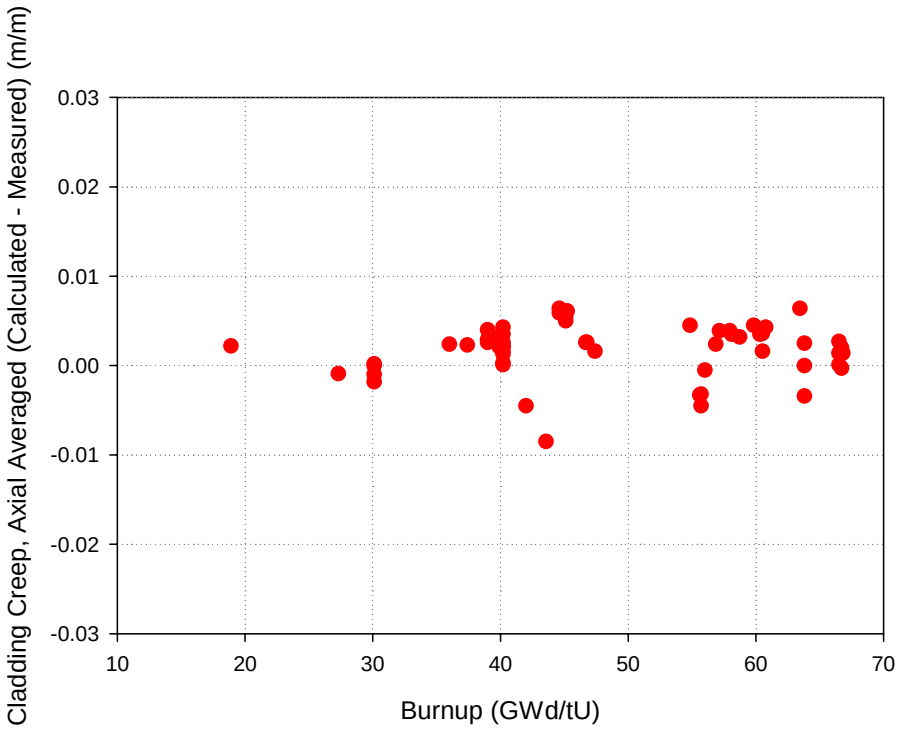

Figure 3-28
Cladding Creep as a Function of Burnup

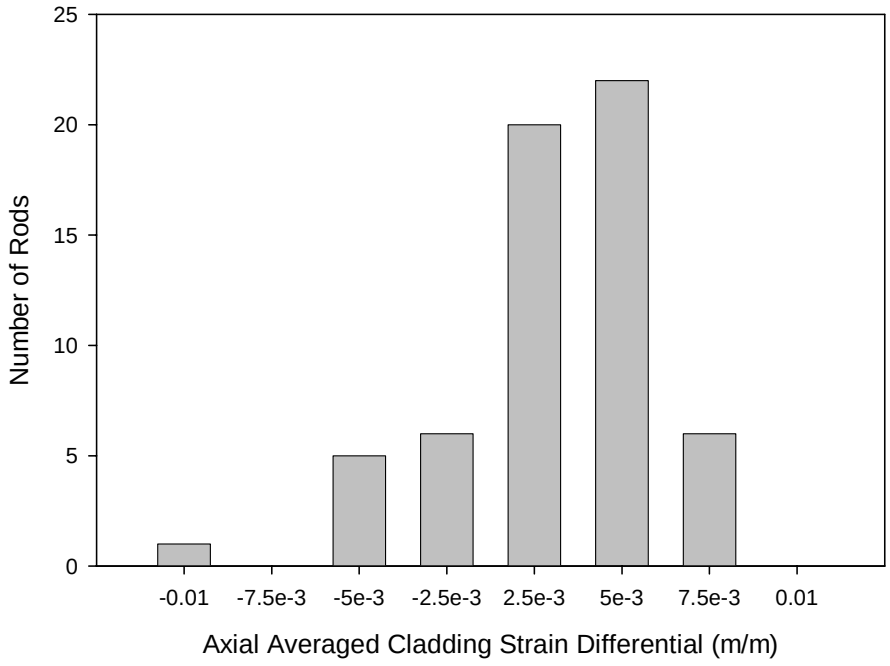

Figure 3-29
Cladding Strain Differential Range Distribution

3.4 Cladding Irradiation Growth

A listing of the fuel rod cases chosen from the FALCON V&V database for evaluation of cladding irradiation growth is shown in Table 3-6. Along with the 14 verification cases, an additional 58 cases, primarily test program and commercial fuel rods, were run during the V&V program, bringing to 72 the total number fuel rod cases used. Irradiation growth was evaluated using the MATPRO axial growth model in both the default (Limbäck and Andersson creep model) and ESCORE-emulation (ESCORE creep model) modes. A summary of the results is provided in Table 3-7. Figures 3-30 through 3-33 provide examples of the performance of the model as compared to measured data for individual rods. A cumulative plot of axial growth performance is shown in Figure 3-34. Irradiation growth differential distribution plots are shown in Figures 3-35 and 3-36 for the both the default and ESCORE-emulation modes, respectively.

Figures 3-30 through 3-33 indicate reasonably good agreement between the irradiation growth calculated and as compared to the measured axial elongation data for the individual rods shown depending upon the calculational mode chosen. In these particular cases, in the default mode the calculated elongation values tend to be larger than the measured data for PWR rods, whereas in the ESCORE emulation mode, the calculated values match very well. Conversely, the trend is reversed for the two BWR rods shown in which the default mode calculated and measured elongation values match very well, while the values calculated in the ESCORE emulation mode under predict axial elongation. Evaluation of the cumulative plot in Figure 3-34, however, indicates that this trend is due to a general over prediction of elongation in the default calculational mode above burnups of ~ 45 GWd/TU. This bias at higher burnups is also noted in the default mode differential distribution presented in Figure 3-35. Early evaluations point to an unintended interaction between radial creep using the Limbäck and Andersson model and axial growth. This is an area that will be a focus of further code development activities. Overall, the mean differential for the default mode calculations, skewed by the high burnup results, is ~ 9.8 mm, whereas for the ESCORE emulation mode calculations it is 1.5 mm.

Table 3-6
Cladding Irradiation Growth Verification and Validation Cases

Verification Cases			
Case	**Average Burnup (GWd/TU)**	**Number of Rods**	**Description Rod Type**
Calvert Cliffs Extended Burnup	59.2	2	PWR
Grand Gulf	36.7	2	BWR
Grohnde	44.9	2	PWR
HB Robinson	62.2	2	PWR
KKL	45.2	2	BWR
Limerick	55.9	2	BWR
Over Ramp	21.0	2	PWR
Validation Cases			
Calvert Cliffs Extended Burnup	57.7	10	PWR
Calvert Cliffs-1	18.9	1	PWR
Dresden-2	30.1	10	BWR
Grand Gulf	39.9	17	BWR
HBEP ABB	46.5	5	BWR
HB Robinson	63.9	9	PWR
KKL	27.3	1	BWR
Limerick	54.7	5	BWR

Table 3-7
Cladding Irradiation Growth Verification and Validation Results

Verification						
Case	**Rod**	**Measured Growth (mm)**	**Default Mode (mm)**	**Default Mode Δ (mm)**	**ESCORE Mode (mm)**	**ESCORE Mode Δ (mm)**
Calvert Cliffs Extended Burnup	BFG092	39.06	54.23	15.17	38.46	-0.6
	BFM043	35.15	58.68	23.53	43.13	7.98
Grand Gulf	A02	31.52	31.59	0.07	45.52	14
	A06	30.84	29.77	-1.07	31.16	0.32
Grohnde	A09	40.44	42.75	2.31	37.93	-2.51
	T09	35.17	45.01	9.84	38.43	3.26
HB Robinson	A10	49.66	53.58	3.92	36.73	-12.93
	R01	51.15	66.84	15.69	45.87	-5.28
KKL	F5	10.6	44.05	33.45	36.63	26.03
	F6	11	35.23	24.23	26.51	15.51
Limerick	J4	19.63	49.78	30.15	37	17.37
	J6	19.84	50.59	30.75	36.76	16.92
Over Ramp	W54R	2.75	4.87	2.12	5.97	3.22
	W55R	3.36	5.05	1.69	6.63	3.27
Validation						
Calvert Cliffs Extended Burnup	BEN013	29.62	54.84	25.22	38.91	9.29
	BFJ027	39.85	54.07	14.22	38.66	-1.19
	BFL009	33.65	51.21	17.56	39.15	5.5
	UFE067	28.35	43.2	14.85	32.07	3.72
	UFE019	28.35	42.63	14.28	31.1	2.75
	BFM034	34.37	59.68	25.31	44.16	9.79
	BFM070	35.58	59.22	23.64	42.52	6.94
	BFM071	32.79	56.89	24.1	41.08	8.29
	BFM073	35.97	58.47	22.5	42.08	6.11
	BFM156	31.83	54.3	22.47	39.52	7.69
Calvert Cliffs-1	AHS008	12.19	25.12	12.93	16.32	4.13

Table 3-7 (continued)
Cladding Irradiation Growth Verification and Validation Results

Verification (continued)						
Case	**Rod**	**Measured Growth (mm)**	**Default Mode (mm)**	**Default Mode Δ (mm)**	**ESCORE Mode (mm)**	**ESCORE Mode Δ (mm)**
Dresden-2	B2	23.34	26.35	3.01	23.08	-0.26
	C3	20.14	18.55	-1.59	16.33	-3.81
	D9	17.5	19.91	2.41	17.19	-0.31
	H2	18.39	19.14	0.75	16.66	-1.73
	K9	15.72	19.77	4.05	16.71	0.99
	220A1	23.34	26.02	2.68	18.89	-4.45
	B9	24.79	20.57	-4.22	17.3	-7.49
	F9	21.16	21.01	-0.15	17.37	-3.79
	H8	23.34	22.37	-0.97	17.32	-6.02
	228A1	21.16	19.87	-1.29	16.75	-4.41
Grand Gulf	901 A05	31.27	30.84	-0.43	36.08	4.81
	901 B01	30.78	32.22	1.44	27.42	-3.36
	901 D02	33.4	31.36	-2.04	21.36	-12.04
	901 E09	31.39	30.18	-1.21	24.53	-6.86
	901 F08	34.49	27.23	-7.26	22.33	-12.16
	901 K05	31.8	29.15	-2.65	23.49	-8.31
	901 B04	35.64	26.75	-8.89	22.67	-12.97
	901 D01	30.15	31	0.85	27.39	-2.76
	901 D09	31.32	30.3	-1.02	26.61	-4.71
	901 E01	32.16	29.93	-2.23	45.06	12.9
	901 F01	31.9	29.53	-2.37	29.51	-2.39
	901 F09	32.18	28.85	-3.33	28.07	-4.11
	901 H06	34.98	27.27	-7.71	21.31	-13.67
	901 H09	32.38	31.09	-1.29	25.11	-7.27
	901 K04	33.25	30.04	-3.21	24.39	-8.86
	901 K06	31.24	29.79	-1.45	24.31	-6.93
	901 K08	31.57	31.28	-0.29	27	-4.57

Table 3-7 (continued)
Cladding Irradiation Growth Verification and Validation Results

Verification (continued)						
Case	**Rod**	**Measured Growth (mm)**	**Default Mode (mm)**	**Default Mode Δ (mm)**	**ESCORE Mode (mm)**	**ESCORE Mode Δ (mm)**
HBEP ABB	A184	13.12	29.13	16.01	21.52	8.4
	A186	17.29	26.91	9.62	20.03	2.74
	A364	14.24	31.4	17.16	23.01	8.77
	H836	11.42	33.29	21.87	24.89	13.47
	H836	29.5	32.34	2.84	24.41	-5.09
HB Robinson	A02	47.98	66.9	18.92	49.11	1.13
	B05	46.76	66.76	20	48.94	2.18
	E02	42.52	67.53	25.01	43.82	1.3
	H05	36.96	54.87	17.91	38.69	1.73
	R05	49.53	68.06	18.53	49.22	-0.31
	B01	46.58	66.83	20.25	48.77	2.19
	F07	45.34	66.28	20.94	43.71	-1.63
	G10	46.28	66.35	20.07	43.63	-2.65
	S02	48.01	68.28	20.27	48.84	0.83
KKL	D02	9.7	33.42	23.72	44.86	35.16
Limerick	E9	18.16	49.55	31.39	37.35	19.19
	F9	18.42	51.25	32.83	37.23	18.81
	G1	46.74	48.08	1.34	37.33	-9.41
	J3	45.85	47.72	1.87	44.08	-1.77
	J7	46.15	48.85	2.7	37.04	-9.11

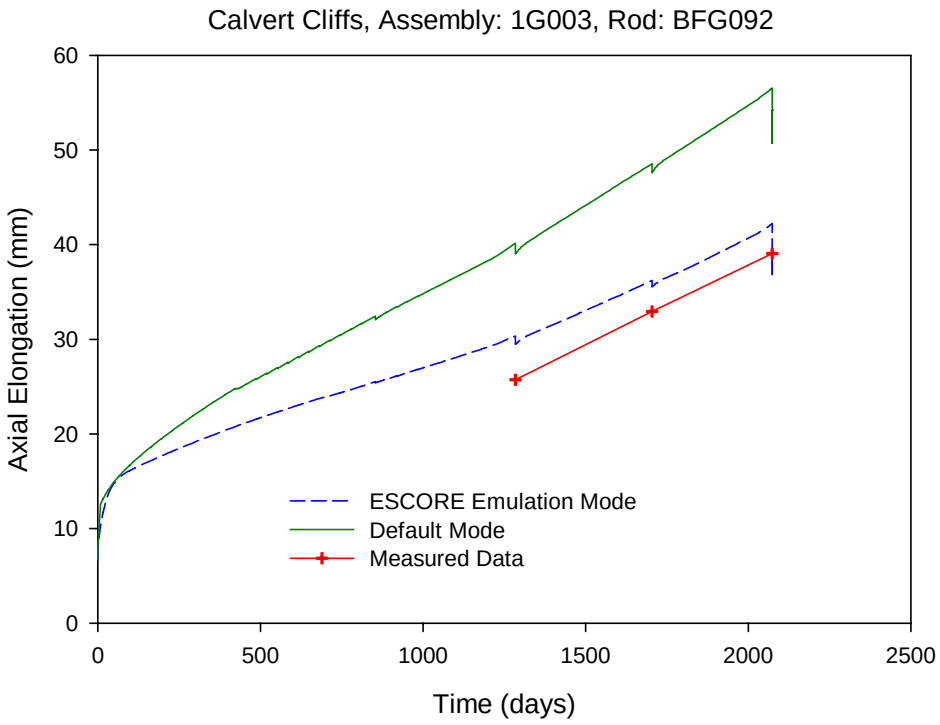

Figure 3-30
Calculated Irradiation Growth Versus Measured Data for Calvert Cliffs Rod BFG092

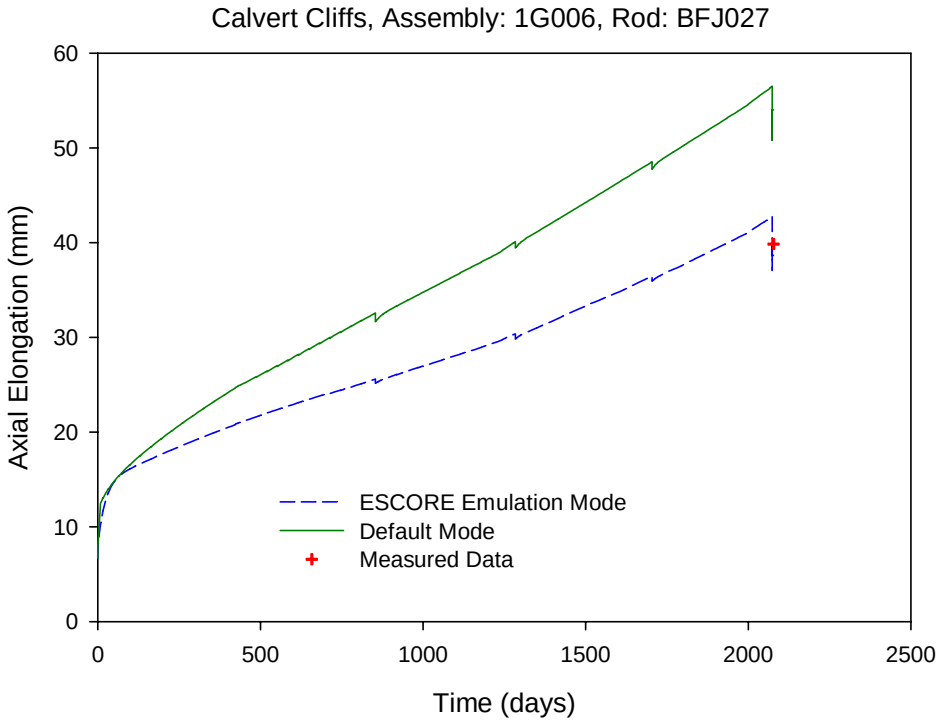

Figure 3-31
Calculated Irradiation Growth Versus Measured Data for Calvert Cliffs Rod BFJ097

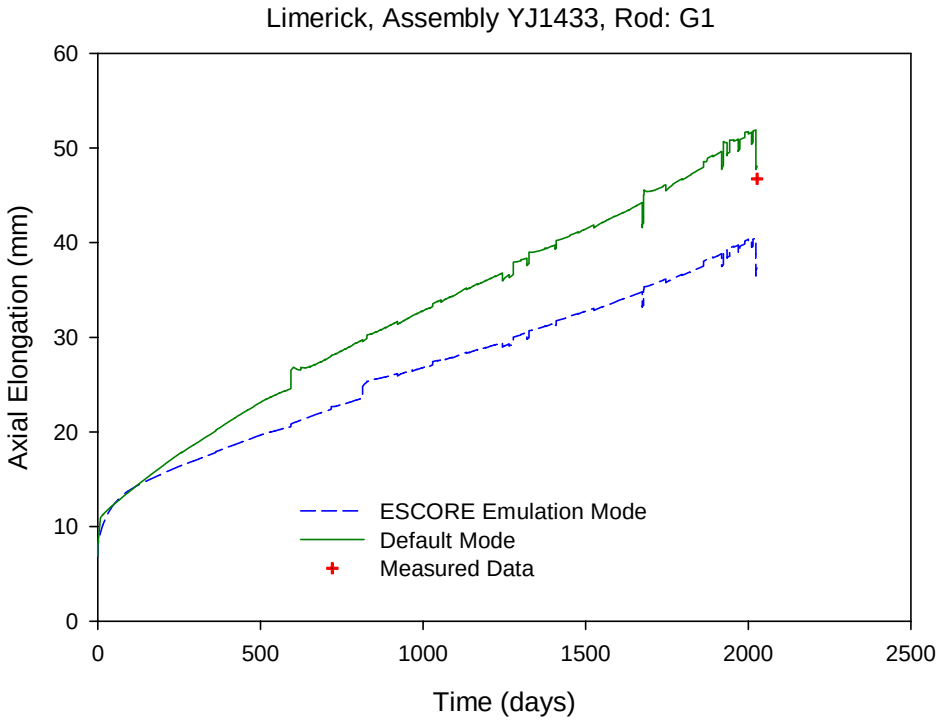

Figure 3-32
Calculated Irradiation Growth Versus Measured Data for Limerick Rod G1

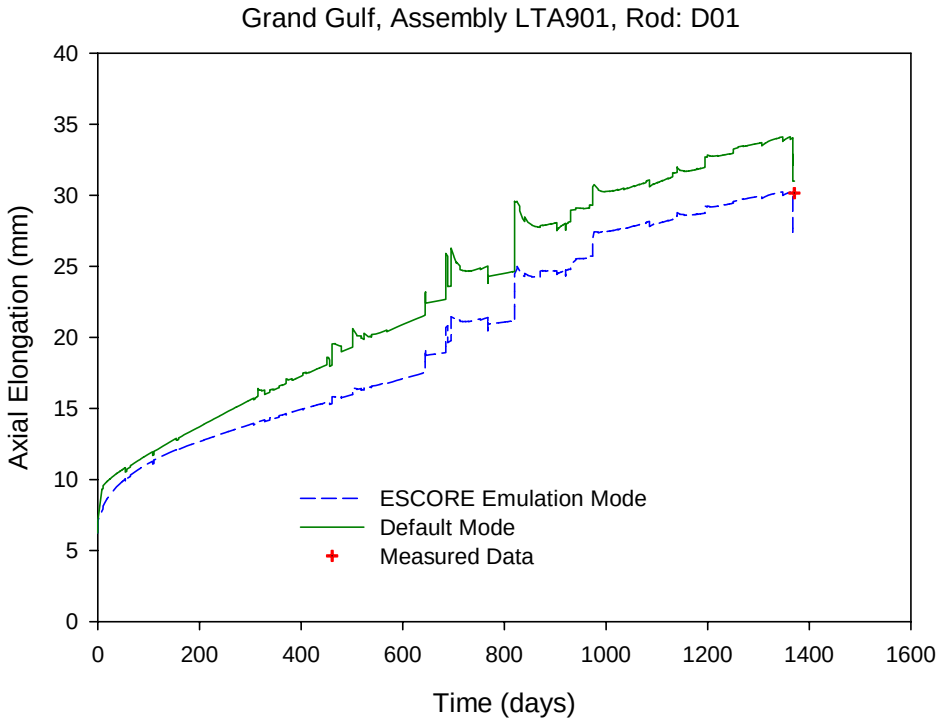

Figure 3-33
Calculated Irradiation Growth Versus Measured Data for Grand Gulf Rod D01

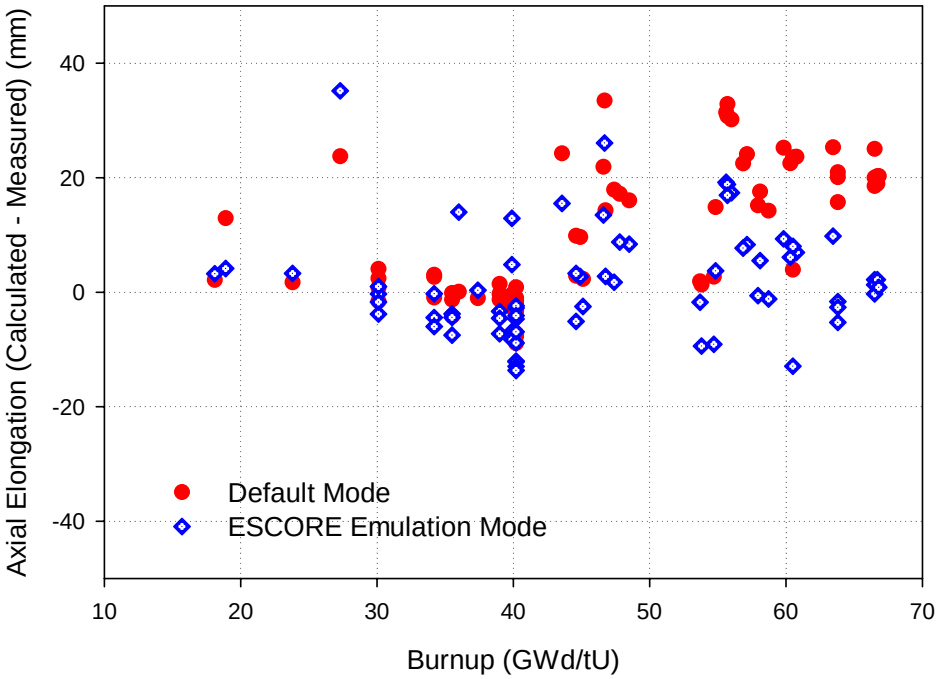

Figure 3-34
Irradiation Growth as a Function of Burnup

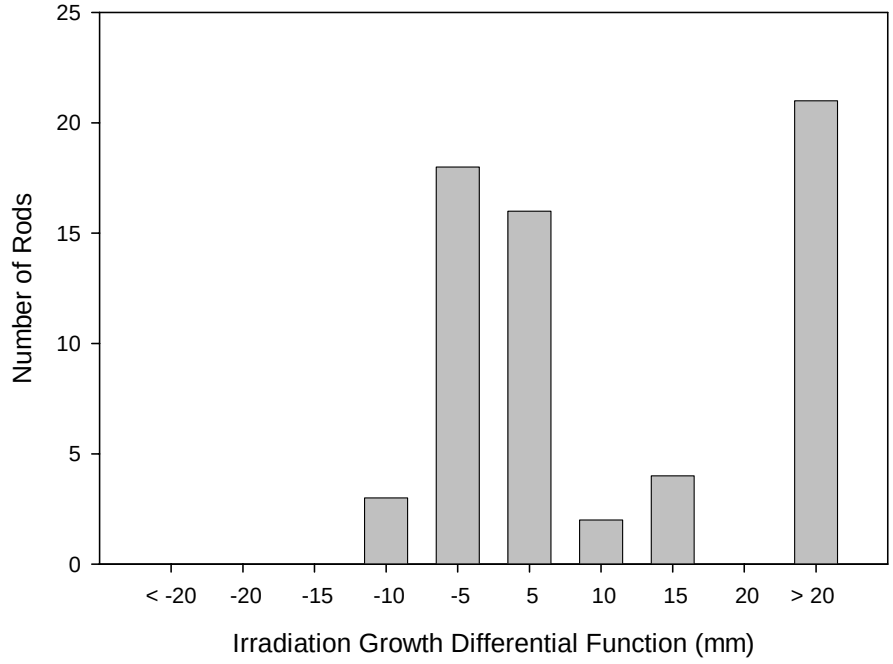

Figure 3-35
Irradiation Growth Default Mode Differential Range Distribution

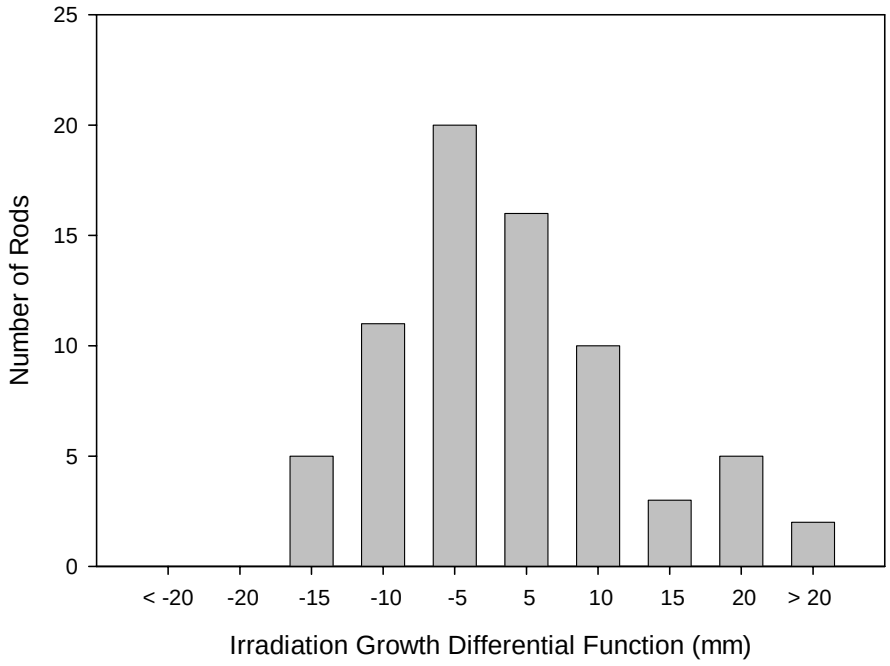

Figure 3-36
Irradiation Growth ESCORE Emulation Mode Differential Range Distribution

3.5 Cladding Corrosion

Table 3-8 lists the fuel rod cases chosen from the FALCON V&V database for cladding corrosion model evaluation. Two different models are used for cladding corrosion under normal operating conditions in FALCON, the EPRI/SLI PFCC model for PWRs and the MATPRO CORROS oxidation model for BWRs. Because these models are well established, having been tested and implemented in several previous versions of FALCON, specific verification of the EPRI/SLI PFCC and the MATPRO CORROS oxidation models was not performed. A total of 49 fuel rod cases, primarily test program and commercial fuel rods, were used for the V&V assessment. Figures 3-37 through 3-41 provide examples of the performance of the model as compared to measured data for individual rods. Cumulative plots of the performance of the corrosion models are shown in Figures 3-42 and 3-43 for the axially averaged and peak oxide thickness, respectively. The axially averaged differential distribution is shown in Figure 3-44.

Figures 3-37 through 3-41 indicate that the two corrosion models (the EPRI/SLI PFCC model for PWRs and the MATPRO CORROS model for BWRs) perform reasonably well. However, in Figure 3-39, although the general trend of the data is represented well, the peak oxide thickness value in the upper portion of the rod is under predicted. Evaluation of this case, revealed a general trend for under prediction of peak oxide thickness in the Grohnde rods. The average peak differential (calculated – measured) is ~ - 12.5 μm. This effect is likely attributable to the highly abbreviated coolant lithium concentration history available for these rods. Reference data available for the Grohnde rods only indicated cycle beginning and ending coolant lithium concentration values. Previous analyses completed during the V&V program have indicated that the EPRI/SLI PFCC model is highly sensitive to coolant lithium concentration. Therefore, it is

likely that the linear interpolation of the coolant lithium concentration values (beginning to end-of-cycle) under estimates the actual lithium concentration and thereby reduces the predicted oxide thicknesses for these rods.

Figure 3-41, shows a large discrepancy in the measured and calculated oxide thickness values on the lower portion of KKL rod D02. The reported oxidation values for the KKL rods are based on eddy current (EC) liftoff data that is not corrected for crud and therefore, the larger reported EC-liftoff values in this region can be attributed to the characteristic crud deposition typically seen at the lower end of the BWR rods. Peaks are also seen at regular intervals in the EC-liftoff trace. These peaks are due to enhanced corrosion at the spacer grid locations. These features can also be seen in the data for the Limerick rods.

Examining Figure 3-42, a comparison between the measured and calculated axially averaged oxide thickness, the data indicate a relatively uniform distribution of oxide thickness differential in a range of ~ –5 to +20 μm throughout the burnup range. The plot also indicates a slight overall trend toward over prediction and wider distribution at higher burnups. A comparison between the measured and calculated peak oxide thickness in Figure 3-43, indicates a relatively larger distribution of oxide thickness differential, roughly in a range of ~ –20 to +35 μm, with a slight overall trend toward over prediction and wider distribution at higher burnups. The over predictions in the peak oxide thickness occur in PWR rods, primarily older Calvert Cliffs rods. The peak oxide thickness for the two higher burnup BWR rods (Limerick and KKL) appear to be under predicted. However, as discussed above, the apparent higher oxide values for BWR rods are due to crud deposition in the lower spans and enhanced corrosion at the spacer grid locations. The more appropriate comparisons for BWR rods are the axially averaged values shown in Figure 3-42 where the effects of localized crud and enhanced oxidation at the spacer grids is diminished. The average differential in the calculated peak oxide thickness for PWR rods using the EPRI/SLI PFCC model is ~ 5.6 μm. Comparing the BWR data, the MATPRO CORROS model has an average differential of ~ 4.8 μm for the peak oxide thickness.

Table 3-8
Cladding Corrosion Validation Cases

Case	Average Burnup (GWd/TU)	Number of Rods	Description Rod Type
Calvert Cliffs Extended Burnup	57.7	10	PWR
Calvert Cliffs-1	30.5	2	PWR
Dresden-2	30.1	4	BWR
Grand Gulf	39.9	17	BWR
Grohnde	45	4	PWR
HB Robinson	63.9	9	PWR
KKL	27.3	1	BWR
Limerick	55.7	2	BWR

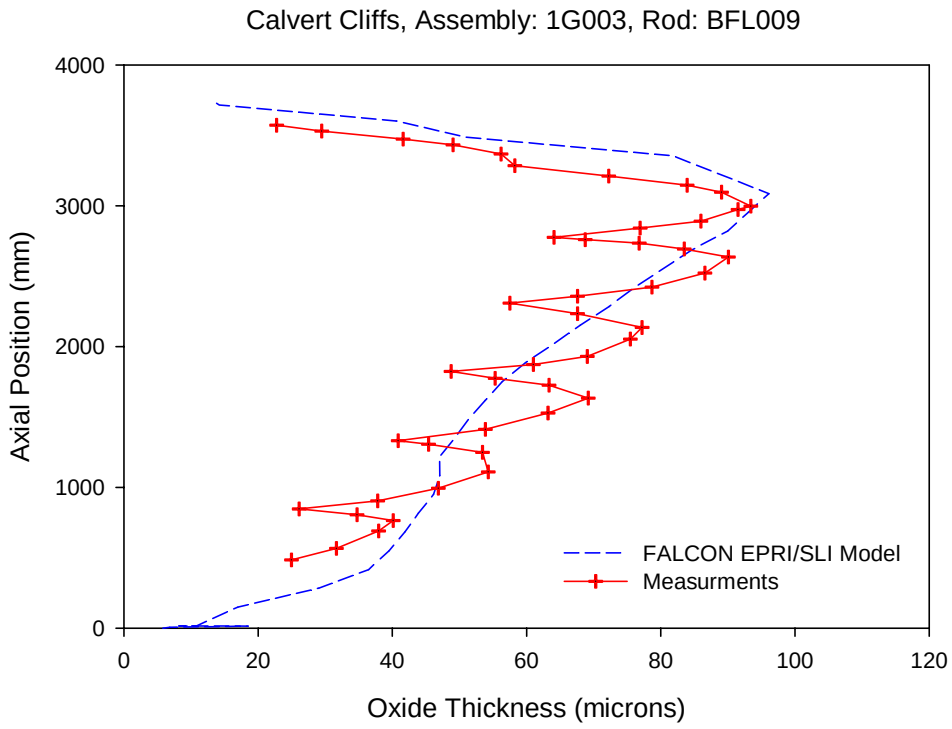

Figure 3-37
Cladding Oxide Thickness Versus Measured Data for Calvert Cliffs Rod UFE019

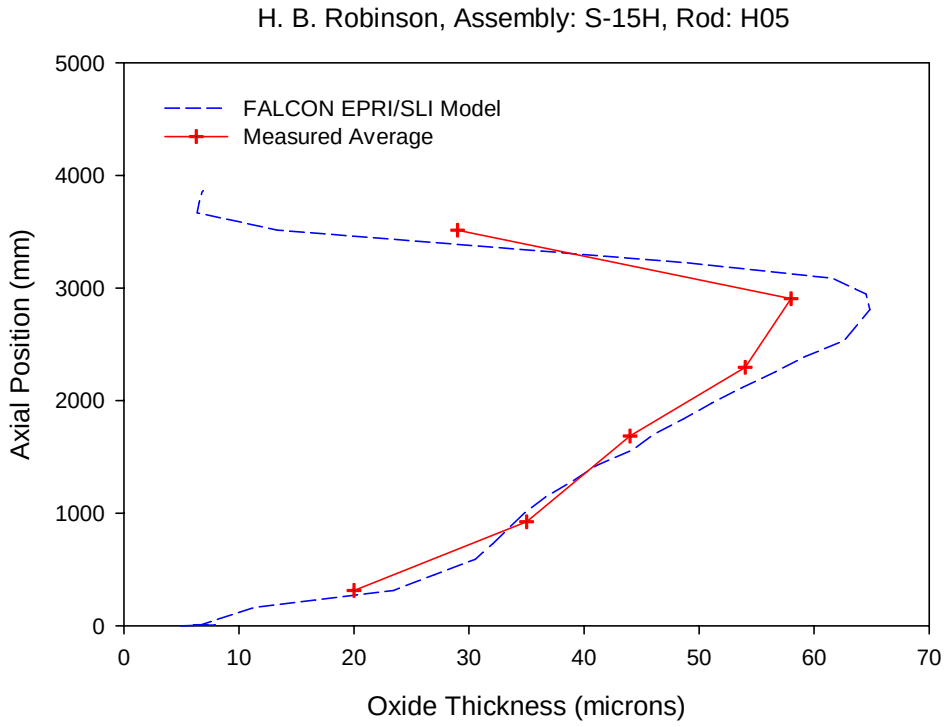

Figure 3-38
Cladding Oxide Thickness Versus Measured Data for H. B. Robinson Rod H05

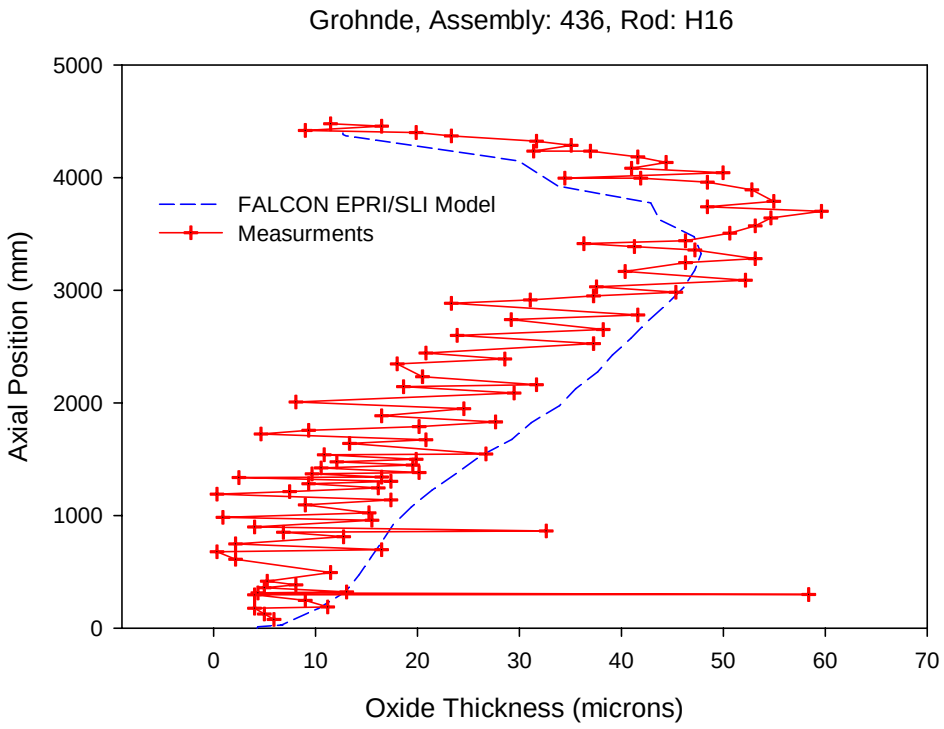

Figure 3-39
Cladding Oxide Thickness Versus Measured Data for Grohnde Rod H16

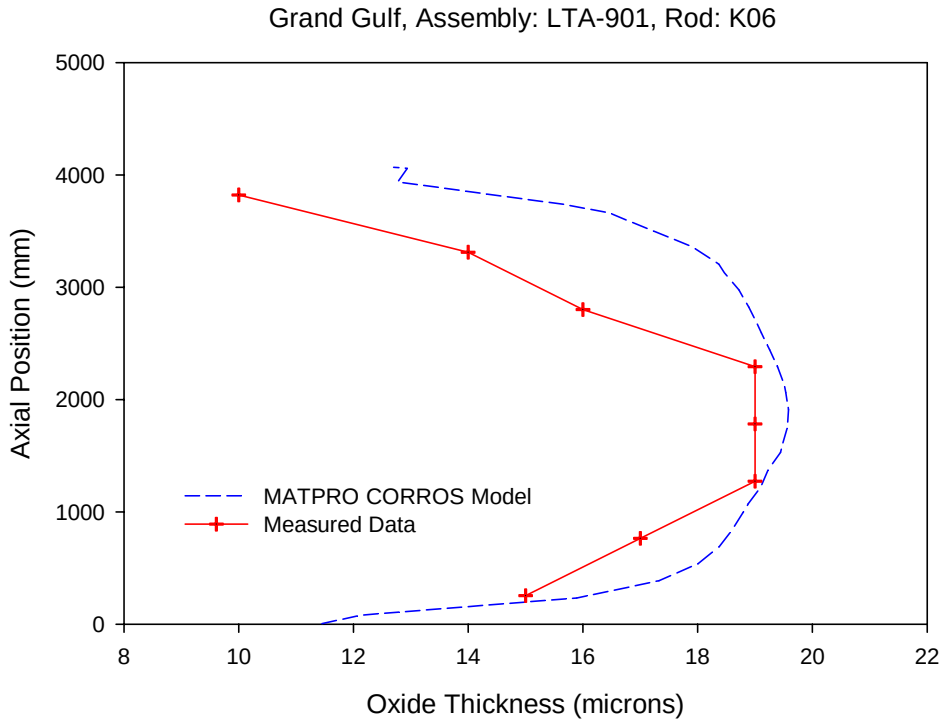

Figure 3-40
Cladding Oxide Thickness Versus Measured Data for Grand Gulf Rod K06

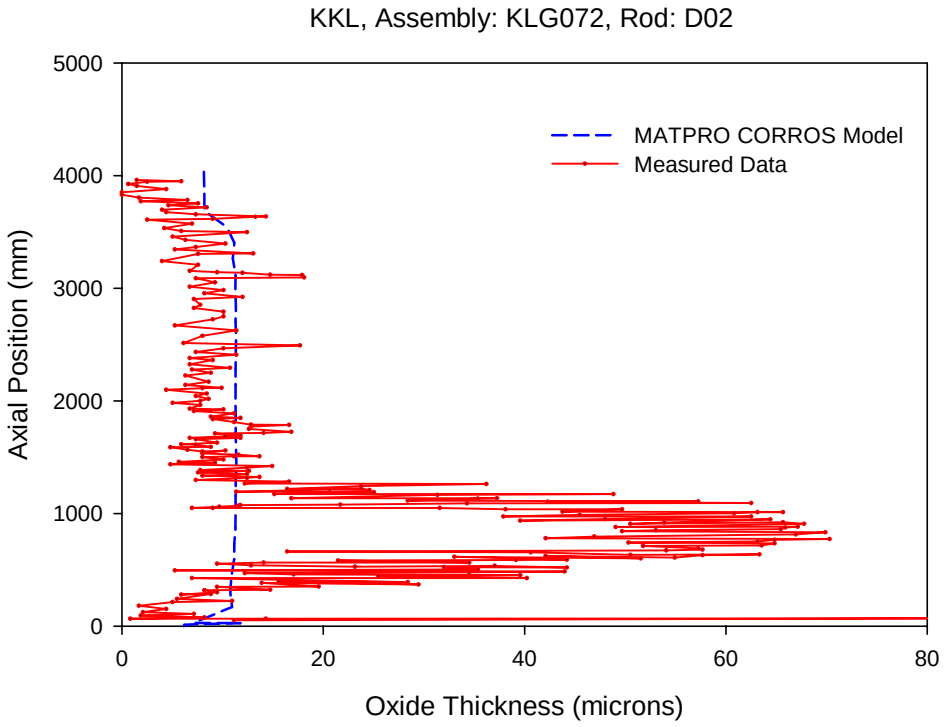

Figure 3-41
Cladding Oxide Thickness Versus Measured Data for KKL Rod D02

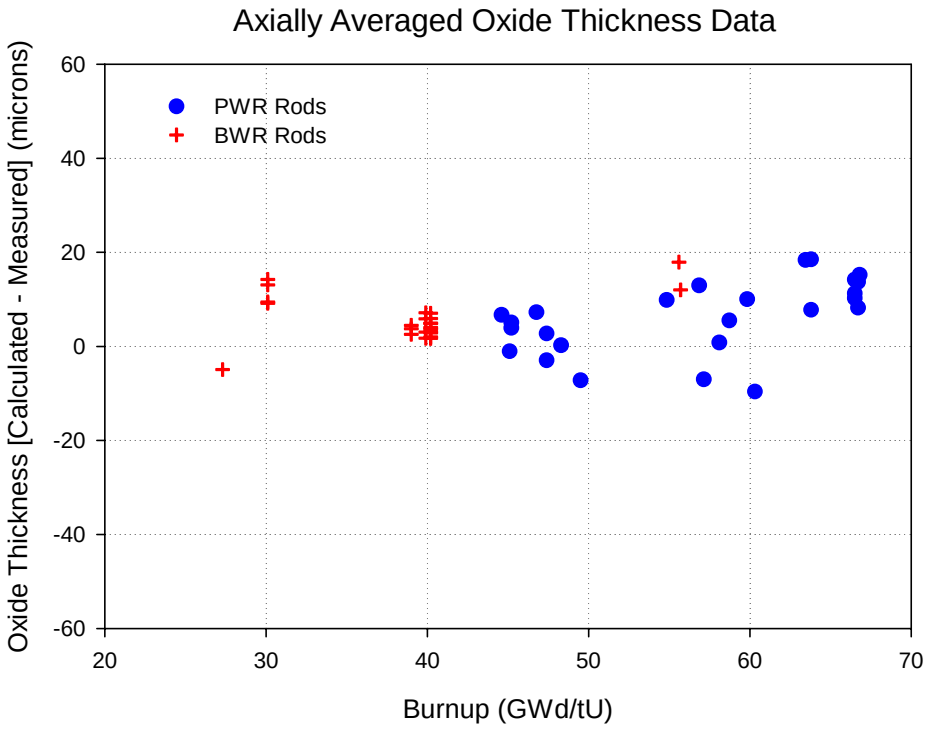

Figure 3-42
Axial Averaged Oxide Thickness as a Function of Burnup

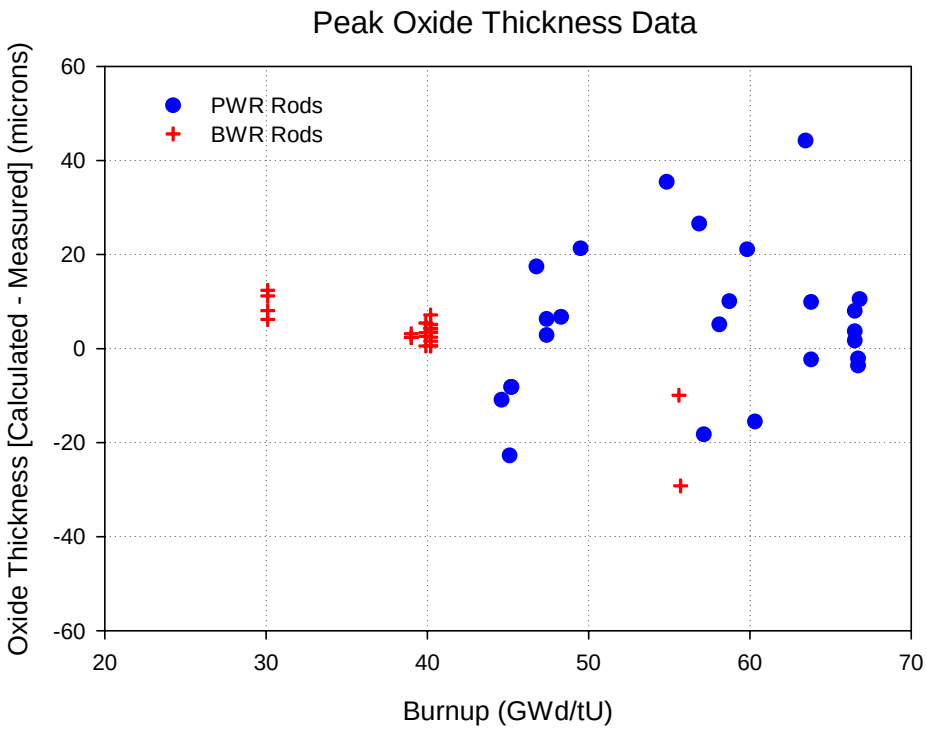

Figure 3-43
Peak Oxide Thickness as a Function of Burnup

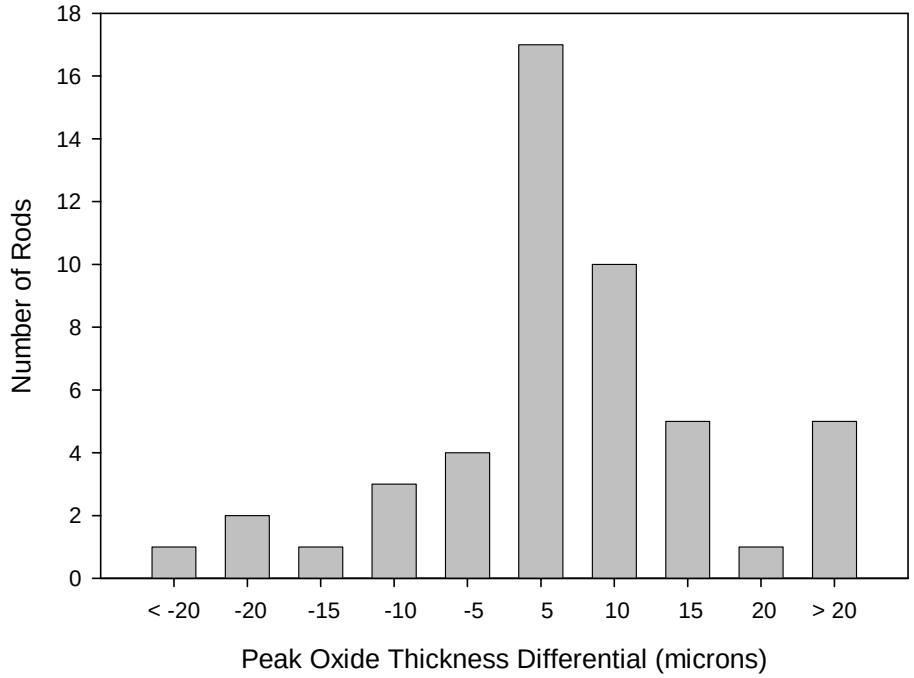

Figure 3-44
Peak Oxide Thickness Differential Range Distribution

3.6 Fuel Rod Internal Void Volume

The calculation of fuel rod internal void volume is an indicator of the integral performance of the material property and behavioral models used in FALCON. And although not a primary modeling parameter in and of itself, it is an important component in the calculation of rod internal pressure. Table 3-9 lists the 69 fuel rod cases, comprised of test program and commercial fuel rods, in the FALCON V&V database with internal void volume measurement data. Table 3-10 contains the measured internal void volume data and the calculated values from FALCON. There were only slight differences between the results from the default and ESCORE emulation modes, so only the default mode data is shown. Comparative and differential distribution plots are shown in Figures 3-45 and 3-46, respectively.

Evaluating Figure 3-45, the overall distribution of rod void volume calculations as compared to the measured data is very good. A slight trend for under prediction can be noted at higher burnups, > ~ 55 GWd/TU, but is not large. Figure 3-46 indicates that the vast majority of the calculated values, ~ 73%, are with a band of +/- 5 cm^3 of the measured values. The overall average differential for all the cases evaluated is -1.2 cm^3, which is equivalent to a value of approximately - 5% of the measured data.

Table 3-9
Fuel Rod Internal Void Volume Validation Cases

Case	Average Burnup (GWd/TU)	Number of Rods	Description Rod Type
Calvert Cliffs Extended Burnup	57.7	10	PWR
Calvert Cliffs-1	30.5	1	PWR
Ft. Calhoun	47.9	2	PWR
Grand Gulf	39.9	17	BWR
HBEP ABB	46.5	5	BWR
HBEP BNFL	42.5	5	PWR
HB Robinson	65.9	8	PWR
KKL	27.3	1	BWR
Limerick	54.7	5	BWR
Oconee	49.5	1	PWR
OPPD	39.3	3	PWR
Peach Bottom – 3	30.8	1	BWR
Zorita	49.6	8	PWR

Table 3-10
Fuel Rod Internal Void Volume Validation Results

Case	Rod	Measured Void Vol. (cm^3)	Calc'd (cm^3)	Δ (cm^3)
Calvert Cliffs Extended Burnup	BEN013	24.71	14.47	-10.24
	BJF027	24.95	14.41	-10.54
	BFL009	38.91	36.6	-2.31
	UFE067	24.66	12.29	-12.37
	UFE019	26.24	12.13	-14.11
	BFM034	26.3	19.37	-6.93
	BFM070	27.14	19.43	-7.71
	BFM071	27.7	18.9	-8.8
	BFM073	27.73	19.37	-8.36
	BFM156	28.2	14.2	-14
Calvert Cliffs - 1	AHS008	33	25.95	-7.05
	NBD144	29	27.36	-1.64
Ft. Calhoun	KJD125	22.97	19.12	-3.85
	KJE076	22.11	19.65	-2.46
Grand Gulf	901A05	22.29	21.71	-0.58
	901B01	22.29	21.44	-0.85
	901D02	19.17	19.12	-0.05
	901E09	22.29	21.11	-1.18
	901F08	19.17	17.25	-1.92
	901K05	22.29	21.13	-1.16
	901B04	19.17	18.07	-1.1
	901D01	22.29	21.22	-1.07
	901D09	22.29	20.62	-1.67
	901E01	22.29	21.82	-0.47
	901F01	22.29	22.06	-0.23
	901F09	22.29	20.93	-1.36
	901H06	22.29	18.07	-4.22
	901H09	22.29	20.76	-1.53
	901K04	22.29	21.34	-0.95
	901K06	22.29	20.26	-2.03
	901K08	22.29	20.49	-1.8

Table 3-10 (continued)
Fuel Rod Internal Void Volume Validation Results

Case	Rod	Measured Void Vol. (cm^3)	Calc'd (cm^3)	Δ (cm^3)
HBEP ABB	A184	27.9	28.16	0.26
	A186	30.1	28.72	-1.38
	A364	28.5	29.59	1.09
	H836	29.2	27.51	-1.69
	H836	29.5	28.69	-0.81
HBEP BNFL	AK	11	13.4	2.4
	BH	9.5	14.65	5.15
	BP	10	15.61	5.61
	CG	9.2	14.97	5.77
	DF	10.5	11.95	1.45
HB Robinson	A02	16.18	13.09	-3.09
	B05	15.14	13.1	-2.04
	E02	16.33	15.58	-0.75
	R05	16.45	14.92	-1.53
	B01	16.54	13.1	-3.44
	F07	17.43	13.17	-4.26
	G10	14.6	13.18	-1.42
	S02	16.38	14.95	-1.43
KKL	D02	27.6	35.36	7.76
Limerick	E9	30.7	30.39	-0.31
	F9	31.2	30.54	-0.66
	G1	29.9	30.3	0.4
	J3	28.4	30.18	1.78
	J7	29.8	30.27	0.47
Oconee	A1	27	35.04	8.04
OPPD	KJE076	23	22.91	-0.09
	KJN052	25	23.88	-1.12
	KKM095	24	23.23	-0.77
Peach Bottom-3	DJD224	45.99	33.65	-12.34

Table 3-10 (continued)
Fuel Rod Internal Void Volume Validation Results

Case	Rod	Measured Void Vol. (cm^3)	Calc'd (cm^3)	Δ (cm^3)
Zorita	328	29	34.89	5.89
	332	31	35.41	4.41
	335	30	34.67	4.67
	384	28.5	36.24	7.74
	386	31	35.52	4.52
	331	28.5	35.37	6.87
	334	31	34.43	3.43
	344	30.5	34.72	4.22
	385	31	34.83	3.83

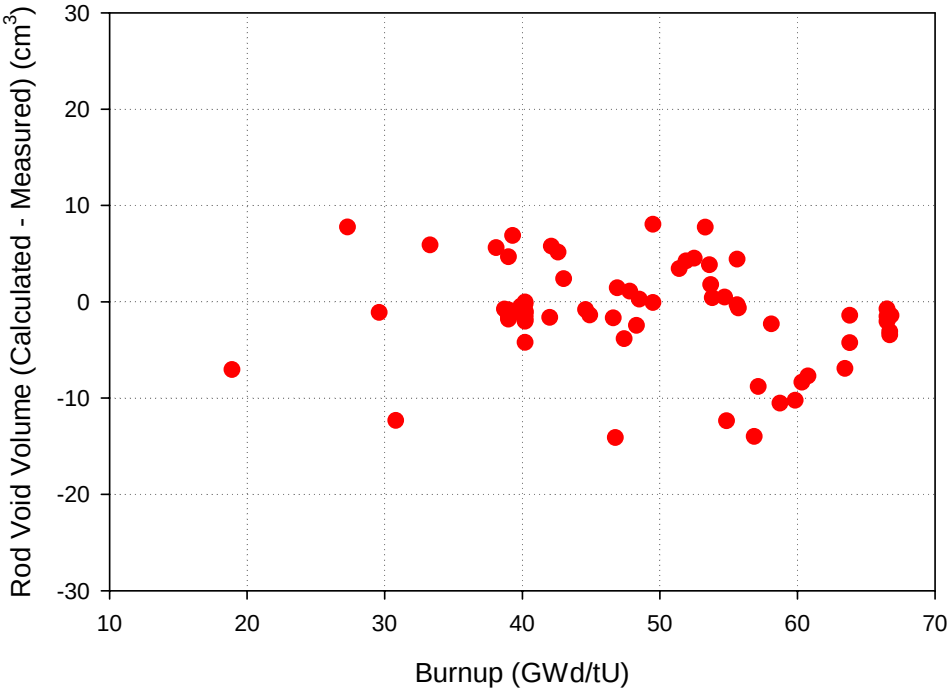

Figure 3-45
Rod Void Volume as a Function of Burnup

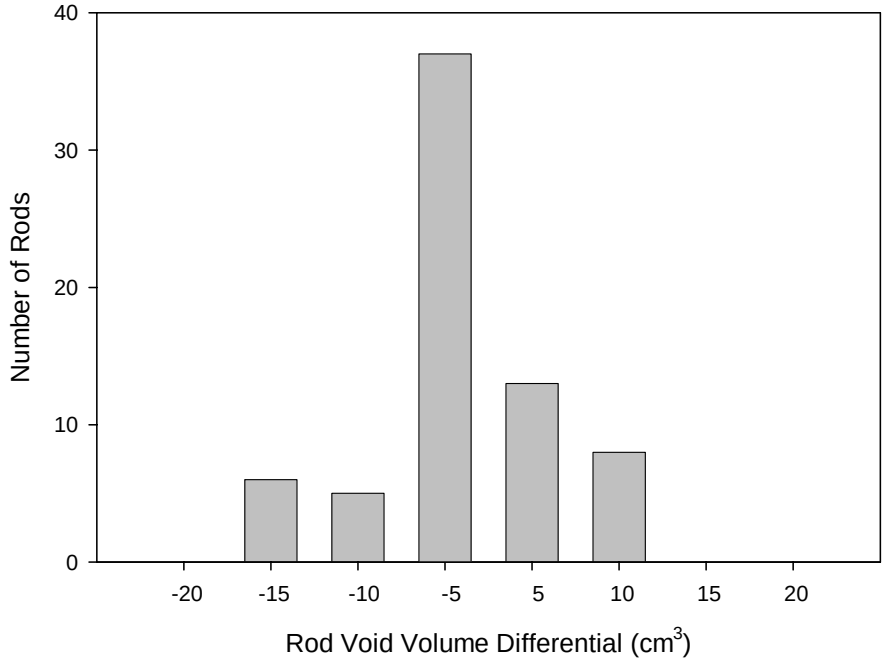

Figure 3-46
Rod Void Volume Differential Range Distribution

3.7 Rod Internal Pressure

Rod internal pressure is another indicator of integral fuel rod modeling performance. Table 3-11 lists the fuel rod cases in the FALCON V&V database with available rod internal pressure measurements. A total of 26 fuel rod cases, primarily test program and commercial fuel rods, were used for the V&V assessment. A summary of the calculated results is provided in Table 3-12. Figure 3-47 presents a cumulative plot of the rod internal pressure as a function of burnup and the differential distribution functions for FALCON in the default and ESCORE emulation modes are shown in Figures 3-48 and 3-49, respectively.

Evaluating Figure 3-47 indicates that the rod internal pressure calculated values reproduce the measured data fairly well. Similar to the distribution of rod void volume calculations, a slight trend for under prediction can be noted at higher burnups, > ~ 60 GWd/TU, but is not large. Figure 3-48 indicates this small bias in the default mode calculations, whereas Figure 3-49 shows a slight over prediction bias in the ESCORE emulation mode calculated values. Looking back at Figure 3-47 these higher values occur in a burnup range of ~ 45 to 60 GWd/TU, but not at higher burnups. The overall average differential for all the cases evaluated in the default mode is –0.44 MPa, and 0.07 MPa for the ESCORE emulation mode.

Table 3-11
Fuel Rod Internal Pressure Validation Cases

Case	Average Burnup (GWd/TU)	Number of Rods	Description Rod Type
Calvert Cliffs Extended Burnup	57.7	10	PWR
HBEP ABB	46.5	5	BWR
HB Robinson	65.9	8	PWR
KKL	27.3	1	BWR
Oconee	49.5	1	PWR
Peach Bottom – 3	30.8	1	BWR

Table 3-12
Fuel Rod Internal Pressure Validation Results

Case	Rod	Measured Int. Pres. (MPa)	Default Mode (MPa)	Default Mode Δ (Mpa)	ESCORE Mode (MPa)	ESCORE Mode Δ (MPa)
Calvert Cliffs Extended Burnup	BEN013	3.705	4.214	0.509	5.002	1.297
	BFJ027	3.587	4.221	0.634	4.973	1.386
	BFL009	3.291	3.213	-0.078	3.501	0.21
	UFE067	3.918	5.311	1.393	5.319	1.401
	UFE019	3.443	4.441	0.998	5.082	1.639
	BFM034	4.203	3.583	-0.62	4.244	0.041
	BFM070	3.989	3.512	-0.477	4.215	0.226
	BFM071	3.769	3.56	-0.209	4.147	0.378
	BFM073	3.893	3.517	-0.376	4.198	0.305
	BFM156	3.458	4.192	0.734	5.011	1.553
HBEP ABB	A184	0.485	0.455	-0.03	0.622	0.137
	A186	0.884	0.445	-0.439	0.585	-0.299
	A364	0.647	0.486	-0.161	0.703	0.056
	H836	2.865	0.632	-2.233	0.845	-2.02
	H836	1.964	0.558	-1.406	0.87	-1.094
HB Robinson	A02	4.39	3.271	-1.119	3.85	-0.54
	B05	4.53	3.321	-1.209	3.849	-0.681
	E02	4.121	2.779	-1.342	3.689	-0.432
	R05	4.236	2.923	-1.313	3.936	-0.3
	B01	3.952	3.324	-0.628	4.002	0.05
	F07	3.628	3.082	-0.546	3.813	0.185
	G10	4.319	3.08	-1.239	3.814	-0.505
	S02	4.265	2.923	-1.342	3.938	-0.327
KKL	D02	1.4	0.717	-0.683	0.654	-0.746
Oconee	A1	4.213	3.796	-0.417	3.885	-0.328
Peach Bottom - 3	DJD224	0.317	0.362	0.045	0.42	0.103

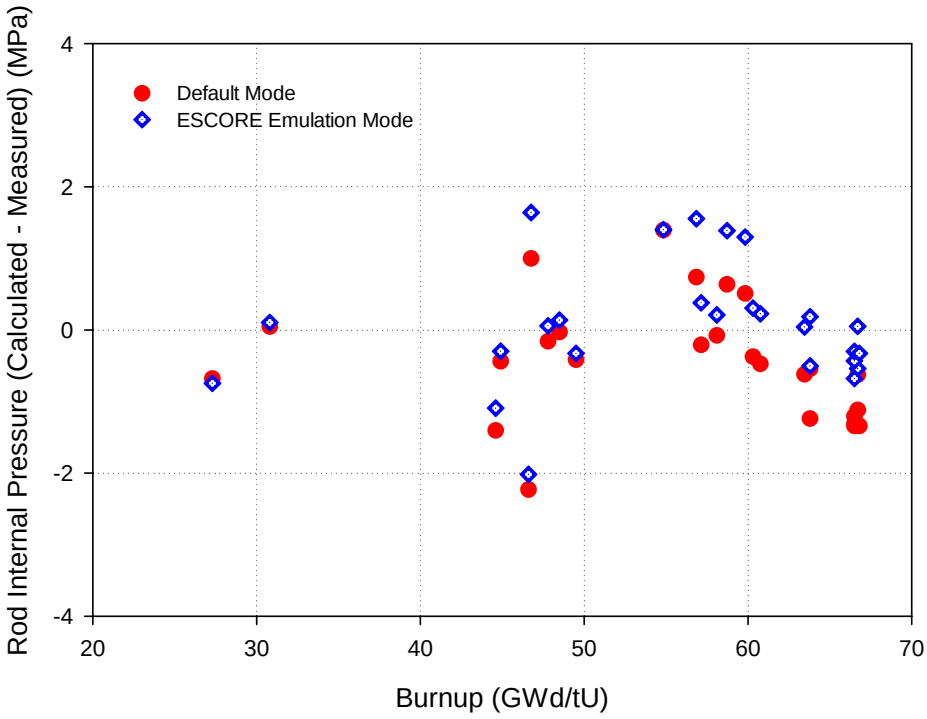

Figure 3-47
Rod Internal Pressure as a Function of Burnup

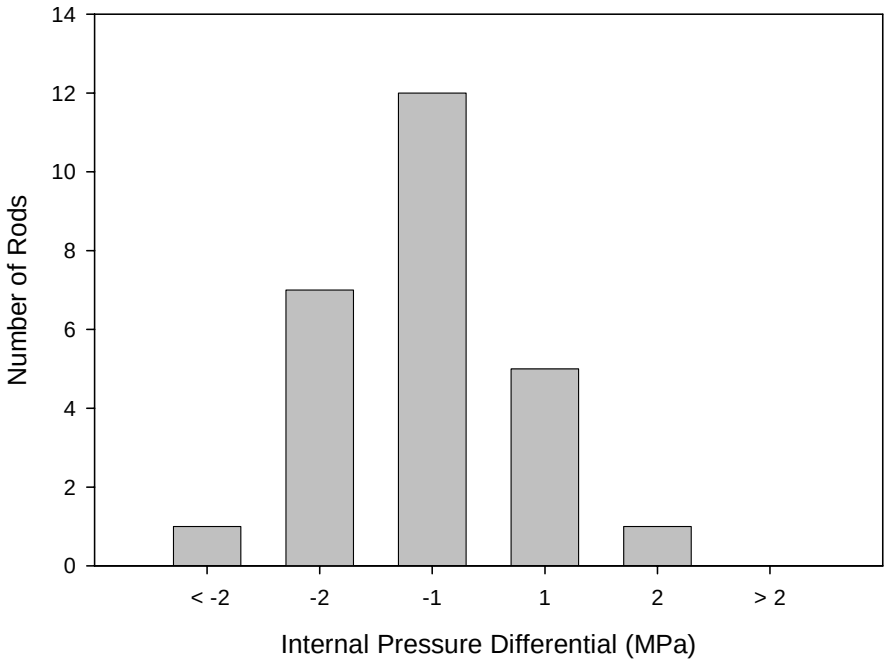

Figure 3-48
Default Mode Rod Internal Pressure Differential Range Distribution

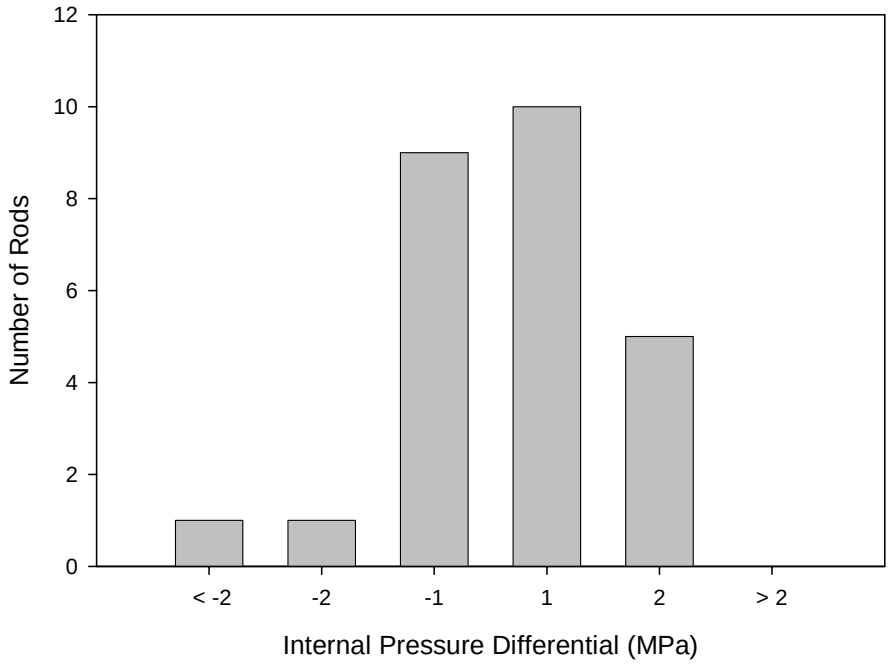

Figure 3-49
ESCORE Emulation Mode Rod Internal Pressure Differential Range Distribution

3.8 Coolant Channel Boundary Conditions

The coolant enthalpy rise model within FALCON is used to calculate the coolant enthalpy, temperature, and mass flow rate distributions along the fuel rod flow channel. These parameters are required to calculate the rod-to-coolant heat transfer coefficients and, along with the coolant temperature, provide the thermal boundary conditions for the cladding and pellet temperature calculations in FALCON. Table 3-13 lists the submodel and separate effects cases selected to verify the coolant channel enthalpy rise model.

Table 3-13
Coolant Channel Enthalpy Rise Model Verification Cases

Case	Description
Enthalpy Rise	Steady state analysis based on the analytical solution of enthalpy rise in a closed channel
Vertical Pipe Flow Experiment	Single and two phase flow experiment with transition from nucleate boiling to film boiling
Annular Flow Experiment	Post-departure from nucleate boiling (DNB) heat transfer, forced convection vaporization experiment

Assuming no mixing between channels, the enthalpy rise in a closed coolant channel is given by the following energy balance equation. [5]

$$\dot{m}\left[h(z)-h_{in}\right]=\int_0^z q''_w(z)P_h dz \tag{2}$$

Where

$\dot{m}$ = mass flow rate,

$h(z)$ = enthalpy at location z,

h_{in} = inlet enthalpy,

$q''_w(z)$ = heat flux (radial average) at location z, and

P_h = heated perimeter.

For a uniform axial heat flux profile, equation (2) simplifies to

$$h(z)=h_{in}+\frac{q''P_h z}{\dot{m}} \tag{3}$$

A cladding-only analysis with uniform heat flux on the inner cladding surface was used in FALCON to compare to the enthalpy distribution given by equation (3). The results shown in Figure 3-50 indicate that the FALCON coolant channel model reproduces well the results of the analytical solution.

Bennett et al. conducted a series of vertical pipe flow experiments consisting of steady state flow in a vertical round tube with a uniformly heated section [6]. In the tests, single-phase water was introduced at the inlet of the uniformly heated test section with boiling conditions varying at the outlet from saturated to stable film boiling. When the input heat flux exceeded the critical heat flux, transition from nucleate boiling to film boiling occurred, precipitating a rapid increase in the wall temperature within the test section of the tube.

A single channel, cladding only model was developed for this experiment to evaluate the pre- and post-CHF heat transfer correlations in FALCON. For these calculations, the Westinghouse critical heat flux correlation and the Jens-Lottes pre-DNB and the Groeneveld 5.7 post-DNB heat transfer correlations were used. Comparisons are made between the predicted cladding wall temperature axial distribution, the axial dryout position, and the maximum wall temperature. Table 3-14 summarizes the axial dryout position and maximum wall temperature results. The computed and measured cladding wall temperatures are compared in Figure 3-51.

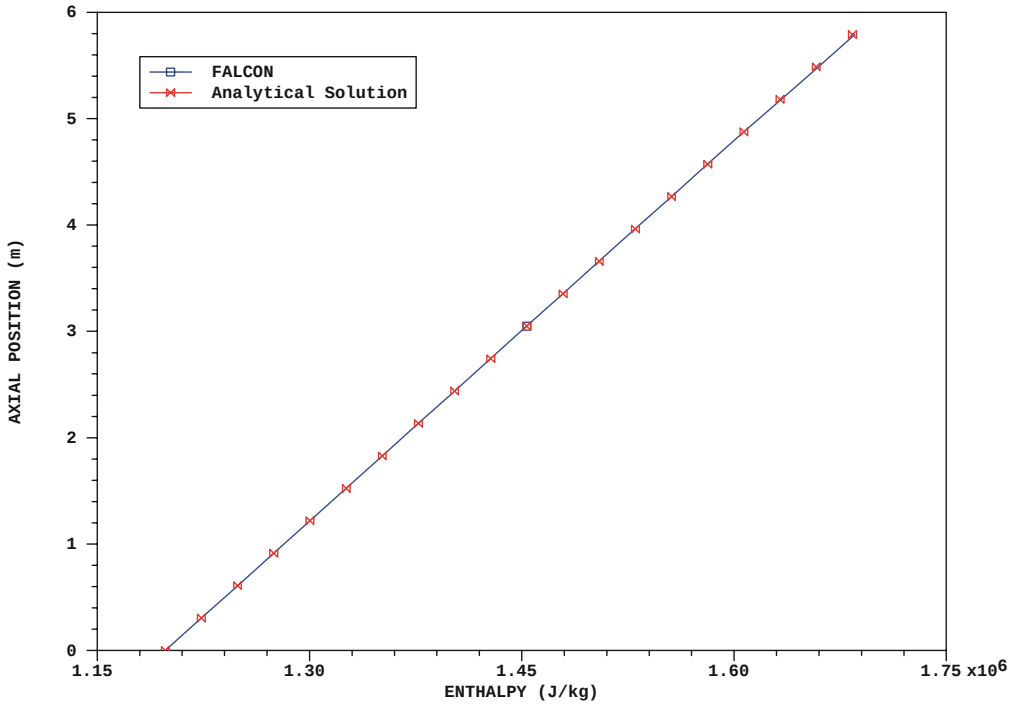

Figure 3-50
Comparison of Coolant Channel Enthalpy Rise

Table 3-14
Vertical Pipe Flow Analysis Results Summary

	Dryout Position (measured from inlet) (m)	Maximum Wall Temperature (˚C)
Measured Data	4.98	779.44
FALCON	4.88	796.78

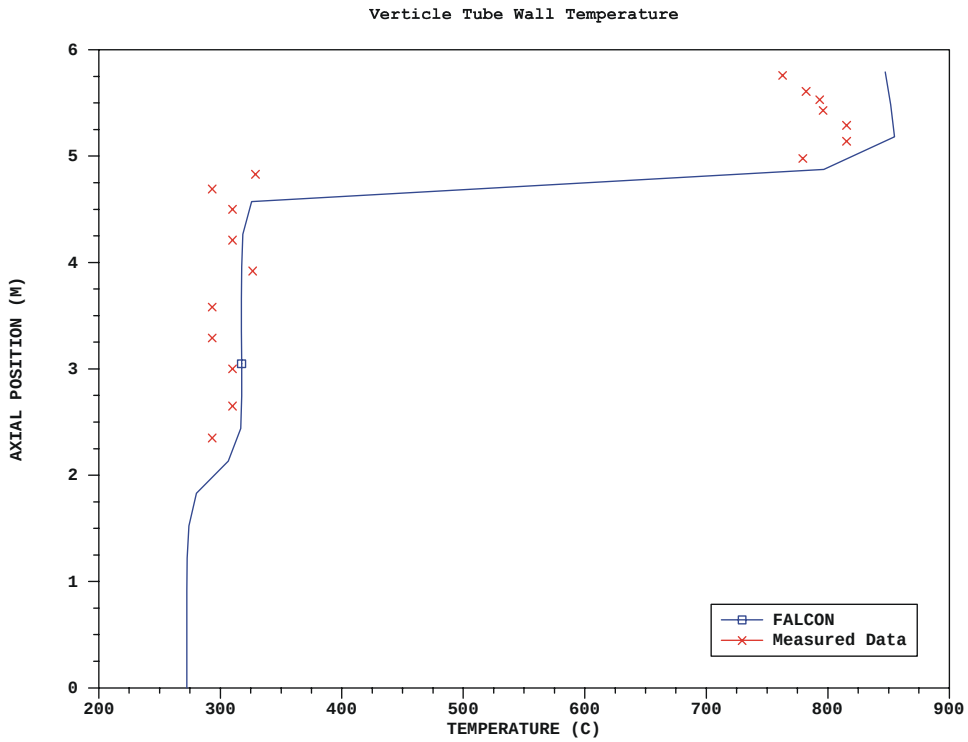

Figure 3-51
Comparison of Tube Wall Temperature for the Vertical Pipe Flow Experiment

The results show that the code predicts the post-DNB dryout position and maximum wall temperature reasonably well using the designated models. Figure 3-51 illustrates that the FALCON computed tube wall temperatures also match the axial distribution of the measured data rather well.

The annular flow experiment was a similar series of heat transfer tests as the aforementioned vertical pipe flow experiment [7]. In this case however, rather than flow through a pipe, this experiment examined a two-phase flow mixture on the exterior of an internally heated annulus encompassed by a shroud. The experiment was conducted by introducing a steam-water mixture at the inlet of the annulus. After a suitable mixing length, the two-phase mixture entered a uniformly heated test section. This flow regime led to a heat transfer condition characterized by forced convection vaporization. As with the previous vertical upflow experiments, a single channel, cladding only model was developed for FALCON to compute the heated wall temperatures for comparison to the measured data. The calculated and measured cladding wall temperatures are compared in Figure 3-52. The results indicate that FALCON calculated wall temperatures match the measured data well (within ~ 3 ˚C) throughout the primary test section of the experiment.

The series of verification cases presented above illustrate that the coolant enthalpy rise model implemented in FALCON performs well for a variety of flow regimes. There are certainly limitations to this model, as noted in the theoretical and numerical bases document [1]. However, for single channel fuel rod conditions with homogeneous flow and for scoping calculations, this model effectively provides the thermal boundary conditions for the thermal solution in FALCON.

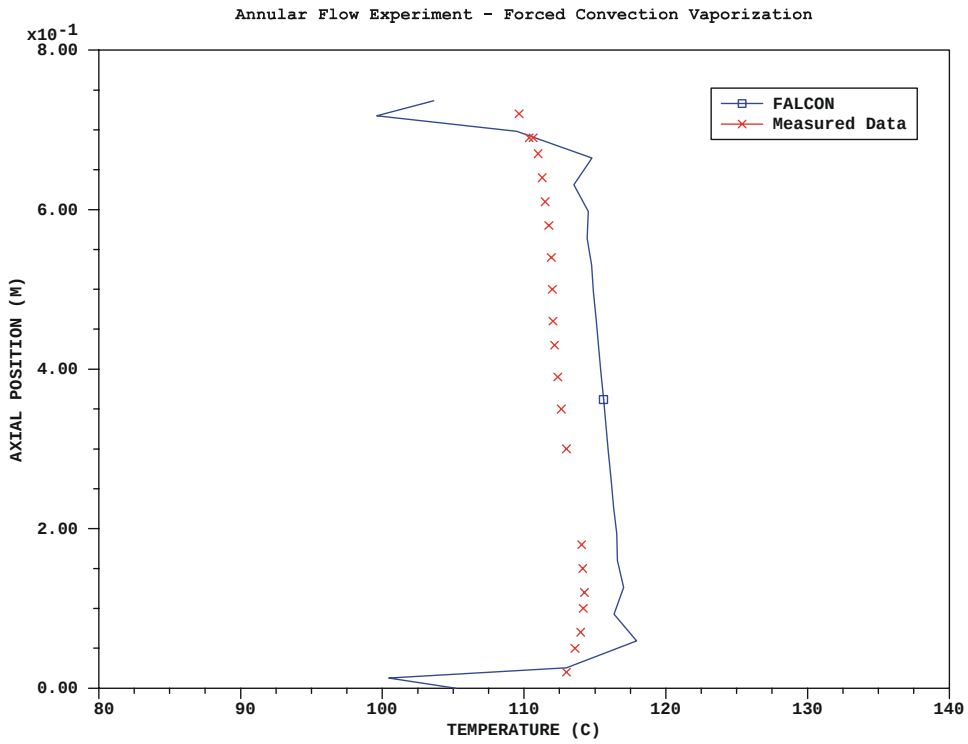

Figure 3-52
Comparison of Annulus Outer Wall Temperatures for the Annular Flow Experiment

3.9 Transient Fuel Rod Analysis

The transient fuel rod behavior capability of FALCON has remained the foundation of the program since its inception. And, as previously noted, FALCON's transient capabilities and applications have been extensively evaluated and documented. The problems chosen for evaluation in this portion of the V&V program are intended to demonstrate the applicability of FALCON MOD01 to the Chapter 15 Design Basis Accidents (DBA's) required in licensing analyses. In this application, the LOCA and RIA represent the worst-case conditions for the analysis of reactor transients and, therefore bound FALCON's application range. Residing between these two extremes, are off-normal-power or cooling conditions, referred to as power/cooling mismatch or PCM transients. PCM-type operational transients represent less severe off-normal conditions that can occur when the coolant cannot adequately remove the energy generated in the fuel rod. In a majority of these transients, DNB can take place, resulting in increased cladding surface temperatures and possible fuel rod failure. Table 3-15 lists the cases selected to demonstrate the transient fuel rod response capabilities of FALCON MOD01.

Table 3-15
Transient Validation Cases

Program	Rod	Description
PBF PCM-2	UTA-008	Program in the PBF to evaluate the behavior of unirradiated PWR fuel rods under normal and post-DNB conditions
FRF-1	L	First Fuel Rod Failure Test (FRF-1) conducted in the TREAT Facility; evaluated the effects of steam flow on cladding behavior following the blow down phase of a LOCA
CABRI	REP Na-5	High burnup RIA simulation test conducted in the CABRI facility; evaluation of high burnup fuel enthalpy limit

3.9.1 Power Burst Facility Power Coolant Mismatch Test 2 (PBF PCM-2)

The PBF PCM-2 test was performed using four unirradiated UO_2-fueled, Zircaloy clad fuel rods [8, 9, 10]. DNB was achieved during the test by decreasing the coolant flow rate while maintaining a constant fuel rod power. The specific parameters of interest during the test were the fuel rod power and coolant flow rate at which DNB occurred and the thermal and mechanical behavior of the test fuel rods following DNB. The experiment consisted of 4 phases; 1) power calibration, 2) preconditioning, 3) fuel rod aging, and 4) eight DNB cycles. The first three phases were used to calibrate the instrumentation and to prepare the fuel rods for DNB operation. The mass fluxes at which DNB was initiated were determined during the first seven DNB test cycles. Fuel rod powers were reduced after DNB was indicated to prevent high cladding temperatures and possible fuel rod failure. The fuel rods were maintained in post-DNB operation only during the eighth DNB cycle.

No fuel rod failures occurred as a result of 145 seconds of high temperature post-DNB operation. Post irradiation examination (PIE) conducted on the test fuel rods revealed cladding outer surface oxide formation on all the fuel rods. A region of cladding collapse was also observed in the high temperature zone. Cladding temperatures were determined by metallographic examination of the cladding microstructures. The measured cladding temperatures from thermocouples placed on the rods generally agreed well with the temperatures determined from metallographic examinations.

A FALCON two-dimensional, full-length fuel rod model was developed for rod UTA-008 and an analysis performed for the DNB cycle 8 (extended post-DNB operation under high temperature film boiling conditions). The analysis was initiated at a power level of 46 kW/m and the flow rate was decreased at a constant rate of 3% per second. The modified Babcock & Wilcox CHF model was used to calculate the initiation of DNB. The calculated fuel temperatures, cladding temperatures, cladding elongation, and rod internal pressure were compared to the measured data available for the eighth DNB cycle.

Results from the FALCON analysis of rod UTA-008 are presented in Figures 3-53 through 3-59. Experimental data evaluated include the cladding temperature, fuel centerline temperature, fuel rod internal pressure, and the mechanical response of the fuel rod.

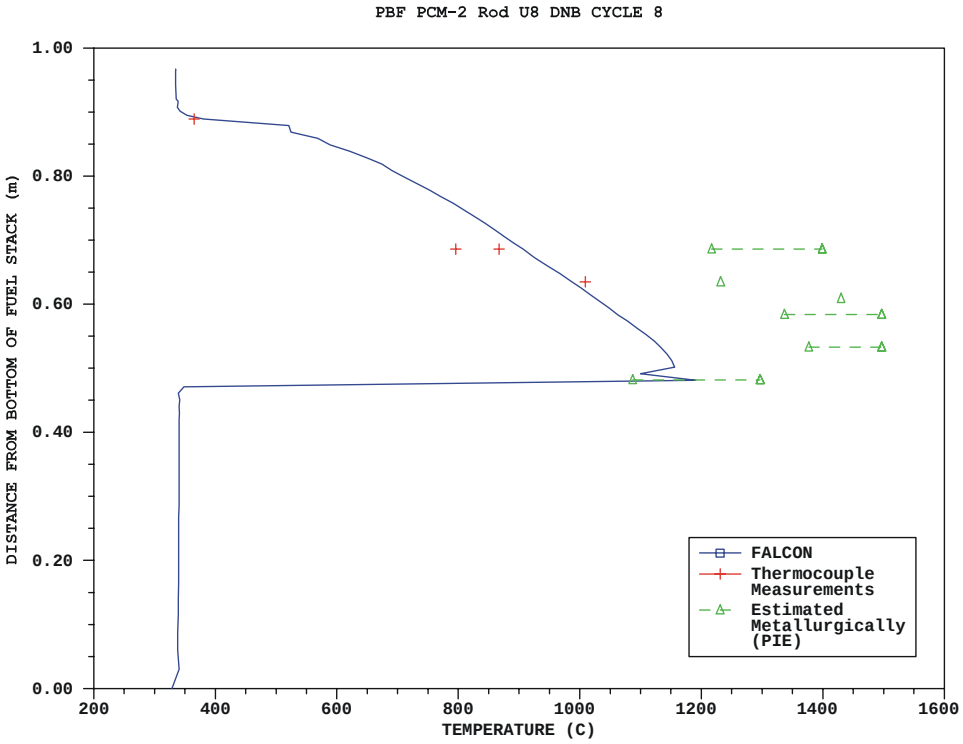

Figure 3-53
Comparison of PBF PCM-2 Cladding Peak Temperatures

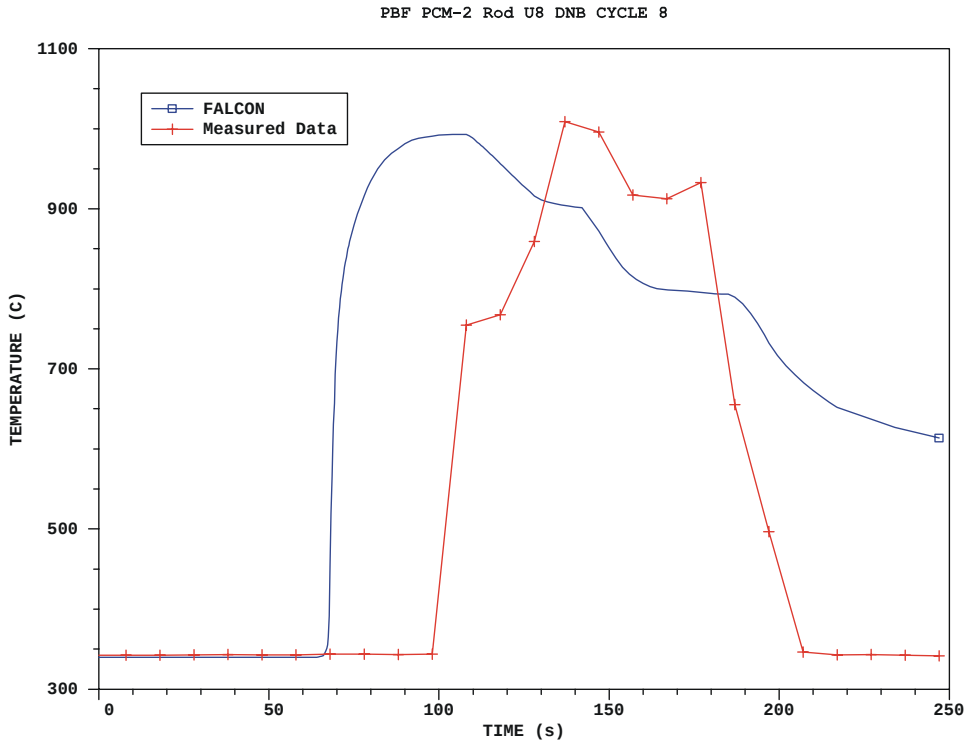

Figure 3-54
Comparison of PBF PCM-2 Cladding Surface Temperatures at 0.635 m Elevation

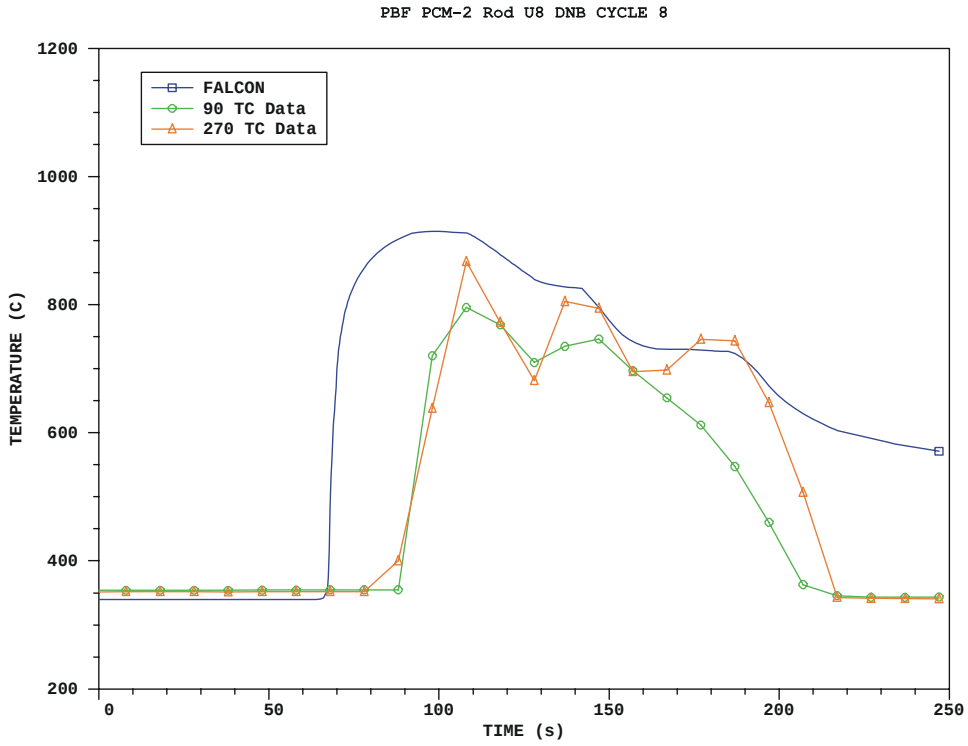

Figure 3-55
Comparison of PBF PCM-2 Cladding Surface Temperatures at 0.686 m Elevation

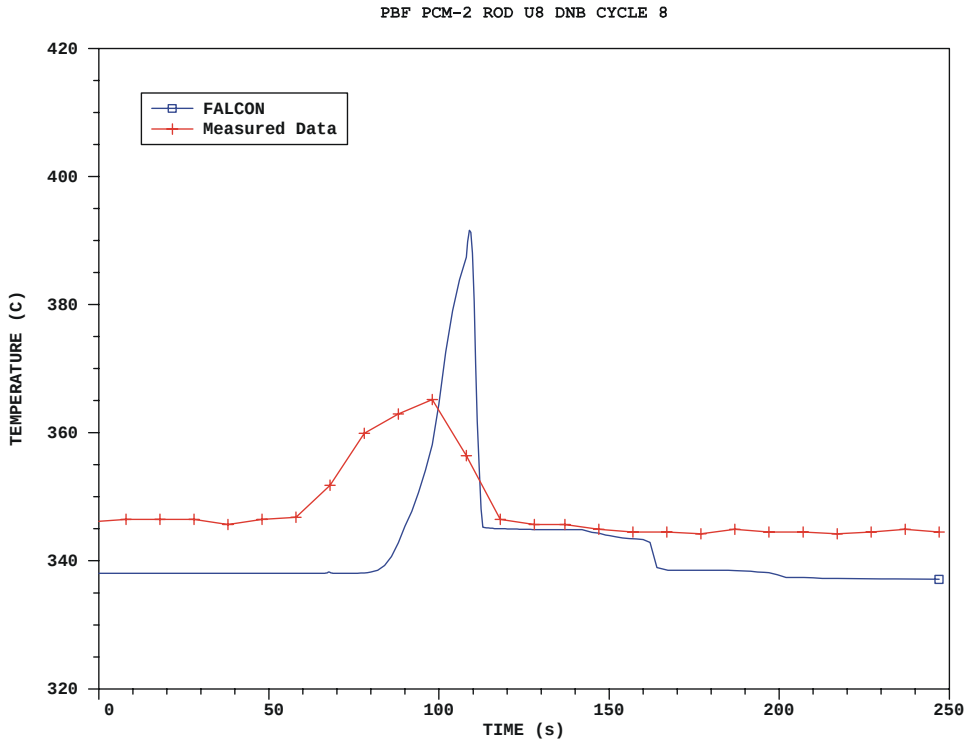

Figure 3-56
Comparison of PBF PCM-2 Cladding Surface Temperatures at 0.889 m Elevation

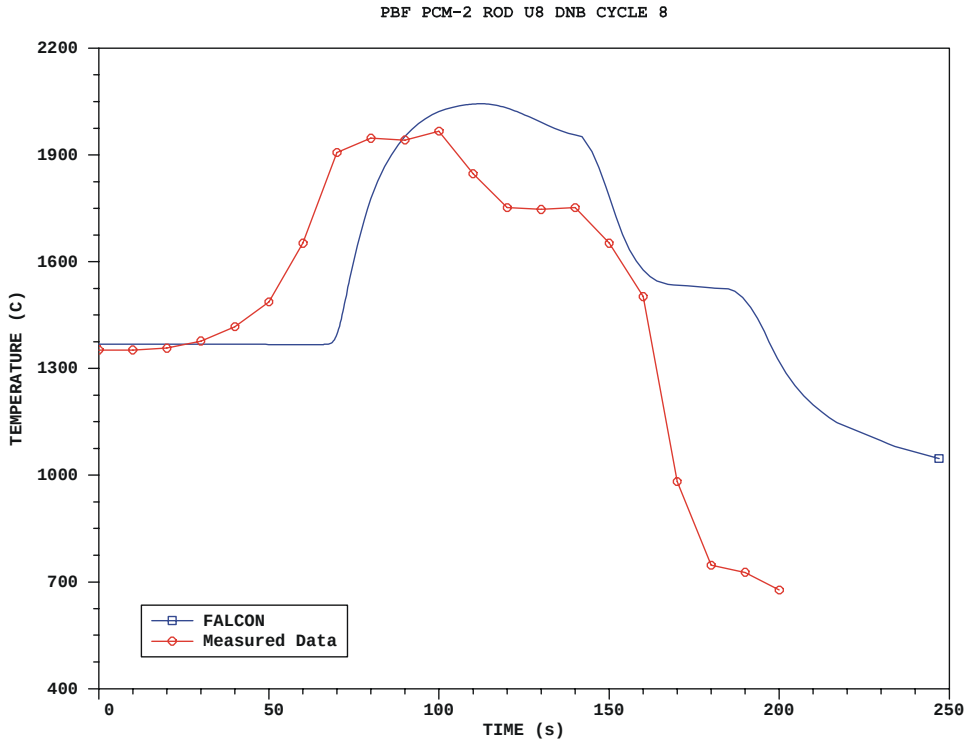

Figure 3-57
Comparison of PBF PCM-2 Fuel Centerline Temperature at 0.686 m Elevation

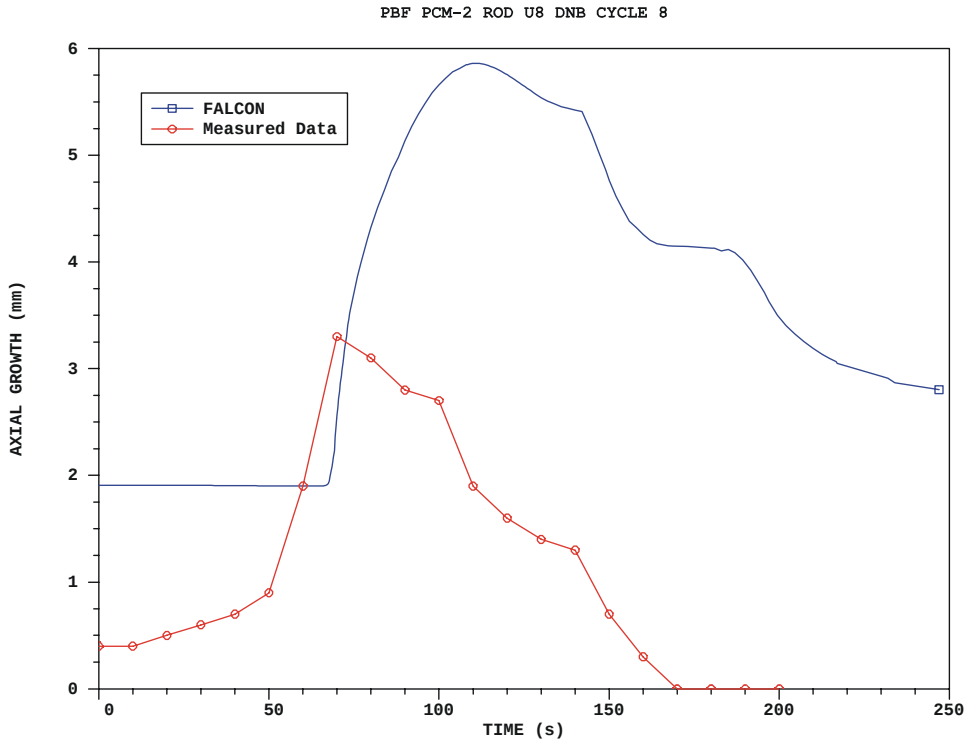

Figure 3-58
Comparison of PBF PCM-2 Cladding Elongation

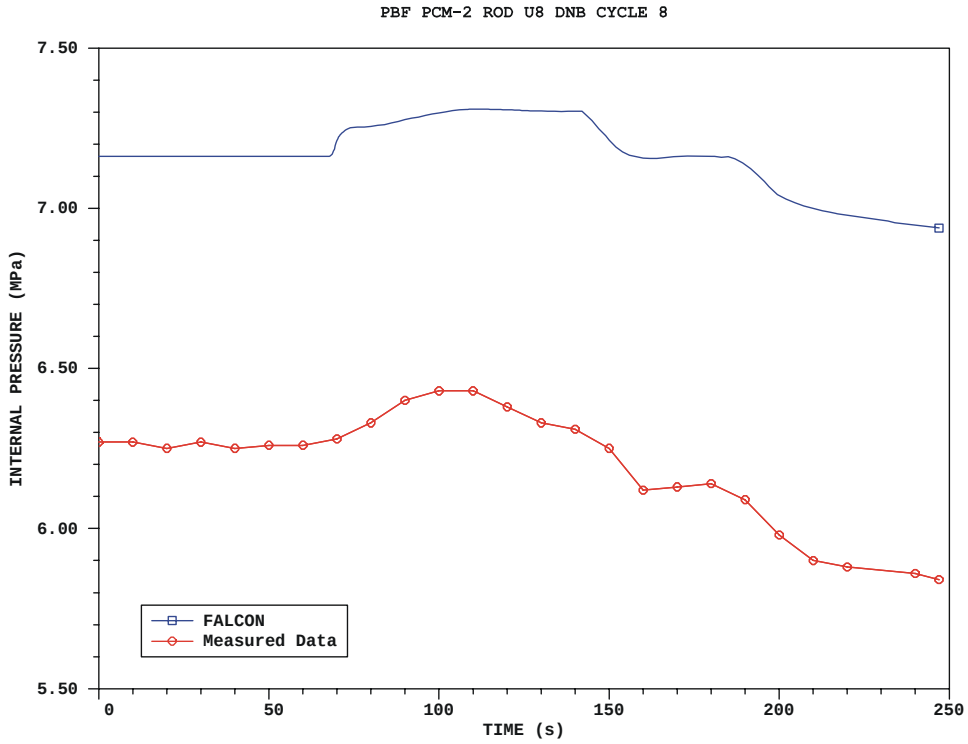

Figure 3-59
Comparison of PBF PCM-2 Rod Internal Gas Pressure

Figure 3-53 shows the axial distribution of the maximum cladding surface temperatures calculated by FALCON during film boiling operation. Temperature data determined from metallographic examinations and peak thermocouple readings are included for comparison. The FALCON calculated peak temperatures and therefore, the extent of film boiling appear to match the data well, particularly the data obtained from the thermocouples. Figures 3-54 through 3-56 show the computed cladding surface temperature time histories corresponding to several thermocouple positions distributed axially, and in one location, azimuthally around the test rod. These plots demonstrate that FALCON predicts DNB to occur ~ 25 to 30 seconds prior to indication from the thermocouples at 0.635 and 0.686m elevation, but ~ 30 afterwards at the higher, 0.889m thermocouple position. With the exclusion of the data at this elevation (Figure 3-56), the FALCON computed peak temperatures match the measured data well. The over prediction of the peak cladding temperatures at the 0.889 m thermocouple location could be due to three-dimensional effects associated with film boiling flow conditions and geometry changes due to rod bowing. The post-DNB heat transfer coefficients calculated by FALCON may also cause the higher predicted temperatures at this location.

The fuel centerline temperature comparison with thermocouple data is presented in Figure 5-57. FALCON over predicts the fuel rod centerline temperature by ~ 75 °C, which is within the uncertainty range of the measured value. The overall predicted time history response shows relatively good agreement with the measured response. The fuel rod cladding elongation is shown in Figure 3-58. FALCON appears to over predict the measured elongation data by ~ 2.5 mm. However, most of the over prediction is a result of the initial cladding elongation prior to DNB. This is most likely an effect of instrument calibration that has not been taken into account properly in the FALCON results. The change in cladding elongation upon DNB initiation calculated by FALCON is only slightly higher than the measured data, ~ 1 mm. Figure 3-59 presents a comparison of the fuel rod internal pressure. The predicted value is ~ 0.7 MPa higher than the measured value. This difference could be attributed to the method used to model the external volume associated with the pressure transducers. However, the pressure response appears to be consistent with the modeled internal volume. A slight increase in pressure is predicted when DNB occurs that is approximately the same as the pressure increase seen in the measured data.

3.9.2 FRF-1 LOCA Experiment

The First Fuel Rod Failure Test (FRF-1) in the Transient Reactor Test (TREAT) facility was performed to study the effects of steam flow on cladding behavior immediately following the blowdown portion of a LOCA [11]. The objectives of the test were to determine: 1) the characteristics and extent of fuel rod failure under LOCA conditions, and 2) the effect of failure on emergency cooling effectiveness. The information obtained from FRF-1 was considered to be validation data for behavior models and tube-burst data under simulated in-pile conditions.

FRF-1 simulated the heat-up stage of a LOCA with a seven-rod bundle in a flowing steam atmosphere. After completion of the test, post-test examinations were carried out to characterize the behavior of the cladding and fuel. PIE indicated that all seven rods experienced cladding ballooning and rupture. Rod-to-rod contact also occurred as a result of the excessive cladding ballooning. Metallographic examinations of the ruptures indicated that they were ductile in

nature. A cladding thermocouple and pressure transducer were located on Test Rod L to monitor the cladding temperature and rod internal pressure responses during the test.

As with PCM-2, FRF-1 rod L was modeled in FALCON using a two-dimensional, full-length fuel rod model. A single channel analysis using a shroud geometry was conducted using the specified rod power and coolant inlet temperature, pressure, and mass flux histories. The analysis was initiated with a power ramp to 21 kW/m at approximately 3 s. The modified Babcock & Wilcox CHF model was used to calculate the initiation of DNB. The rod-to-rod contact noted in the PIE was not modeled in the analysis. The calculated fuel temperatures, rod internal pressure, and cladding deformation were compared to the available measured data. These comparisons are presented in Figures 3-60 through 3-62.

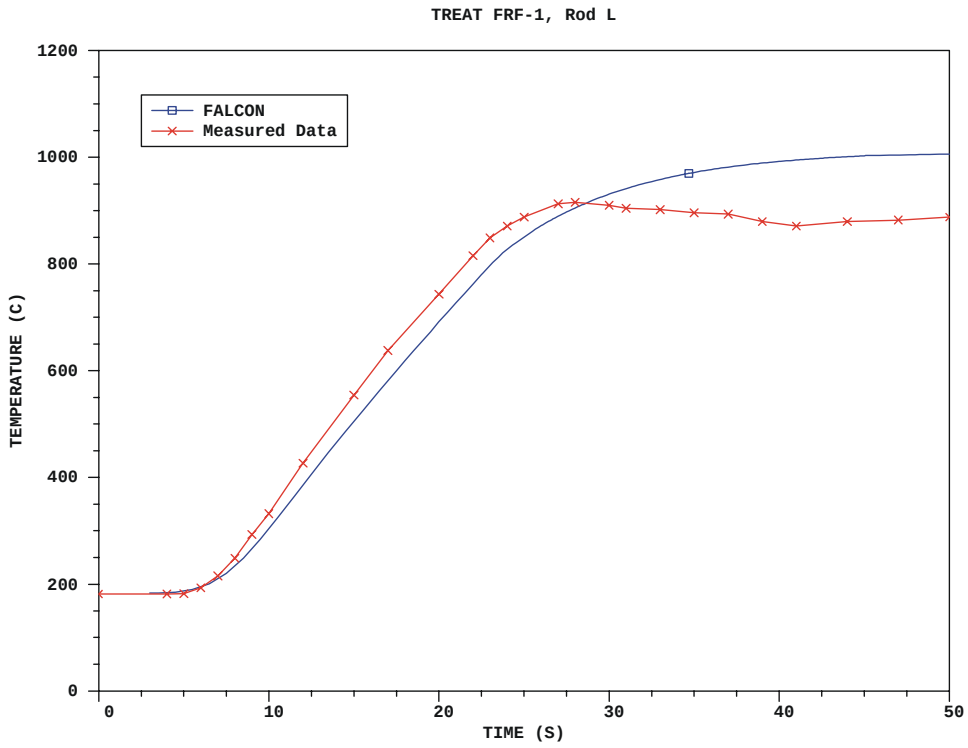

Figure 3-60
Comparison of FRF-1 Rod L Cladding Surface Temperature

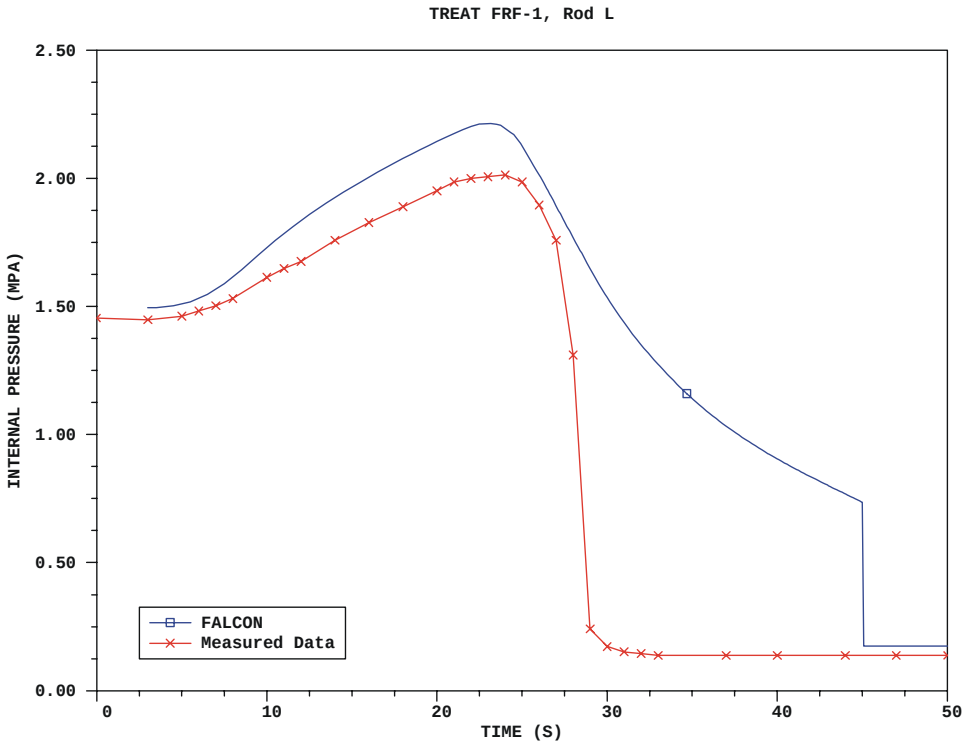

Figure 3-61
Comparison of FRF-1 Rod L Internal Rod Press

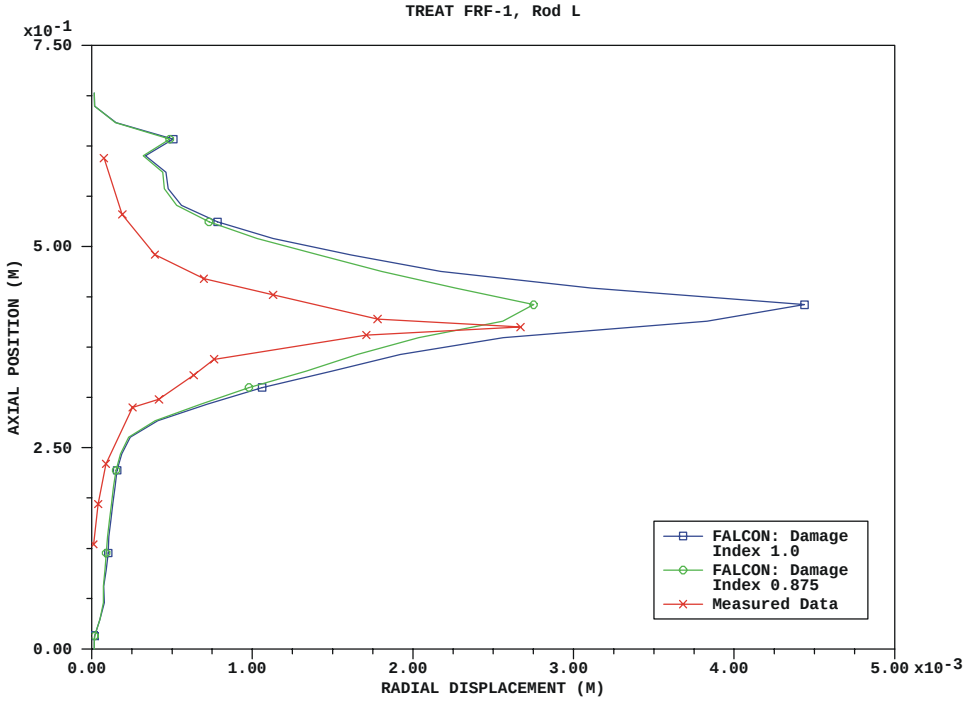

Figure 3-62
Comparison of FRF-1 Rod L Cladding Swelling

The cladding surface temperature response, shown in Figure 3-60, indicates that the predicted heat up rate and temperatures agree well with the measured data. The fuel rod internal pressure history is shown in Figure 3-61. This plot indicates that FALCON slightly over predicts the peak internal pressure and drops off less quickly indicating a slower response to cladding rupture. However, the pressure increase due to fuel rod heat up tracks the response of the measured data quite well. As with the PCM-2 analysis, the difference in the pressure response could be related to the method used to represent the pressure transducer volume. During the experiment, extensive cladding ballooning begins to occur at approximately 23 s, resulting in an increase in the internal volume. This effect can be seen in the measured pressure data as the rate of pressure increase slows. Fuel rod failure occurs at approximately 28 s, as indicated by the rapid decrease in pressure to a value equal to the coolant pressure. The FALCON calculated cladding ballooning and subsequent volume increase agrees well with the experimental data. However, the predicted time to failure, at 45 s, is several seconds after the indicated failure at 28 s.

As discussed in the numerical bases and theory manual, the high temperature cladding rupture determination in FALCON is based on a time-temperature-stress failure approach using the cumulative damage concept [1]. This approach assumes that a material accumulates damage due to sustained stress. A damage index value of unity is used in FALCON to represent a best-estimate failure probability. This value is determined through calibration of the time-temperature-stress failure threshold based on internal pressure induced uniform stress and strain states throughout the cladding wall thickness under constant heating rates. Non-uniform variance under actual experimental conditions introduces uncertainty into the predicted point of cladding failure initiation.

A comparison of the predicted and measured cladding deformation is presented Figure 3-62. Two FALCON computational results are shown, one for a damage index of 1.0 and one for a damage index of 0.875. The predicted cladding deformation using a damage index of 1.0 sustains larger radial displacement before failure, reaching a maximum displacement of 4.44 mm as compared to the measured value of 2.67 mm. The larger displacement prior to failure corresponds to the longer failure time indicated by the pressure response curve in Figure 3-61. Using a damage index of 0.875, however, FALCON calculates a radial displacement 2.75 mm, very near the experimental value. The differences noted in the cladding ballooning and failure predictions can be attributable to a variety of factors. For example, rod-to-rod contact was noted in the PIE of FRF-1. This may have affected the measured cladding deformations. Rod bowing and ovality can also impact the formation and extent of cladding ballooning. Because of the FALCON modeling approach, these effects are not implicitly accounted for and can contribute to differences between computed and observed cladding deformation. Additionally, recent changes in the cladding creep and axial growth models may have had an impact on the calibration of the damage index. Evaluation of this potential effect is an area that will be a focus of further code development activities.

3.9.3 CABRI REP Na-5 RIA Experiment

The REP Na-5 test was part of a series of tests conducted in CABRI test reactor designed to evaluate high burnup cladding behavior under RIA conditions and to establish bases for a high burnup fuel enthalpy limit [12, 13, 14]. The rod segment selected for REP Na-5 was originally irradiated in a standard 17x17 PWR fuel assembly and reached a burnup of ~ 64 GWd/TU. The

refabricated rod segment was placed in a test capsule containing in-pile instrumentation and tested in a flowing sodium loop inside the central flux area of the CABRI reactor. Although the test capsule coolant, pressure, and the pulse widths experienced during these tests are different from LWR conditions, precluding direct evaluation of LWR fuel performance, the coolant conditions are considered representative to study the response of the test rods prior to DNB.

A two-dimensional, full-length fuel rod model was developed to simulate this experiment. A single channel analysis using a shroud geometry with sodium coolant was conducted using a narrow Gaussian-shaped power pulse (9.5 ms FWHM) peaking at ~ 19.5 MW/m at 0.08 s to provide data for comparison to the measured axial growth and residual cladding strains. Additional parameters available from the model included fuel enthalpy, fuel and cladding temperatures, and cladding strain energy density (SED). Comparison of SED to the critical SED (CSED) can provide a basis for determination of rod failure. Plots of the experimental pulse width and fuel enthalpy, cladding axial elongation, and cladding hoop strains are presented in Figures 3-63 through 3-65. Table 3-16 summarizes the measured data and comparable modeling results.

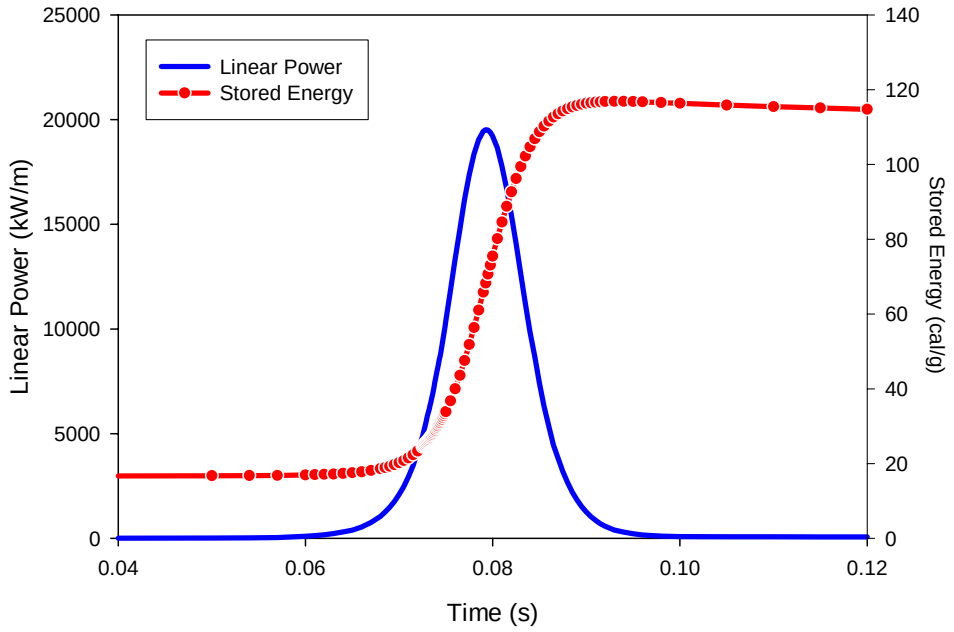

Figure 3-63
REP Na-5 Pulse Linear Power and Enthalpy

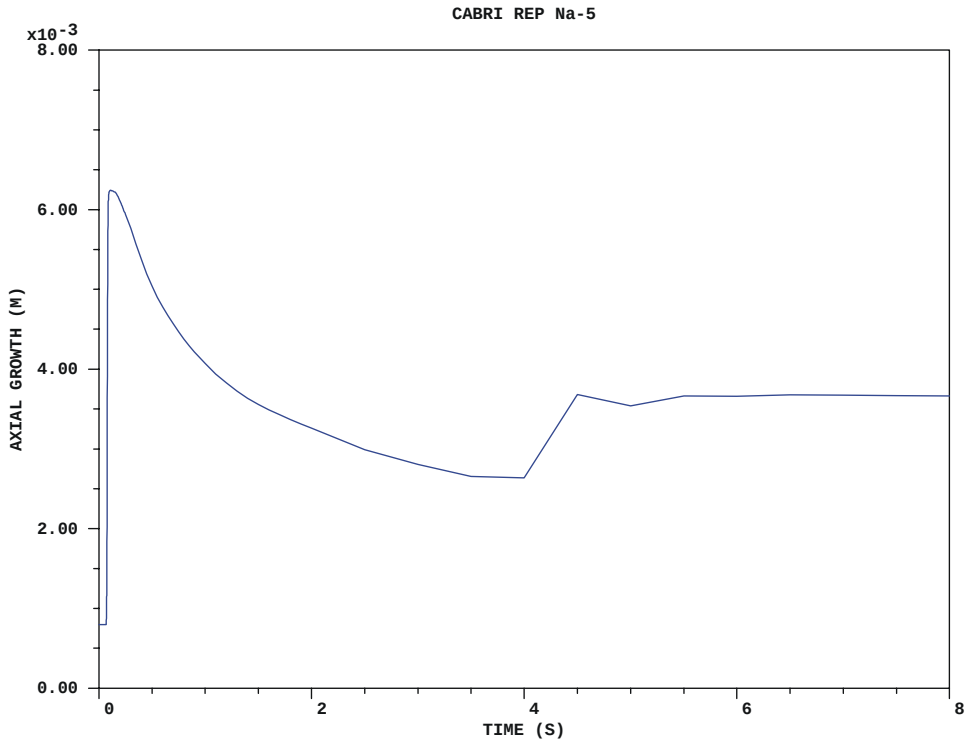

Figure 3-64
REP Na-5 Calculated Cladding Axial Elongation

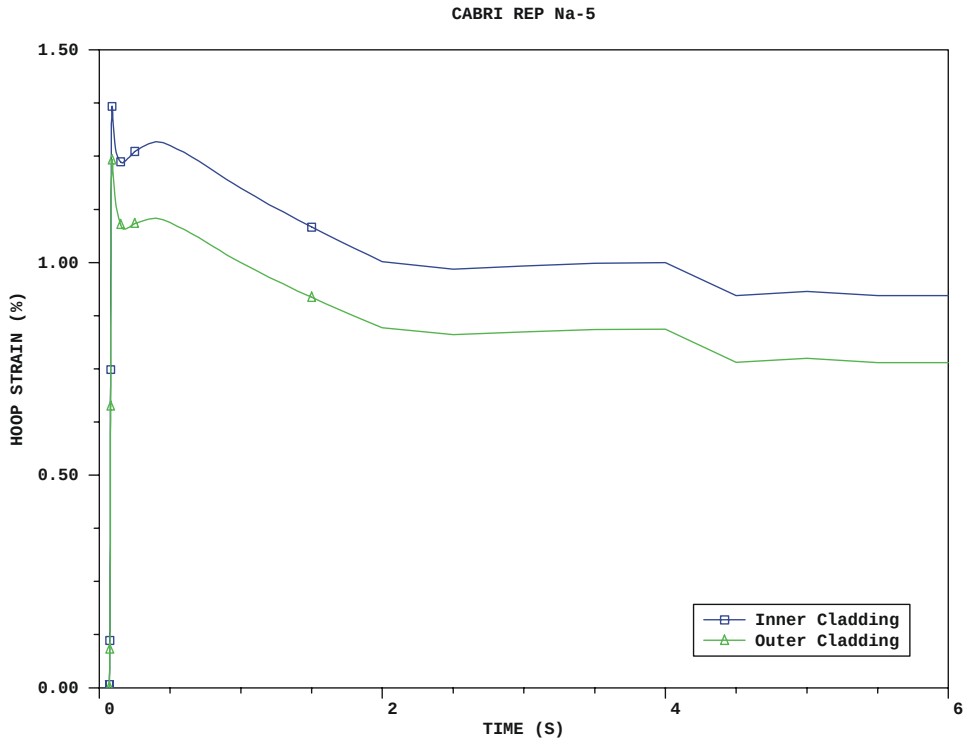

Figure 3-65
REP Na-5 Calculated Cladding Strain

Table 3-16
REP Na-5 Analysis Results Summary

	Cladding Elongation (mm)	Cladding Residual Strain (%)
Measured Data	6.3	1.1
FALCON	6.2	Inner Wall 0.92 Outer Wall 0.76

The power pulse used in the FALCON analysis of REP Na-5 was developed as an idealized Gaussian in the absence of more detailed information. In Figure 3-63, the power plotted is the linear power of the peak power node that represents a peaking factor of ~ 1.16 as compared to the segment average linear power. The fuel rod response to the narrow pulse used in REP Na-5 is essentially adiabatic. Meaning that the pulse terminates before heat conduction within the fuel decreases the fuel enthalpy. As shown in Figure 3-63, at the beginning of the transient the fuel enthalpy is ~ 16.7 cal/g corresponding to the pre-transient sodium temperature of 280 ˚C. The fuel enthalpy then rises in response to the energy deposited into the fuel as a result of the power pulse. After stabilizing at a peak value of 116.8 cal/g, the fuel enthalpy eventually drops back down to its pretest value ~ 100 s after the test (not shown due to the time scale in the plot).

Figures 3-64 and 3-65 present the computed transient response of the cladding axial elongation and hoop strains, respectively, during the test. As shown in Table 3-16 the FALCON predicted values match the measured data quite well. The peak axial elongation occurred at 0.11 s into the transient and reached a value of 6.2 mm. The peak cladding hoop strains occurred slightly earlier at 0.9 s and were 1.37% and 1.24% for the inner and outer cladding wall locations, respectively. A more detailed description of the RIA capabilities of FALCON can be found in Reference 14.

3.10 References

1. *Fuel Analysis and Licensing Code: Falcon MOD01: Volume 1: Theoretical and Numerical Bases,* EPRI, Palo Alto, CA: 2004. 1011307.
2. Lyon, W.F., Montgomery, R,.O., Zangari, A.J., Sunderland, D.J., Rashid, Y.R., and Dunham, R.S., "Fuel Performance Analysis Capability in FALCON," Final Report, TR-1002866, EPRI, Palo Alto, CA, December 2002.
3. Garner, R.W., Sparks, D.T., Smith, R.H., Klink, P.H., Schwieder, D.H., and MacDonald. P.E., “Gap Conductance Test Series-2, Test Results Report for Tests GC2-1, GC2-2, and GC2-3,” NUREG/CR-0300, TREE-1268, EG&G Idaho, November 1978.
4. Bird, R.E., Stewart W.E., and Lightfoot E.N., Transport Phenomena, John Wiley and Sons, Inc., p. 357.
5. Montgomery, R.O., Zangari, A.J., Rashid, Y.R., "FREY-01 – Fuel Rod Evaluation System, Vol. 4 Verification and Validation Manual," ANATECH Research Corporation, NP-3277-CCM, Rev. 2, January 1993.

6. Bennett, A.W., Hewitt, G.F., Kearsy, K.A. Keeys, R.K.F., "Heat Transfer to Steam-Water Mixtures Flowing in Uniformly Heated Tubes in which the Critical Heat Flux has been Exceeded," AERE-R 5373, 1967.
7. Bennett, J.A.R., Collier, J.G., Pratt, H.R.C., Thronton, J.D.T., "Heat Transfer to Two-Phase Gas-Liquid Systems, Part 1: Steam-Water Mixtures in the Liquid Dispersed Region in an Annulus" AERE-R 3159, 1959.
8. Mehner, A.S., Vinjamuri, K., “Fuel Rod Behavior During the Test PCM-2,” NUREG/CR-0647, Idaho National Engineering Laboratory, April 1979.
9. Martinson, Z.R., McCardell, R.K., “Power-Cooling-Mismatch Test Series Test PCM-2 Test Results Report,” TREE-NUREG-1038, Idaho National Engineering Laboratory, February 1977.
10. Seiffert, S.L., “Power-Cooling-Mismatch Test Series Test PCM-2 Post-Irradiation Examinations,” TREE-NUREG-1069, Idaho National Engineering Laboratory, March 1977.
11. Lorenz, R. A., et al., “Final Report on the First Fuel Rod Failure Transient Test of a Zircaloy-Clad Fuel Rod Cluster in TREAT,” ORNL-4635, Oak Ridge National Laboratory, March 1971.
12. Montgomery, R.O., Rashid, Y.R., "Evaluation of Irradiated Fuel During RIA Simulation Tests," TR-106387, EPRI, Palo Alto, CA. 1996.
13. Frizonnet, J.M., Breton, J.P., Rigat, R., Papin, J., "The Main Outcomes from the Interpretation of the CABRI REP-Na Experiments for RIA Study," proceedings of the AND Topical Meeting on Light Water Reactor Fuel Performance, Portland, OR, March 2-6, 1997.
14. Montgomery, R.O., Sunderland, D., "Analysis of Reactivity Initiated Accident-Simulation Tests Conducted at the CABRI and NSRR Facilities in France and Japan," EPRI, Palo Alto, CA. 2004. 1002863.

4
SUMMARY

The verification and validation program for FALCON MOD01 has been completed. Its primary goal was to demonstrate the predictive capability of FALCON for both PWR and BWR LWR fuels under steady state and transient operating conditions and to provide guidance for future development activities. To achieve this, a fuel rod database was developed and used to evaluate the implementation of the numerous material property and behavioral model modifications and additions made to FALCON MOD01.

The FALCON fuel rod database contains 159 cases comprised of analytical models and instrumented, test program, and commercial fuel rods. The rods chosen for inclusion into the database represented a wide range of fuel design variants, irradiation environments, and burnups. The sources for these cases included the ESCORE and FREY fuel rod databases, Halden test reactor programs, and EPRI, U.S. Department of Energy, NRC, and commercial utility fuel test programs. An analysis data request form was developed to facilitate gathering data for inclusion into the FALCON V&V database. This form lists detailed data requirements including fuel and cladding dimensions, thermal hydraulic parameters, rod design data, and power history/axial shape data needed for FALCON fuel performance analyses. The fuel cases were prioritized using selection criteria based on a variety of factors: high rod average burnup (up to or exceeding ~ 70 GWd/TU), relevancy of fuel rod design, and availability of applicable/required experimentally measured data. The selection criteria also took into consideration the results of earlier reviews of the ESCORE validation, the recommendations made during the FALCON peer review, and the FREY transient validation database.

The verification activity was conducted as an iterative benchmark testing and revision process on newly added or developed primary material property and behavioral models affecting the steady state analysis capability of the code. The technical areas of verification testing were fuel rod thermal performance, fission gas release, cladding creep, and cladding irradiation growth. The evaluation of these areas was accomplished by using several selected subsets from the fuel rod database. The selection of these subsets was determined by the availability of the required measured data. The verification process led to several changes in FALCON that substantially improved its performance. These included the modification of the overall thermal/mechanical iteration scheme. This change eliminated gap closure oscillations (“gap chatter”) under low gap conductivity conditions such as present with Xe or Ar fill gases. Adjustments to the Forsberg – Massih FGR model saturation and release criteria and the addition of an athermal release model improved FGR performance. Feedback from the analysis of cladding creep data led to changes in the fuel swelling model that greatly improved cladding creep strain predictions.

After the completion of the verification process, validation testing was conducted as a single run of the remaining inventory of fuel rod cases. Comparisons of the calculated values to analytical and experimentally measured data for fuel temperature, fission gas release, cladding diametral

creep strain, cladding irradiation (axial) growth, cladding corrosion, fuel rod internal void volume, fuel rod internal pressure, and coolant channel enthalpy and temperature were completed. The performance of FALCON MOD01 in each of these categories was evaluated based on these comparisons. Additionally, several transient cases were run to demonstrate the applicability of FALCON in the areas of power/coolant mismatch, LOCA, and RIA.

With the completion of the verification and validation program, the applicability of FALCON MOD01 for steady state and transient analyses has been established. This activity has provided a solid basis for evaluation of the code and its material property and behavioral models and will provide guidance for the continued development of FALCON.

A
APPENDIX A: FALCON V&V FUEL ROD DATABASE

The following pages contain a listing of the rods and/or analytical cases populating the FALCON MOD01V&V database. The rods are organized by testing or commercial program. Information regarding the rod type, characteristics, and measured data available are also included in the listings. References for the data listed are noted in brackets and refer to the numerical reference list following the rod listing tables.

Appendix A: FALCON V&V Fuel Rod Database

Rod/ Group	Type/ Loction	No. of Rods	Avg Burnup	Temp	FGR	Cladding Creep	Corrosion	Axial Growth	Void Volume	Internal Pressure
Annular Flow	**Channel**	**1**	**GWd/tU**	**(^{0}C)**	**(%)**	**Dia Strain(%)**	**Avg. Ox. (μm)**	**(mm)**	**(cc)**	**(MPa)**
annular flow channel				[46]						
CABRI	**17x17 PWR**	**1**	**GWd/tU**	**(^{0}C)**	**(%)**	**Dia Strain(%)**	**Avg. Ox. (μm)**	**(mm)**	**(cc)**	**(MPa)**
REP NA-5	5-cycle rod		64			1.1 [47,48]	20 [47,48]	6.3 [47,48]		
Calvert Cliffs - I	**14X14 PWR**	**2**	**GWd/tU**	**(^{0}C)**	**(%)**		**Avg. Ox. (μm)**	**(inch)**	**(cc)**	**(MPa)**
AHS008	1-cycle rod		18.9		**0.3** [3]	[3]		**0.48** [3]	29-36 [3]	
NBD 144	4-cycle Rod		42		**1.5** [3]	[2]			29-36 [3]	
Calverts Cliffs Ext BU	**14X14 PWR**	**12**	**GWd/tU**	**(^{0}C)**	**(%)**	**Dia Strain(%)**	**Avg. Ox. (μm)**	**(inch)**	**(cc)**	**(Psia)**
BFJ027	STD/STD 1G006		58.726		**2** [4]	[5]	[5]	**1.569** [5]	**24.95** [4]	**535** [4]
BFL009	Anlr/STD 1G003		58.106		**1.6** [4]	[5]	[5]	**1.325** [5]	**38.91** [4]	**492** [4]
BEN013	STD/STD 1G003		59.835		**2.3** [4]	[5]	[5]	**1.166** [5]	**24.71** [4]	**552** [4]
UFE067 (higher enrich)	STD/STD C1H038		54.841		**2.6** [4]	[5]	[5]	**1.116** [5]	**24.66** [4]	**583** [4]
UFE019 (higher enrich)	STD/STD C1H038		46.791		**0.9** [4]	[5]	[5]	**1.116** [5]	**26.24** [4]	**514** [4]
BFM073	RL/STD 1G006		60.319		**2.9** [4]	[5]	[5]	**1.416** [5]	**27.73** [4]	**579** [4]
BFM070	RL/STD 1G006		60.761		**3.1** [4]	[5]	[5]	**1.322** [5]	**27.14** [4]	**593** [4]
BFM071	RL/STD 1G006		57.143		**2.3** [4]	[5]	[5]	**1.291** [5]	**27.7** [4]	**561** [4]
BFM034	STD/STD 1G003		63.451		**3.8** [4]	[5]	[5]	**1.353** [5]	**26.3** [4]	**624** [4]
BFM156	STD/STD 1G003		56.854		**1.4** [4]	[5]	[5]	**1.253** [5]	**28.2** [4]	**516** [4]
BFG092	STD/STD 1G003		57.95		**1.7** [4]	[5]	[5]	**1.54** [5]	**24.65** [4]	**527** [4]
BFM043	RL/STD 1G003		60.51		**3.0** [4]	[5]	[5]	**1.38** [5]	**27.35** [4]	**589** [4]

Rod/ Group	Type/ Loction	No. of Rods	Avg Burnup	Temp	FGR	Cladding Creep	Corrosion	Axial Growth	Void Volume	Internal Pressure
DOE/BR-3	**PWR**	**1**	**GWd/tU**	**(^{0}C)**	**(%)**	**Dia Strain(%)**	**Avg. Ox. (μm)**	**(mm)**	**(cc)**	**(MPa)**
ROD 36I8V			59.60		**33.8** [6]					
Dresden 2	**9X9 BWR**	**7**	**GWd/tU**	**(^{0}C)**	**(%)**	**Dia Strain(%)**	**Avg. Ox. (μm)**	**(inch)**	**(cc)**	**(MPa)**
228 D9	CFR EOC-11		30.1		**-**	[7]	[7]	**0.689** [7]		
228 K9	CFR EOC-11		30.1		**-**	[7]	[7]	**0.619** [7]		
228 H2	CFR/NAF EOC-11		30.1		**-**	[7]	[7]	**0.724** [7]		
228 C3	CFR/NAF EOC-11		30.1		**-**	[7]	[7]	**0.793** [7]		
228 A01	CFR EOC-12		35.5		**0.88** [8]	[7]	[7]	**0.833** [8]		
228 B09	Zr4 EOC-12		35.5		**0.65** [8]	[7]	[7]	**0.976** [8]		
228 F09	CFR EOC-12		35.5		**0.24** [8]	[7]	[7]	**0.833** [8]		
Dresden 2	**8X8 BWR**	**3**	**GWd/tU**	**(^{0}C)**	**(%)**	**Dia Strain(%)**	**Peak Ox.(μm)**	**(inch)**	**(cc)**	**(MPa)**
220 B2	CFR/NAF EOC-12		34.2		**0.06** [8]	[8]	**31** [8]	**0.919** [8]		
220 A01	CFR EOC-12		34.2		**0.12** [8]	[8]		**0.919** [8]		
220 H8	CFR EOC-12		34.2		**0.13** [8]	[8]		**0.919** [8]		

CFR - Characterized Fuel Rod

NAF - Neutron Absorbing Fuel Rod (Gd2O3)

Zr4 - Zircaloy-4 Cladding

Rod/ Group	Type/ Loction	No. of Rods	Avg Burnup	Temp	FGR	Cladding Creep	Corrosion	Axial Growth	Void Volume	Internal Pressure
Enthalpy Rise	**channel**	**1**	**GWd/tU**	**(J/kg)**	**(%)**	**Dia Strain(%)**	**Avg. Ox. (μm)**	**(mm)**	**(cc)**	**(MPa)**
coolant channel				coolant enthalpy [49]						
FRF-1	**BWR**	**1**	**GWd/tU**	**(^{0}C)**	**(%)**	**Dia Strain (m)**	**Avg. Ox. (μm)**	**(mm)**	**(cc)**	**(MPa)**
L			0	[50]		[50]				[50]
Ft. Calhoun	**14X14 PWR**	**2**	**GWd/tU**	**(^{0}C)**	**(%)**	**Dia Strain(%)**	**Avg. Ox. (mils)**	**(mm)**	**(inch3)**	**(MPa)**
KJD-125	Assembly D005		47.4		**0.45** [9]		[9]		**1.402** [9]	
KJE-076	Assembly D005		48.3		**0.62** [9]		[9]		**1.349** [9]	
Grand Gulf	**9X9 BWR**	**19**	**GWd/tU**	**(^{0}C)**	**(%)**	**Dia Strain(%)**	**Avg. Ox. (μm)**	**(inch)**	**(cc)**	**(MPa)**
LTA901-A05	Large Pellet/ Medium Gap		39.9		**4.4** [11]	[11]	[11]	**1.231** [11]	**22.29** [11]	
LTA901-B01	Large Pellet/ Large Gap		39		**9** [11]	[11]	[11]	**1.212** [11]	**22.29** [11]	
LTA901-D02	Small Pellet/ Medium Gap		40.2		**1.2** [11]	[11]	[11]	**1.315** [11]	**19.17** [11]	
LTA901-E09	Large Pellet/ Medium Gap		39.9		**0.8** [11]	[11]	[11]	**1.236** [11]	**22.29** [11]	
LTA901-F08	Small Pellet/ Small Gap		40.2		**0.3** [11]	[11]	[11]	**1.358** [11]	**19.17** [11]	
LTA901-K05	Large Pellet/ Medium Gap		39.9		**2.3** [11]	[11]	[11]	**1.252** [11]	**22.29** [11]	
LTA901-B04	Small Pellet/ Medium Gap		40.2		**2.0** [11]	[11]	[11]	**1.403** [11]	**19.17** [11]	
LTA901-D01	Large Pellet/ Small Gap		40.2		**1.8** [11]	[11]	[11]	**1.187** [11]	**22.29** [11]	
LTA901-D09	Large Pellet/ Medium Gap		40.2		**1.3** [11]	[11]	[11]	**1.233** [11]	**22.29** [11]	
LTA901-E01	Large Pellet/ Medium Gap		39.9		**2.9** [11]	[11]	[11]	**1.266** [11]	**22.29** [11]	
LTA901-F01	Large Pellet/ Large Gap		40.2		**3.1** [11]	[11]	[11]	**1.256** [11]	**22.29** [11]	
LTA901-F09	Large Pellet/ Large Gap		40.2		**3.8** [11]	[11]	[11]	**1.267** [11]	**22.29** [11]	
LTA901-H06	Small Pellet/ Lagre Gap		40.2		**2.1** [11]	[11]	[11]	**1.377** [11]	**22.29** [11]	

Rod/ Group	Type/ Loction	No. of Rods	Avg Burnup	Temp	FGR	Cladding Creep	Corrosion	Axial Growth	Void Volume	Internal Pressure
Grand Gulf	**9X9 BWR**	**19**	**GWd/tU**	**(^{0}C)**	**(%)**	**Dia Strain(%)**	**Avg. Ox. (μm)**	**(inch)**	**(cc)**	**(MPa)**
LTA901-H09	Large Pellet/ Large Gap		39		**2.9** [11]	[11]	[11]	**1.275** [11]	**22.29** [11]	
LTA901-K04	Large Pellet/ Large Gap		40.2		**3.7** [11]	[11]	[11]	**1.309** [11]	**22.29** [11]	
LTA901-K06	Large Pellet/ Small Gap		40.2		**2.1** [11]	[11]	[11]	**1.230** [11]	**22.29** [11]	
LTA901-K08	Large Pellet/ Small Gap		39		**1.2** [11]	[11]	[11]	**1.243** [11]	**22.29** [11]	
LTA901-A02	Large Pellet/ Large Gap		39		**5.2** [11]	[11]	[11]	**1.241** [11]	**22.29** [11]	
LTA901-A06	Large Pellet/ Large Gap		40.2		**3.5** [11]	[11]	[11]	**1.214** [11]	**22.29** [11]	
Grohnde	**16X16 PWR**	**6**	**GWd/tU**	**(^{0}C)**	**(%)**	**Dia Strain(%)**	**Peak Ox.(μm)**	**(%)**	**(cc)**	**(MPa)**
436-H16	R2 Clad		45.2			[12]	[12]			
436-k01	R2 Clad		44.6			[12]	[12]			
436-k16	R1 Cladding		45.1			[12]	[12]			
437-A08	R2 Cladding		45.2			[12]	[12]	**0.79** [12]		
437-A09	R1 Cladding		45.1			[12]	[12]	**0.92** [12]		
437-T09	R2 Cladding		44.6			[12]	[12]	**0.80** [12]		
HB Robinson	**15X15 PWR**	**11**	**GWd/tU**	**(^{0}C)**	**(%)**	**Dia Strain(%)**	**Avg. Ox. (μm)**	**(inch)**	**(cc)**	**(MPa)**
RA18235	S-15H, A02 G-38, D05		66.7		**2.4** [13]	[13]	[13]	**1.889** [13]	**16.18** [13]	**4.39** [13]
RA18229	S-15H, B05 G-38, D06		66.5		**2.3** [13]	[13]	[13]	**1.841** [13]	**15.14** [13]	**4.53** [13]
RA18293	S-15H, E02 G-38, F04		66.5		**2.1** [13]	[13]	[13]	**1.674** [13]	**16.33** [13]	**4.121** [13]

Rod/ Group	Type/ Loction	No. of Rods	Avg Burnup	Temp	FGR	Cladding Creep	Corrosion	Axial Growth	Void Volume	Internal Pressure
HB Robinson	**15X15 PWR**	**11**	**GWd/tU**	**(^{0}C)**	**(%)**	**Dia Strain(%)**	**Avg. Ox. (μm)**	**(inch)**	**(cc)**	**(MPa)**
RA19867	S-15H, R05 G-38, N06		66.5		**2.2** [13]	[13]	[13]	**1.950** [13]	**16.45** [13]	**4.236** [13]
BL219926 (contain 10% Gd)	S-15H, H05 S-31, H05		47.4		**1.4** [13]	[13]	[13]	**1.455** [13]		
RA18300	S-15H, G10 G-38, G10		63.8		**1.9** [13]	[13]	[13]	**1.822** [13]	**14.6** [13]	**4.3194** [13]
RA18308	S-15H, F07 G-38, F07		63.8		**1.4** [13]	[13]	[13]	**1.785** [13]	**17.43** [13]	**3.6283** [13]
RA19865	S-15H, S02 G-38, N05		66.8		**2.4** [13]	[13]	[13]	**1.89** [13]	**16.38** [13]	**4.2646** [13]
RA18302	S-15H, B01 G-38, E04		66.7		**2.0** [13]	[13]	[13]	**1.834** [13]	**16.54** [13]	**3.9523** [13]
BG02 438	S-15H, A10 S15, A10		62.8		**2.5** [13]	[13]	[13]	**1.955** [13]	**16.11** [13]	**4.4812** [13]
RA11 0889	S-15H, R01 G-38, M04		66.9		**1.6** [13]	[13]	[13]	**2.014** [13]	**14.91** [13]	**1.256** [13]
HBC	**PWR**	**1**	**GWd/tU**	**(^{0}C)**	**(%)**	**Dia Strain(%)**	**Avg. Ox. (μm)**	**(mm)**	**(cc)**	**(MPa)**
HBC BN 1066			48.20		**5.3** [14]					
HBEP	**PWR/BWR**	**4**	**GWd/tU**	**(^{0}C)**	**(%)**	**Dia Strain(%)**	**Avg. Ox. (μm)**	**(mm)**	**(cc)**	**(MPa)**
HBEP GE 10-1			31.4		**5.2** [15]					
HBEP GE 10-2			28.9		**0.1** [15]					
HBEP GE 14-2			32.1		**0.15** [15]					
HBEP W 17A			46.1		**0.5** [15]					
HBEP ABB	**8X8 BWR**	**6**	**GWd/tU**	**(^{0}C)**	**(%)**	**Avg Strain(%)**	**Avg. Ox. (μm)**	**(mm)**	**(cc)**	**(MPa)**
A1/8-4	TVO-1 6-cycle		48.5		**0.3** [16]	**0.8** [16]	[17]	**13.12** [16]	**27.9** [16]	**0.485** [16]
A1/8-6	TVO-1 5-cycle		44.9		**3.4** [16]	**0.5** [16]	[17]	**17.29** [16]	**30.1** [16]	**0.884** [16]

Rod/ Group	Type/ Loction	No. of Rods	Avg Burnup	Temp	FGR	Clad Creep	Corrosion	Axial Growth	Void Volume	Internal Pressure
HBEP ABB	**8X8 BWR**	**6**	**GWd/tU**	**(^{0}C)**	**(%)**	**Avg Strain(%)**	**Avg. Ox. (μm)**	**(mm)**	**(cc)**	**(MPa)**
A3/6-4	TVO-1 6-cycle		47.8		**1** [16]	(**-0.1**) [16]	[17]	**14.24** [16]	**28.5** [16]	**0.647** [16]
E8/27-6	TVO-1 5-cycle		43.7		**1** [16]	**0** [16]	[17]	**18.36** [16]	**30.9** [16]	**0.62** [16]
H8/36-4	TVO-1 6-cycle		46.6		**17.3** [16]	**0.4** [16]	[17]	**11.42** [16]	**29.2** [16]	**2.865** [16]
H8/36-6	TVO-1 5-cycle		44.6		**11.2** [16]	**0.7** [16]	[17]	**12.68** [16]	**29.5** [16]	**1.964** [16]
HBEP BNFL	**PWR**	**5**	**GWd/tU**	**(^{0}C)**	**(%)**	**Dia Strain(%)**	**Avg. Ox. (μm)**	**(mm)**	**(cc)**	**(MPa)**
373 Rod AK	Pressurized		43		**4.1** [15]				**10.24** [15]	
373 Rod BH	Non-pressurized		42.6		**7.6** [15]				**9.81** [15]	
373 Rod BP	Non-pressurized		38.1		**7.3** [15]				**9.91** [15]	
373 Rod CQ	Non-pressurized		42.1		**6.6** [15]				**9.45** [15]	
373 Rod DF	Pressurized		46.9		**4** [15]				**9.67** [15]	
IFA 418	**HBWR**	**1**	**GWd/tU**	**(^{0}C)**	**(%)**	**Dia Strain(%)**	**Avg. Ox. (μm)**	**(mm)**	**(cc)**	**(MPa)**
IFA-418 Rod 2			13.6		**0.2** [3]					
IFA 432	**HBWR**	**1**	**GWd/tU**	**(^{0}C)**	**(%)**	**Dia Strain(%)**	**Avg. Ox. (μm)**	**(mm)**	**(cc)**	**(MPa)**
IFA-432.3			28.9		**10.0** [20]					
IFA 504	**HBWR**	**3**	**GWd/tU**	**(^{0}C)**	**(%)**	**Dia Strain(%)**	**Avg. Ox. (μm)**	**(mm)**	**(cc)**	**(MPa)**
IFA 504	Argon Filled		26.4	[22]						
IFA 504	Helium Filled		26.4	[22]						
IFA 504	Xenon Filled		26.4	[22]						

Appendix A: FALCON V&V Fuel Rod Database

Rod/ Group	Type/ Loction	No. of Rods	Avg Burnup	Temp	FGR	Cladding Creep	Corrosion	Axial Growth	Void Volume	Internal Pressure
IFA 505.5	**HBWR**	**3**	**GWd/tU**	**(^{0}C)**	**(%)**	**Dia Strain(%)**	**Avg. Ox. (μm)**	**(mm)**	**(cc)**	**(MPa)**
IFA 505.5 Rod 1			40	[23]						
IFA 505.5 Rod 2			40	[23]						
IFA 505.5 Rod 3			40	[23]						
IFA 509.1	**HBWR**	**3**	**GWd/tU**	**(^{0}C)**	**(%)**	**Dia Strain(%)**	**Avg. Ox. (μm)**	**(mm)**	**(cc)**	**(MPa)**
IFA 509.1 Rod 1			14	[23]						
IFA 509.1 Rod 2			14	[23]						
IFA 509.1 Rod 3			14	[23]						
IFA 515.10	**HBWR**	**2**	**GWd/tU**	**(^{0}C)**	**(%)**	**Dia Strain(%)**	**Avg. Ox. (μm)**	**(mm)**	**(cc)**	**(MPa)**
Rod A1			55	[23]						
Rod A2	contain 8% Gd		55	[23]						
IFA 519.9	**HBWR**	**1**	**GWd/tU**	**(^{0}C)**	**(%)**	**Dia Strain(%)**	**Avg. Ox. (μm)**	**(mm)**	**(cc)**	**(MPa)**
Rod DH			91.2		**57.4** [23]					
IFA 533.2	**HBWR**	**1**	**GWd/tU**	**(^{0}C)**	**(%)**	**Dia Strain(%)**	**Avg. Ox. (μm)**	**(mm)**	**(cc)**	**(MPa)**
Rod 808			51.5		**7.0** [27]					
IFA 562.1	**HBWR**	**6**	**GWd/tU**	**(^{0}C)**	**(%)**	**Dia Strain(%)**	**Avg. Ox. (μm)**	**(mm)**	**(cc)**	**(MPa)**
Rod-5			14.0	[23]						
Rod-6			14.0	[23]						
Rod-7			14.0	[23]						

Rod/ Group	Type/ Loction	No. of Rods	Avg Burnup	Temp	FGR	Cladding Creep	Corrosion	Axial Growth	Void Volume	Internal Pressure
IFA 562.1	**HBWR**	**6**	**GWd/tU**	**(^{0}C)**	**(%)**	**Dia Strain(%)**	**Avg. Ox. (μm)**	**(mm)**	**(cc)**	**(MPa)**
Rod-10			14.0	[23]						
Rod-11			14.0	[23]						
Rod-12			14.0	[23]						
IFA 597	**HBWR**	**1**	**GWd/tU**	**(^{0}C)**	**(%)**	**Dia Strain(%)**	**Avg. Ox. (μm)**	**(mm)**	**(cc)**	**(MPa)**
Rod-8	Base Irradiation		63.3		**10.0** [23]					
IFA 636.1	**HBWR**	**2**	**GWd/tU**	**(^{0}C)**	**(%)**	**Dia Strain(%)**	**Avg. Ox. (μm)**	**(mm)**	**(cc)**	**(MPa)**
Rod 2	contain 8% Gd		21.0	[29]						
Rod-7			21.0	[29]						
KKL	**8X8 BWR**	**3**	**GWd/tU**	**(^{0}C)**	**(%)**	**Dia Strain(%)**	**Avg. Ox. (μm)**	**(mm)**	**(ml)**	**(Bar)**
Rod D2	GE-10 KLG072		27.3		**8.2** [30]	[30]	[30]	**9.7** [30]	**27.6** [30]	**14** [30]
Rod F5 (contain 3% Gd)	GE-10 KLG105		46.69		**11.64** [31]	[31]	[31]	**10.60** [31]	**37.6** [31]	**21.1** [31]
Rod F6	GE-11 LYT982		43.57		**8.1** [31]	[31]	[31]	**11.0** [31]	**29.9** [31]	**21.5** [31]
Limerick	**9X9 BWR**	**7**	**GWd/tU**	**(^{0}C)**	**(%)**	**Dia Strain(%)**	**Avg. Ox. (μm)**	**(inch)**	**(cc)**	**(MPa)**
YJ1433 E9	GE11 UO_2 Rod		55.6		**19.31** [33]	[32]	[32]	**0.715** [32]	**30.7** [33]	
YJ1433 F9	GE11 UO_2 Rod		55.7		**19.40** [33]	[32]	[32]	**0.725** [32]	**31.2** [33]	
YJ1433 G1	GE11 UO_2 Tie Rod		53.8		**15.59** [33]			**1.84** [32]	**29.9** [33]	
YJ1433 J3	GE11 UO_2 Tie Rod		53.7		**10.88** [33]			**1.805** [32]	**28.4** [33]	

Rod/ Group	Type/ Loction	No. of Rods	Avg Burnup	Temp	FGR	Cladding Creep	Corrosion	Axial Growth	Void Volume	Internal Pressure
Limerick	**9X9 BWR**	**7**	**GWd/tU**	**(^{0}C)**	**(%)**	**Dia Strain(%)**	**Avg. Ox. (μm)**	**(inch)**	**(cc)**	**(MPa)**
YJ1433 J7	GE11 UO_2 Tie Rod		54.7		**6.33** [33]			**1.817** [32]	**29.8** [33]	
YJ1433 J4	GE11 UO_2 Rod		57.0		**13.12** [33]			**0.773** [32]	**29.4** [33]	
YJ1433 J6	GE11 UO_2 Rod		56.0		**16.72** [33]			**0.781** [32]	**30.1** [33]	
Oconee	**15X15 PWR**	**1**	**GWd/tU**	**(^{0}C)**	**(%)**	**Avg Strain(%)**	**Avg. Ox. (μm)**	**(mm)**	**(cc)**	**(Psi)**
15159 A1	Assembly 1D45		49.5		**2.2** [34]	**(-1.0465)** [34]	[34]		**27** [34]	**611** [34]
OPPD/DOE	**PWR**	**3**	**GWd/tU**	**(^{0}C)**	**(%)**	**Dia Strain(%)**	**Avg. Ox. (μm)**	**(mm)**	**(cc)**	**(MPa)**
D005	KJE076		49.5		**0.6** [3]				**22-29** [3]	
D013	KJN052		29.6		**0.3** [3]				**22-29** [3]	
D038	KKM095		38.7		**0.4** [3]				**22-29** [3]	
Over Ramp	**PWR**	**3**	**GWd/tU**	**(^{0}C)**	**(%)**	**Dia Strain(%)**	**Avg. Ox. (μm)**	**(mm)**	**(cc)**	**(MPa)**
A10/3 Studsvik Over Ramp			12.72		**30.3** [37]			**0.6** [37]		
W 5/4 Studsvik Over Ramp			18.1		**4.37** [37]			**2.75** [37]		
W 5/5 Studsvik Over Ramp			23.8		**5.14** [37]			**3.36** [37]		
PBF GC2-2	**BWR**	**2**	**GWd/tU**	**(^{0}C)**	**(%)**	**Avg Strain(%)**	**Avg. Ox. (μm)**	**(mm)**	**(cc)**	**(MPa)**
522-2	Ar-filled		0	[51]						
522-4	He-filled		0	[51]						
PBF PCM-2	**PWR**	**1**	**GWd/tU**	**(^{0}C)**	**(%)**	**Avg Strain(%)**	**Avg. Ox. (μm)**	**(mm)**	**(cc)**	**(MPa)**
UTA-008			0	[52,53,54]						
Peach Bottom 3	**8X8 BWR**	**2**	**GWd/tU**	**(^{0}C)**	**(%)**	**Avg Strain(%)**	**Avg. Ox. (μm)**	**(mm)**	**(cc)**	**(Psi)**
F4	DJD-0224		30.8		**4.8** [38]				**45.99** [38]	**45.99** [38]
C3	DJD-0220		33		[38]				[38]	[38]
PETTEN/DOE	**PWR**	**9**	**GWd/tU**	**(^{0}C)**	**(%)**	**Dia Strain(%)**	**Avg. Ox. (μm)**	**(mm)**	**(cc)**	**(MPa)**
DOE 1/23			33		**40.8** [3]					

Rod/ Group	Type/ Loction	No. of Rods	Avg Burnup	Temp	FGR	Cladding Creep	Corrosion	Axial Growth	Void Volume	Internal Pressure
PETTEN/DOE	**PWR**	**9**	**GWd/tU**	**(^{0}C)**	**(%)**	**Dia Strain(%)**	**Avg. Ox. (μm)**	**(mm)**	**(cc)**	**(MPa)**
V30/05			31.4		**25.6** [3]					
V40/4			42.6		**12.6** [3]					
V40/1			46.9		**26.6** [3]					
V40/2			46.8		**42.2** [3]					
V40/3			46.2		**29.5** [3]					
V30/2			32.1		**35.0** [3]					
DOE 1/24			33.5		**33.6** [3]					
V 40/5			45		**11.4** [3]					
Quad Cities 1	**8X8 BWR**	**1**	**GWd/tU**	**(^{0}C)**	**(%)**	**Dia Strain(%)**	**Avg. Ox. (μm)**	**(mm)**	**(cc)**	**(MPa)**
Rod G7	Assembly LJB-586		42		**0.3** [9]					
RISO III	**PWR/BWR**	**4**	**GWd/tU**	**(^{0}C)**	**(%)**	**Dia Strain(%)**	**Avg. Ox. (μm)**	**(mm)**	**(cc)**	**(MPa)**
RISO III AN2			41.54		**29.7** [39]					
RISO III AN3			42.18		**35.5** [39]					
RISO III GE4			23.3		**27.0** [39]					
RISO III GE7			40.7		**14.4** [39]					
Super Ramp	**PWR**	**1**	**GWd/tU**	**(^{0}C)**	**(%)**	**Dia Strain(%)**	**Avg. Ox. (μm)**	**(mm)**	**(cc)**	**(MPa)**
PK2/1	Studsvik Super Ramp		45.2		**28.3** [39]					

Appendix A: FALCON V&V Fuel Rod Database

Rod/ Group	Type/ Loction	No. of Rods	Avg Burnup	Temp	FGR	Cladding Creep	Corrosion	Axial Growth	Void Volume	Internal Pressure
Transient Cond.		**1**	**GWd/tU**	**(^{0}C)**	**(%)**	**Dia Strain(%)**	**Avg. Ox. (μm)**	**(mm)**	**(cc)**	**(MPa)**
pellet	bare fuel pellet			[55]						
Tribulation	**PWR**	**4**	**GWd/tU**	**(^{0}C)**	**(%)**	**Dia Strain(%)**	**Avg. Ox. (μm)**	**(mm)**	**(cc)**	**(MPa)**
Tribulation W 109			49.3		**0.75** [39]					
Tribulation W 217			29.3		**0.2** [39]					
Tribulation W 220			51.1		**1.3** [39]					
Tribulation W 324			57.2		**6.7** [39]					
Vertical Pipe Flow	**Channel**	**1**	**GWd/tU**	**(^{0}C)**	**(%)**	**Dia Strain(%)**	**Avg. Ox. (μm)**	**(mm)**	**(cc)**	**(MPa)**
verical tube				[56]						
Zorita	**PWR**	**9**	**GWd/tU**	**(^{0}C)**	**(%)**	**Dia Strain(%)**	**Avg. Ox. (μm)**	**(mm)**	**(cc)**	**(MPa)**
Rod 328	Pressurized		34.9		**11.7** [44]				**30.5** [44]	
Rod 332	Pressurized		57.5		**20.9** [44]				**28.3** [44]	
Rod 335	Pressurized		40.5		**12.4** [44]				**29.5** [44]	
Rod 384	Non-pressurized		54.1		**23.9** [44]				Not Measured	
Rod 386	Pressurized		54.4		**22.6** [44]				**29.0** [44]	
Rod 331	Pressurized		40.8		**7.3** [44]				**31.0** [44]	
Rod 334	Non-pressurized		53.6		**23.0** [44]				**22.2** [44]	
Rod 344	Pressurized		53.8		**16.9** [44]				Not Measured	
Rod 385	Pressurized		550		**13.2** [44]				**28.0** [44]	

A.1 References

1. Bessette, D. E., Hatfield, S. C., Van Saun, P. A., Baciarelli, R. M., " Examination of Calvert Cliffs-1 Test Fuel Assemblies at End of Cycles 1 and 2," EPRI, Palo Alto, CA, Sept 1978, RP 586-1
2. Ruzauskas, E. J., Lavake, J. C., Weber, R. G., " Examination of Calvert Cliffs-1 Test Fuel Assemblies After Cycle 4," EPRI, Palo Alto, CA, Oct 1981, CE NPSD-146
3. Fancher, R. B., Fiero, I. B., Freeburn, H. R., Garde, A. M., Kennard, M. W., Krammen, M. A., Smerd, P. G., Yackle, N. T., " ESCORE: The EPRI Steady-State Core Reload Evaluator Code," Vol-1, EPRI, Palo Alto, CA, August 1986, EPRI NP-4492-CCMP
4. Smith, G. P., Pirek, R. C., Griffiths, M., " Hot Cell Examination of Extended Burnup Fuel From Calvert Cliffs-1," EPRI, Palo Alto, CA, July 1994, Vol-2, TR-103302-V2
5. Examination of the PROTOTYPE and 1H038 Assemblies after Reactor Cycle 9 in Calvert Cliffs Unit 1, EPRI, Palo Alto, CA, Nov 1992, CE NPSD-493-NP
6. Balfour, M. G., Chubb, W. C., Boyle, R. F., "BR-3 High Burnup Fuel Rod Hot Cell Program, Volume 2: Data Summary," Westinghouse Electric Corporation Report, November 1982, WCAP-10238.
7. Bain, G. M., " 9X9 BWR Fuel Demonstration, Third Poolside Examination of Lead Test Assemblies," Advanced Nuclear Fuels Corporation, Sept 1989, ANF-89-100
8. Bain, G. M., "Performance of 9X9 Demonstration Assemblies in Dresden-2," EPRI, Palo Alto, CA, June 1992, TR-100752
9. Montgomery, R., Kurkchubasche, I., Parker, D., "ESCORE Re-evaluation with Expanded Validation Set," ANA-92-0126
10. Dey, W. C., Packard, D. R., "Preirradiation Characterization of Two of Four 9X9-5 Grand Gulf XN-1.3 Lead Fuel Assemblies," July 1989, ANF-89-092 (P)
11. Painter, D. B., "Inspection of SPC 8X8 and 9X9 Fuel Assemblies at Grand Gulf," Sept 1994, EMF-94-195 (P)
12. Bain, G. M., " Behavior of Duplex and Reference Fuel Cladding in the Grohnde PWR," EPRI, Palo Alto, CA, Nov 1995, TR-105358
13. Design, Operation, and performance Data for High Burnup PWR Fuel from the H. B. Robinson Plant for Use in the NRC Experimental Program at Argonne National Laboratory, EPRI, Palo Alto, CA: 2001. 1001558
14. Blanpain, P., "Task 3: Power-To-Melt Experiment," HBC International Program Report, January 1989, BN Reference No.: 06324/221
15. Lanning, D. D., Cunningham, M. E., Bradley, E. R., Barner., J. O., "Qualification of Fission Gas Release Data from Task 2 Rods," Battelle Pacific Northwest Laboratories, Richland, WA, November 1987, HBEP-25 (2P4)
16. Cunningham, M. E., Lanning, D. D., Barner., J. O., "Qualification of Fission Gas Release Data from Task 3 Rods," Battelle Pacific Northwest Laboratories, Richland, WA, January 1990, HBEP-60 (3P26)

17. Barner., J. O., Cunningham, M. E., Freshley, M. D., Lanning, D. D., "High Burnup Effects Program Final Report," Battelle Pacific Northwest Laboratories, Richland, WA, April 1990, HBEP-61 (3P27)

18. Thompson, J. F., Bell, A. W., Pearce, J. H., Taylor, C., " Destructive and Special Examinations of Three BWR Fuel Rods Irradiated in TVO-1- Task 3," Battelle Pacific Northwest Laboratories, Richland, WA, July 1989, HBEP-58 (3P24)

19. Lanning, D.D., Bradley, E.R., " Final Irradiation And Postirradiation Data From The NRC/PNL Instrumented Assembly IFA-432," Pacific Northwest Laboratory, Richland, Washington, HPR 329/7.

20. Turnbull, J. A., "Database for Halden Irradiation Experiment IFA-432," IFPE Database, CD 1, May 2002

21. Killen, J., Skattum, E., Haaland, A., " Review of Thermal Behavior and Fission Product Release From the Gas Flow Rig IFA-504," OECD Halden Reactor Project Report, April 1987, HWR-187

22. White, R. J., Haaland, A., Skattum, E., " Thermal Performance of Fuel in the Gas Flow Rods IFA-430 (USNRC/EG&G) and IFA-504 (HP)," OECD Halden Reactor Project Report, HWR-0086, May 1983.

23. Beguin, S., Claudel, J., " Halden Input Deck for EPRI," EDF Report, Report ID # E-N-T-CN/01-00569.

24. Sheppard, D. O., " IFA-505 Data Report From Beginning of Life to August 1982," OECD Halden Reactor Project Report, May 1983, HPR 299

25. Patrakka, E., Stall, H. U., Kolstad, E., Granta, S., " 3-Rod Diameter Rig IFA-509 Data Report on Rod No. 3," OECD Halden Reactor Project Report, May 1983, HWR-93

26. Turnbull, J. A., " Concluding Report on Three PWR Rods Irradiated to 90 MWD/KG UO_2 in IFA-519.9: Analysis of Measurements Obtained In-Pile and by PIE," OECD Halden Reactor Project Report, January 2001, HWR-668

27. Devold, H., " Steady State and Transient Temperature Measurements on BWR-Type Fuel up to 70 MWd/Kg UO_2. (IFA-533.2)," OECD Halden Reactor Project Report, January 1998, HWR-531

28. Smith, M. R., " Final Report on the In-Pile Results from the Pellet Roughness Test in Rig IFA-562," OECD Halden Reactor Project Report, November 1989, HWR-245

29. Ruhmann, H., Beere, W., Lee, B., " Irradiation Performance Of Commercial UO_2 and (U, GD)O_2 Fuel; Updated of the Test IFA-636.1," OECD Halden Reactor Project Report, February 2001, HWR-672

30. Failure Root Cause of PCI Suspect Fuel Rods from Kernkraftwerk Leibstadt (KKL) Reactor: Part 2: PIE of Failed and Sibling Rods, EPRI, Palo Alto, CA: 2000. TR-111065-P2

31. Failure Root Cause of PCI Suspect Fuel Rods from Kernkraftwerk Leibstadt (KKL) Reactor: Part 1: PIE of High Burn-up Sound Fuel Rods, EPRI, Palo Alto, CA: 2000. TR-111065-P1.

32. Poolside Examination Data on High-Duty BWR Fuel Exposed to 52 GWd/MTU: Limerick 1 EOC7 GE11 Reload Assembly Poolside Examination, EPRI, Palo Alto, CA: 1999. TR-112048.

33. Hot Cell Examination of GE11 BWR Fuel Exposed to 52 GWd/MTU in Limerick 1: Volume 1, Fuel Characteristics, Operational History and Integral Fuel Rod Measurements, EPRI, Palo Alto, CA: 2001. 1003130.

34. The Hot Cell Examination of Oconee 1 Fuel Rods After Five Cycles of Irradiation. Babcock & Wilcox, DOE/ET/34212-50, BAW-1874, Oct 1986

35. Survey of Cladding Oxide Thickness on Extended Burnup Fuel Rods. Babcock & Wilcox, DOE/ET/34212-53, BAW-1819, Sept 1987

36. The Hot Cell Examination of Gadolina Lead Test Assembly Rods after One Cycle of Irradiation. Babcock & Wilcox, DOE/ET/34212-55, BAW-2003, Nov 1990

37. Djurle, S., " The Studsvik Over-Ramp Project," Final Report, April 1983, EPRI, Palo Alto, CA, NP-3007

38. Final Report of Boiling Water Reactor Fuel Rod Performance Evaluation Program, General Electric Report, NEDC-30845, Dec 1984

39. IFPE Database, OECD Nuclear Energy Data Back, CD 2, Release May 2002.

40. Knudsen, P., Bagger, C., Carlsen, H., Johansen, B. S., Misfeldt, I., Mogensen, M., "Final Report On The Risϕ Transient Fission Gas Release Project," Volume 1, December 1986, RISϕ-TFGP-R29.

41. Knudsen, P., Bagger, C., Carlsen, H., Johansen, B. S., Misfeldt, I., Mogensen, M., "Final Report On The Risϕ Transient Fission Gas Release Project," Volume 2, December 1986, RISϕ-TFGP-R29.

42. Djurle, S., "Final Report Of The Super-Ramp Project," Studsvik Report, December 1984, STUDSVK-STSR-32

43. Lange, R. A., and Sugarman, A. C., " Zorita Irradiation Program; Fuel Rod Fabrication," Westinghouse Report WCAP-7250 Rev. 1, October 1982.

44. Balfour, M. G., Roberts, E., DeQuidt E., and Blanc, P., "Zorita Research and Development Program: Volume 1, Final Report, Westinghouse Report, WCAP-10180 Volume 1, September 1982.

45. Balfour, M. G., Roberts, E., DeQuidt E., and Blanc, P., "Zorita Research and Development Program: Volume 2, Data Summary, Westinghouse Report, WCAP-10180 Volume 2, September 1982.

46. Bennett, J.A.R., Collier, J.G., Pratt, H.R.C., Thronton, J.D.T., "Heat Transfer to Two-Phase Gas-Liquid Systems, Part 1: Steam-Water Mixtures in the Liquid Dispersed Region in an Annulus" AERE-R 3159, 1959.

47. Montgomery, R.O., Rashid, Y.R., "Evaluation of Irradiated Fuel During RIA Simulation Tests," TR-106387, EPRI, Palo Alto, CA. 2004.

48. Montgomery, R.O., Sunderland, D., "Analysis of Reactivity Initiated Accident-Simulation Tests Conducted at the CABRI and NSRR Facilities in France and Japan," EPRI, Palo Alto, CA. 2004. 1002863.

49. Montgomery, R.O., Zangari, A.J., Rashid, Y.R., "FREY-01 – Fuel Rod Evaluation System, Vol. 4 Verification and Validation Manual," ANATECH Research Corporation, NP-3277-CCM, Rev. 2, January 1993.

50. Lorenz, R. A., et al., "Final Report on the First Fule Rod Failure Transient Test of a Zircaloy-Clad Fuel Rod Cluster in TREAT," ORNL-4635, Oak Ridge National Laboratory, March 1971.

51. Garner, R.W., Sparks, D.T., Smith, R.H., Klink, P.H., Schwieder, D.H., and MacDonald. P.E., "Gap Conductance Test Series-2, Test Results Report for Tests GC2-1, GC2-2, and GC2-3," NUREG/CR-0300, TREE-1268, EG&G Idaho, November 1978.

52. Mehner, A.S., Vinjamuri, K., "Fuel Rod Behavior During the Test PCM-2," NUREG/CR-0647, Idaho National Engineering Laboratory, April 1979.

53. Martinson, Z.R., McCardell, R.K., "Power-Cooling-Mismatch Test Series Test PCM-2 Test Results Report," TREE-NUREG-1038, Idaho National Engineering Laboratory, February 1977.

54. Seiffert, S.L., "Power-Cooling-Mismatch Test Series Test PCM-2 Post-Irradiation Examinations," TREE-NUREG-1069, Idaho National Engineering Laboratory, March 1977.

55. Bird, R.E., Stewart W.E., and Lightfoot E.N., Transport Phenomena, John Wiley and Sons, Inc., p. 357.

56. Bennett, J.A.R., Collier, J.G., Pratt, H.R.C., Thronton, J.D.T., "Heat Transfer to Two-Phase Gas-Liquid Systems, Part 1: Steam-Water Mixtures in the Liquid Dispersed Region in an Annulus" AERE-R 3159, 1959.

WARNING: This Document contains information classified under U.S. Export Control regulations as restricted from export outside the United States. You are under an obligation to ensure that you have a legal right to obtain access to this information and to ensure that you obtain an export license prior to any re-export of this information. Special restrictions apply to access by anyone that is not a United States citizen or a Permanent United States resident. For further information regarding your obligations, please see the information contained below in the section titled "Export Control Restrictions."

Export Control Restrictions

Access to and use of EPRI Intellectual Property is granted with the specific understanding and requirement that responsibility for ensuring full compliance with all applicable U.S. and foreign export laws and regulations is being undertaken by you and your company. This includes an obligation to ensure that any individual receiving access hereunder who is not a U.S. citizen or permanent U.S. resident is permitted access under applicable U.S. and foreign export laws and regulations. In the event you are uncertain whether you or your company may lawfully obtain access to this EPRI Intellectual Property, you acknowledge that it is your obligation to consult with your company's legal counsel to determine whether this access is lawful. Although EPRI may make available on a case by case basis an informal assessment of the applicable U.S. export classification for specific EPRI Intellectual Property, you and your company acknowledge that this assessment is solely for informational purposes and not for reliance purposes. You and your company acknowledge that it is still the obligation of you and your company to make your own assessment of the applicable U.S. export classification and ensure compliance accordingly. You and your company understand and acknowledge your obligations to make a prompt report to EPRI and the appropriate authorities regarding any access to or use of EPRI Intellectual Property hereunder that may be in violation of applicable U.S. or foreign export laws or regulations.

About EPRI

EPRI creates science and technology solutions for the global energy and energy services industry. U.S. electric utilities established the Electric Power Research Institute in 1973 as a nonprofit research consortium for the benefit of utility members, their customers, and society. Now known simply as EPRI, the company provides a wide range of innovative products and services to more than 1000 energy-related organizations in 40 countries. EPRI's multidisciplinary team of scientists and engineers draws on a worldwide network of technical and business expertise to help solve today's toughest energy and environmental problems.

EPRI. Electrify the World

SINGLE USER LICENSE AGREEMENT

THIS IS A LEGALLY BINDING AGREEMENT BETWEEN YOU AND THE ELECTRIC POWER RESEARCH INSTITUTE, INC. (EPRI). PLEASE READ IT CAREFULLY BEFORE REMOVING THE WRAPPING MATERIAL.

BY OPENING THIS SEALED PACKAGE YOU ARE AGREEING TO THE TERMS OF THIS AGREEMENT. IF YOU DO NOT AGREE TO THE TERMS OF THIS AGREEMENT, PROMPTLY RETURN THE UNOPENED PACKAGE TO EPRI AND THE PURCHASE PRICE WILL BE REFUNDED.

1. GRANT OF LICENSE

EPRI grants you the nonexclusive and nontransferable right during the term of this agreement to use this package only for your own benefit and the benefit of your organization. This means that the following may use this package: (I) your company (at any site owned or operated by your company); (II) its subsidiaries or other related entities; and (III) a consultant to your company or related entities, if the consultant has entered into a contract agreeing not to disclose the package outside of its organization or to use the package for its own benefit or the benefit of any party other than your company.

This shrink-wrap license agreement is subordinate to the terms of the Master Utility License Agreement between most U.S. EPRI member utilities and EPRI. Any EPRI member utility that does not have a Master Utility License Agreement may get one on request.

2. COPYRIGHT

This package, including the information contained in it, is either licensed to EPRI or owned by EPRI and is protected by United States and international copyright laws. You may not, without the prior written permission of EPRI, reproduce, translate or modify this package, in any form, in whole or in part, or prepare any derivative work based on this package.

3. RESTRICTIONS

You may not rent, lease, license, disclose or give this package to any person or organization, or use the information contained in this package, for the benefit of any third party or for any purpose other than as specified above unless such use is with the prior written permission of EPRI. You agree to take all reasonable steps to prevent unauthorized disclosure or use of this package. Except as specified above, this agreement does not grant you any right to patents, copyrights, trade secrets, trade names, trademarks or any other intellectual property, rights or licenses in respect of this package.

4. TERM AND TERMINATION

This license and this agreement are effective until terminated. You may terminate them at any time by destroying this package. EPRI has the right to terminate the license and this agreement immediately if you fail to comply with any term or condition of this agreement. Upon any termination you may destroy this package, but all obligations of nondisclosure will remain in effect.

5. DISCLAIMER OF WARRANTIES AND LIMITATION OF LIABILITIES

NEITHER EPRI, ANY MEMBER OF EPRI, ANY COSPONSOR, NOR ANY PERSON OR ORGANIZATION ACTING ON BEHALF OF ANY OF THEM:

(A) MAKES ANY WARRANTY OR REPRESENTATION WHATSOEVER, EXPRESS OR IMPLIED, (I) WITH RESPECT TO THE USE OF ANY INFORMATION, APPARATUS, METHOD, PROCESS OR SIMILAR ITEM DISCLOSED IN THIS PACKAGE, INCLUDING MERCHANTABILITY AND FITNESS FOR A PARTICULAR PURPOSE, OR (II) THAT SUCH USE DOES NOT INFRINGE ON OR INTERFERE WITH PRIVATELY OWNED RIGHTS, INCLUDING ANY PARTY'S INTELLECTUAL PROPERTY, OR (III) THAT THIS PACKAGE IS SUITABLE TO ANY PARTICULAR USER'S CIRCUMSTANCE; OR

(B) ASSUMES RESPONSIBILITY FOR ANY DAMAGES OR OTHER LIABILITY WHATSOEVER (INCLUDING ANY CONSEQUENTIAL DAMAGES, EVEN IF EPRI OR ANY EPRI REPRESENTATIVE HAS BEEN ADVISED OF THE POSSIBILITY OF SUCH DAMAGES) RESULTING FROM YOUR SELECTION OR USE OF THIS PACKAGE OR ANY INFORMATION, APPARATUS, METHOD, PROCESS OR SIMILAR ITEM DISCLOSED IN THIS PACKAGE.

6. EXPORT

The laws and regulations of the United States restrict the export and re-export of any portion of this package, and you agree not to export or re-export this package or any related technical data in any form without the appropriate United States and foreign government approvals.

7. CHOICE OF LAW

This agreement will be governed by the laws of the State of California as applied to transactions taking place entirely in California between California residents.

8. INTEGRATION

You have read and understand this agreement, and acknowledge that it is the final, complete and exclusive agreement between you and EPRI concerning its subject matter, superseding any prior related understanding or agreement. No waiver, variation or different terms of this agreement will be enforceable against EPRI unless EPRI gives its prior written consent, signed by an officer of EPRI.

Program: 1011309

Nuclear Power

EPRI • 3412 Hillview Avenue, Palo Alto, California 94304 • PO Box 10412, Palo Alto, California 94303 • USA
800.313.3774 • 650.855.2121 • askepri@epri.com • www.epri.com